Method for Predicting Lateral Displacement of PVD-improved Deposits under Embankment Loading

September 2015

Department of Science and Advanced Technology
Graduate School of Science and Engineering
Saga University, Japan

FANG XU

Method for Predicting Lateral Displacement of PVD-improved Deposits under Embankment Loading

A dissertation submitted in partial fulfillment of the requirement for the degree of Doctor of Philosophy in Geotechnical Engineering

By

FANG XU

Dissertation Supervisor:	Prof. Jinchun Chai
Examination Committee:	Prof. Jinchun Chai Prof. Koji Ishibashi Prof. Takenori Hino Associate Prof. Daisuke Suetsugu
External Examiner:	Prof. Suksun Horpibusuk Suranaree University of Technology, Thailand
Nationality:	Chinese
Previous Degrees:	Bachelor of Civil Engineering Central South University, Changsha, China Master of Geotechnical Engineering Central South University, Changsha, China

Department of Science and Advanced Technology
Graduate School of Science and Engineering
Saga University, Japan
September 2015

ACKNOWLEDGEMENT

Abstract

A method has been proposed for predicting the maximum net lateral displacement (δ_{nm}, the maximum outward lateral displacement subtracting the maximum inward lateral displacement) of prefabricated vertical drains (PVDs) improved deposits under embankment loading with and without the application of vacuum pressure. The method is based on the results of a series of large-scale laboratory model tests and more than 30 field case histories.

For the laboratory model tests, the model box has dimension of 1.5 m in length, 0.62 m in width and 0.85 m in height. The embankment load was applied using air pressure through Bellofram cylinder systems. The model tests were mainly designed to investigate the effects of embankment loading rate (LR) and the undrained shear strength (s_u) of the model ground on the lateral displacement. The test results indicate that: (1) the normalized lateral displacement (NLD), i.e. the ratio of maximum lateral displacement (δ_m) to the ground surface settlement (S_f) at the centerline of the surcharge loading area ($NLD = \delta_m/ S_f$), almost linearly increased with the increase of LR; (2) Under the same loading condition, NLD reduced with the increase of s_u.

Except the embankment loading rate and undrained shear strength of the ground, there are other important parameters affecting the values of NLD, i.e. magnitude of embankment load, ratio of vacuum pressure to the embankment load, and deformation and consolidation properties of soft subsoils. To consider the effects of all these factors on NLD, a synthetic parameter termed as a ratio of an index load (p_n) to s_u of the deposit (RLS) has been adopted. p_n is calculated as the total embankment load (p_{em}) subtracting the sum of p_{em} and the absolute value of vacuum pressure (p_{vac}) multiplied by the average degree of consolidation (U) of the PVD-improved zone corresponding to the end of embankment construction. The reason for using the values of U and s_u corresponding to the end of embankment construction to calculate RLS is that at that time the system has the largest applied surcharge load and a relatively small undrained shear strength, i.e. lower factor of safety (FS). There are many field cases showed that the maximum lateral displacement

occurred at this time point. For each model test, the values of *NLD* and *RLS* have been analyzed and the laboratory test results verified that *RLS* is a controlling factor of *NLD*.

Further, more than 30 field case histories of embankments constructed on PVD-improved grounds have been collected from different countries and the corresponding values of *NLD* and *RLS* were analyzed. The all analyzed results of *NLD* and *RLS* from both the laboratory tests and the field case histories were depicted together in a *NLD-RLS* plot. It shows a general trend of *NLD* increases with the increasing of *RLS*. Using regression analysis, a bilinear range was proposed for the *NLD-RLS* relationship for predicting the maximum net lateral displacement (δ_{nm}) of PVD-improved deposits under embankment loading with and without the application of vacuum pressure.

In using this method, the value of *RLS* and the settlement, S_f, can be calculated prior to an embankment construction. And then from the *NLD-RLS* relationship, a value of *NLD* is obtained, and therefore δ_{nm} can be predicted. It is recommended that the proposed method can be used as a design tool in engineering practice.

TABLE OF CONTENTS

LIST OF TABLES

LIST OF FIGURES

LIST OF NOTATIONS

a	Width of PVD
A_1	Area of inward lateral displacement under the toe of an embankment
A_2	Area of outward lateral displacement under the toe of an embankment
b	Thickness of PVD
B	Half width of the vacuum preloading treated area
B_1	With of embankment slope
B_2	Half with of the top of an embankment
c_h	Coefficient of consolidation of soil in the horizontal direction
c_v	Coefficient of consolidation of soil in the vertical direction
c'	Effective cohesion stress
C_c	Compression index
C_s	Swelling index
d_m	Diameter of the cross section of mandrel
d_s	Diameter of smear zone
d_w	Equivalent diameter of PVD
D	Diameter of mini-vane
D_0	A constant (= 1.5 m)
D_e	Diameter of unit cell of PVD-improvement
DR	Displacement ratio
e	Void ratio
e_0	Initial void ratio
E_s	Compression modulus
E_{s1-2}	Compression modulus corresponding to stress increment of 100 to 200 kPa
FS	Factor of safety
g	An integer
G	A parameter equal to $(2g+1)\pi/2$
G_s	Specific gravity
H	Thickness of soil layer
H_d	Length of drainage path

H_{em}	Height of embankment
H_L	Thickness of PVD-improved zone
I	A factor used to calculate the increment of vertical stress due to embankment load
k	Hydraulic conductivity
k_h	Hydraulic conductivity of the intact soil in the horizontal direction
k_s	Hydraulic conductivity of the smear zone in the horizontal direction
k_v	Hydraulic conductivity of the intact soil in the vertical direction
K_0	At-rest horizontal earth pressure coefficient
K_a	Rankine active earth pressure coefficient
l	Drainage length of PVD
LR	Loading rate
m	Constant for calculating undrained shear strength
n	Spacing ratio of PVD-improvement
NLD	Normalized lateral displacement
$NLD\text{-}L$	Normalized lateral displacement at the left side of the loading area
$NLD\text{-}R$	Normalized lateral displacement at the right side of the loading area
OCR	Overconsolidation ratio
p_{em}	Embankment load
p_i	Load at ith loading step
p_j	Load at jth loading step
p_n	An index pressure
p_{vac}	Vacuum pressure
Δp_j	Load increment at jth loading step
q_w	Discharge capacity of PVD
r	Radial coordinate
RLS	Ratio of index pressure to undrained shear strength
s	Smear ratio PVD
s_u	Representative undrained shear strength of PVD-improved zone
s_{ui}	Initial undrained shear strength of the model ground
S	Spacing of PVD
S_1	Constant for calculating undrained shear strength
S_c	Consolidation settlement

S_f	Ground surface settlement on the embankment centerline
ΔS_f	Increment of ground surface settlement on the embankment centerline
t	Time
t_i	Time at ith loading step
t_{j0}	Imaginary time
Δt	Increment of time
T_1	Time for a time-dependent load to be fully applied
T_h	Time factor for radial consolidation
T_v	Time factor for vertical consolidation
T_{max}	Measured maximum torque in vane shear test
u	Excess pore water pressure
u_0	Initial excess pore water pressure
$\bar{u}$	Average excess pore water pressure
$\bar{u}_0$	Initial average excess pore water pressure
U	Degree of consolidation
U_2	Average degree of consolidation for the layer without PVD
U_{av}	Overall average degree of consolidation
U_h	Average degree of consolidation in horizontal direction
U_i	Average degree of consolidation at ith loading step
U_j	Average degree of consolidation at jth loading step
U_p	Average degree of consolidation of the layer with PVDs located above the unimproved layer
U_T	Average degree of consolidation of the layer without PVD calculated by Terzaghi's 1D consolidation theory
U_v	Average degree of consolidation in vertical direction
w	Water content
w_L	Liquid limit
w_n	Initial water content of clay slurry
w_P	Plastic limit
z	Depth
z_c	The maximum depth of crack caused by vacuum pressure
z_L	Depth where no lateral displacement occurs
z_w	Depth of ground water level

z'	Vertical distance between z_L and z_c
α	A factor used to calculate ε_{vv} from ε_{vol}
α_2	A factor used to calculate the degree of consolidation of unimproved layer
γ_{em}	Unit weight of embankment fill
γ_t	Total unit weight of soil
γ_w	Unit weight of water
γ'	Effective unit weight of soil
δ	Lateral displacement
δ_{av}	Average lateral displacement
δ_m	Maximum lateral displacement
δ_{mi}	Maximum inward lateral displacement
δ_{mo}	Maximum outward lateral displacement
δ_{mL}	Measured maximum lateral displacement at left side of the loading area
δ_{mR}	Measured maximum lateral displacement at right side of the loading area
$\Delta\delta_m$	Increment of maximum lateral displacement
ε_h	Average inward lateral strain
ε_{vol}	Volumetric strain
ε_{vv}	Vertical strain
λ	Slope of virgin compression line in e-ln(p') plot
μ	A parameter considering the effect of PVD spacing, smear and well resistance
ν	Poisson's ratio
σ'_v	Vertical effective stress
σ'_{v0}	Initial vertical effective stress
σ'_{vp}	Vertical pre-consolidation pressure
$\Delta\sigma'_v$	Increment of vertical effective stress
$\Delta\sigma_{vac}$	Increment of vacuum pressure
$\Delta\sigma_z$	Increment of vertical stress due to embankment load
ϕ'	Effective friction angle of soil

CHAPTER ONE
INTRODUCTION

1.1   General Background

In recent years, the demand for constructing embankments on coastal regions increases with the development of modern transport infrastructures, such as highway, railway and airports. Usually, there are soft deposits with high water content, high compressibility, low permeability and low shear strength in these regions. Constructions on those soft soils may experience excessive deformation or even bearing capacity failure. Preloading with installation of prefabricated vertical drains (PVDs) is one of the commonly used ground improvement methods (Chai *et al*. 2010; Pothiraksanon *et al*. 2010; Ghandeharioon *et al*. 2011; Karunaratne 2011; Mesri and Khan 2012; Deng *et al*. 2013; Oliveira; 2013; Chai *et al*. 2014; Parsa-Pajouh *et al*. 2014; Kim *et al*. 2014; Karim and Lo 2015; Lu *et al*. 2015). With PVD-improvement the soft ground consolidates in both vertical and horizontal directions, and usually the length of drainage path between PVDs in the horizontal direction is much less than that in the vertical direction of the natural deposit. Therefore, it remarkably accelerates the consolidation process of the soft clayey deposits and increases the rate of strength gain of the ground under a preloading pressure (Liu *et al*. 2008; Xu and Chai 2014). As a result, an embankment can be constructed faster than that on natural deposit.

The embankment load induces not only vertical stresses but also shear stresses to the soft ground. Consequently, it results in settlements and lateral displacements of the ground, and predicting or controlling the ground deformation is a main issue considered in design of an embankment. There have been many researches on predicting the vertical settlement of the embankment foundation, and generally, relative good agreements can be achieved between the predicted and measured values for both the cases of embankment constructed on natural and PVD-improved deposit (e.g. Devata and Darch 1973; Asaoka 1978; Tan

1995; Cascone and Biodi 2013; Hu *et al*. 2014). However, predictions of lateral displacement remains as a difficult task.

In the case of an embankment to be constructed near some existing buildings or structures, predicting the lateral displacement of the soft ground will often be a crucial issue and sometimes may in fact control the design. Because of the anisotropy, nonhomogeneity, nonlinear stress-strain behavior of soft clayey soil and the difficulties to consider the embankment stiffness and foundation roughness (Poulos 1972), there is not a theoretical way as for predicting vertical settlement to predict the lateral displacement of natural deposit under embankment loading. So researchers tried to find some empirical ways, e.g. Tavenas *et al*. (1979); Tavenas and Leroueil (1980); Suzuki (1988); Loganathan *et al*. (1993); Ma (1995) and Smadi (2001). However, these studies simply provided statistics between the maximum lateral displacements under the toe of an embankment (δ_m) and the ground surface settlements on the embankment centerline (S_f), and predicted the value of δ_m as a percentage of the value of S_f. Because different field cases have different ground conditions and different construction procedures, these empirical methods cannot give an accordance prediction.

For the case of embankment on PVD-improved deposit, Ong and Chai (2011) and Chai *et al*. (2013) reported that the main factors affecting the ground lateral displacement are magnitudes of embankment load and vacuum pressure, loading rate, deformation, consolidation and strength properties of the soft subsoil and the properties of PVDs. If a theoretical or empirical method can consider the effects of these main influencing factors, acceptable predictions of lateral displacement may be achieved for PVD-improved deposit.

Based on investigation of filed case histories, Chai *et al*. (2013) proposed an empirical method with theoretical considerations of the effects of the main influencing factors to predict the maximum lateral displacement of the ground for PVD-improved deposit under the combination of vacuum pressure and embankment loading. However, to date there is no systematic investigation of the lateral displacement of PVD-improved deposit under only embankment loading.

1.2   Objectives and Scopes

Prefabricated vertical drain (PVD) has been widely used to accelerate the consolidation process, increase the rate of strength gain and reduce the post construction deformation of

embankments on soft clayey deposits. This study focused on investigating the lateral displacement of PVD-improved deposit under embankment loading by laboratory model tests and analyses of field case histories. The main objective is to propose a method for predicting the maximum lateral displacement of PVD-improved ground under embankment loading. This objective has been achieved by the following three steps.

(1) Investigation by laboratory model tests

For a specific embankment, the ground deformation, especially lateral displacement is not only influenced by the magnitude of the embankment load, but also loading rate. In this study a series of large scale laboratory model tests were conducted in a metal box with inner dimensions of 1.50 m in length, 0.62 m in width and 0.85 m in height. The model tests were conducted under different surcharge loading rate, while the total applied surcharge load was kept the same. Under such kind of loading manner, the effects of the loading rate on lateral displacement were investigated.

(2) Investigation by field case histories

The ratio of the maximum ground lateral displacement (δ_m) under the toe of the embankment to the ground surface settlement on the embankment centerline (S_f) was defined as normalized lateral displacement (NLD). The relationship between NLD and the ratio of load to undrained shear strength of the ground (RLS) has been investigated. Totally, 18 field case histories collected in five different countries were analyzed.

(3) Method for predicting lateral displacement

Combining the results from laboratory model tests and case histories, an empirical method with theoretical considerations of the main factors influencing lateral displacement was proposed for predicting the lateral displacement of PVD-improved deposits under embankment loading.

1.3 Organization of the Dissertation

This dissertation contains six chapters. Fig. 1.1 shows the flow chart of the research. Chapter 1 describes the general background, objectives and scopes of the study.

Chapter 2 reviews the literatures about consolidation theory for PVD-improvement, lateral displacement of natural and PVD-improved ground under embankment loading, and factors affecting lateral displacement.

Chapter 3 presents the large scale laboratory model test and test results. It contains test devices, cases tested as well as the test results in terms of ground surface settlements, variations of excess pore water pressure in the model ground and lateral displacement profiles.

Chapter 4 investigates the lateral displacements of PVD-improved deposits by analyzing 18 field case histories collected in five different countries.

Chapter 5 presents the proposed method for predicting the maximum lateral displacement of PVD-improved deposits under embankment loading.

Finally, the conclusions drawn from this study and the recommendations for future works are given in Chapter 6.
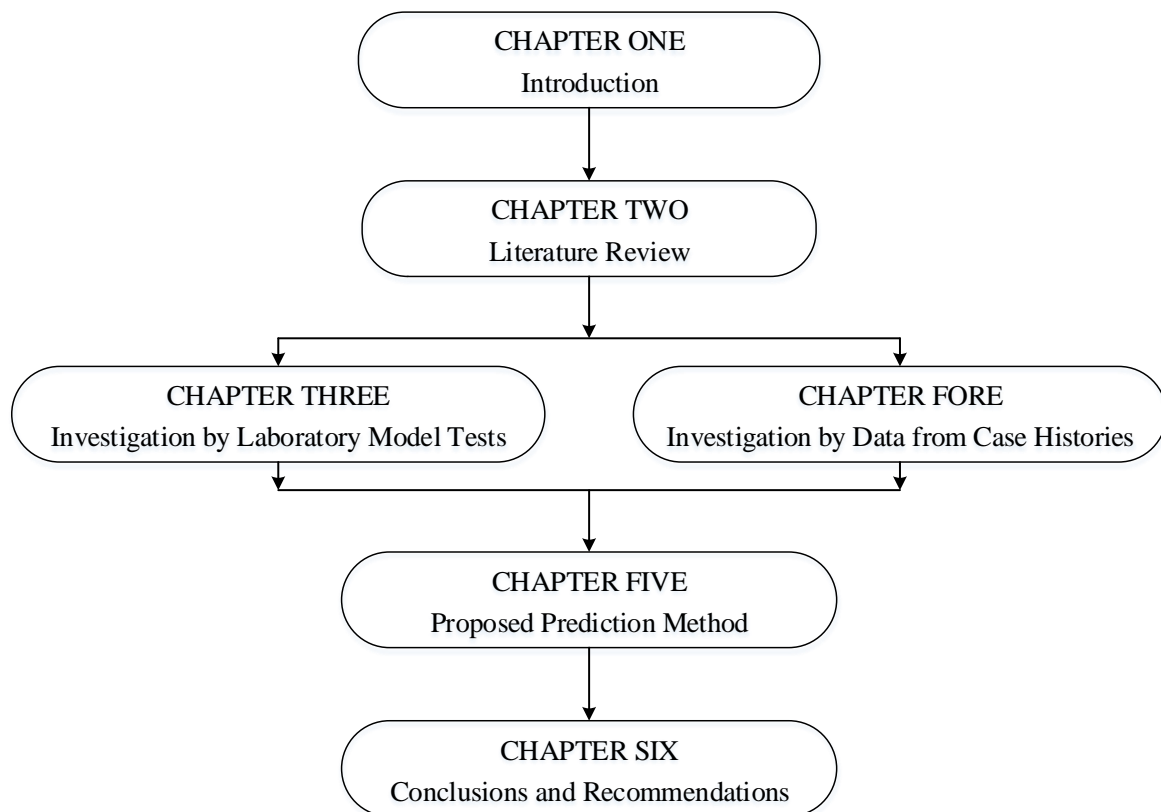
Fig. 1.1 Flow chart of this study

CHAPTER TWO
LITERATURE REVIEW

2.1   Introduction

In 1930s, prefabricated vertical drains (PVDs) were first introduced into geotechnical engineering practice, almost the same time as the application of sand drains (SDs) (Hansbo 1977). Subsequently, several types of PVD were developed (Hansbo 1979). Today there are more than 100 types of PVD available in the market and the number is still increasing (Ong 2011).

Usually, a PVD consists of a plastic core with holes and longitudinal drainage channels covered with a filter sleeve of geotextiles or other geosynthetic materials, as shown in Fig. 2.1.

Fig. 2.1 Typical type of PVD

Preloading with installation of PVDs has become one of the most efficient and cost-effective soft clayey ground improvement technique and it is widely used worldwide (e.g. Chai *et al*. 2010; Pothiraksanon *et al*. 2010; Ghandeharioon *et al*. 2011; Karunaratne 2011; Mesri and Khan 2012; Deng *et al*. 2013; Oliveira; 2013; Chai *et al*. 2014; Parsa-Pajouh *et al*. 2014; Kim *et al*. 2014; Karim and Lo 2015; Lu *et al*. 2015). The PVDs provide drainage paths along which excess pore water pressures caused by a surcharge load can be

dissipated faster than by a vertical drainage path of natural soil alone (Chai *et al.* 2010; Walker *et al.* 2012; Indraratna *et al.* 2012). And the consolidation theory for PVD-improvement has been well established (e.g. Barron 1948; Hansbo 1981).

The preloading pressure, e.g. embankment load and/or vacuum pressure, can cause settlements and lateral displacements of the ground, and they are the main issues considered in design of an embankment on PVD-improved ground. In some cases, the shear stresses caused by the embankment load will induce large lateral displacement in the ground, result in stability problem of the system and detrimental effect on the behavior of adjacent structures or buildings. Especially in the case of piles installed close to the embankment, lateral displacement may cause significant bending moments or even structural failure of the piles.

In engineering practice, excessive lateral deformation of the ground is not allowed, even though the embankment-foundation system has sufficient factor of safety. For example, in Japan the maximum lateral displacement at the property boundary of a highway or railway is restricted to be less than ±50 mm (Chai and Carter 2011). Sometimes, constructing retaining structures, such as cement deep mixing columns or dry jet mixing columns, is required near the toe of the embankment to reduce the lateral displacement, as illustrated in Fig 2.2. Therefore, predicting the lateral displacement of the ground is an essential design requirement.
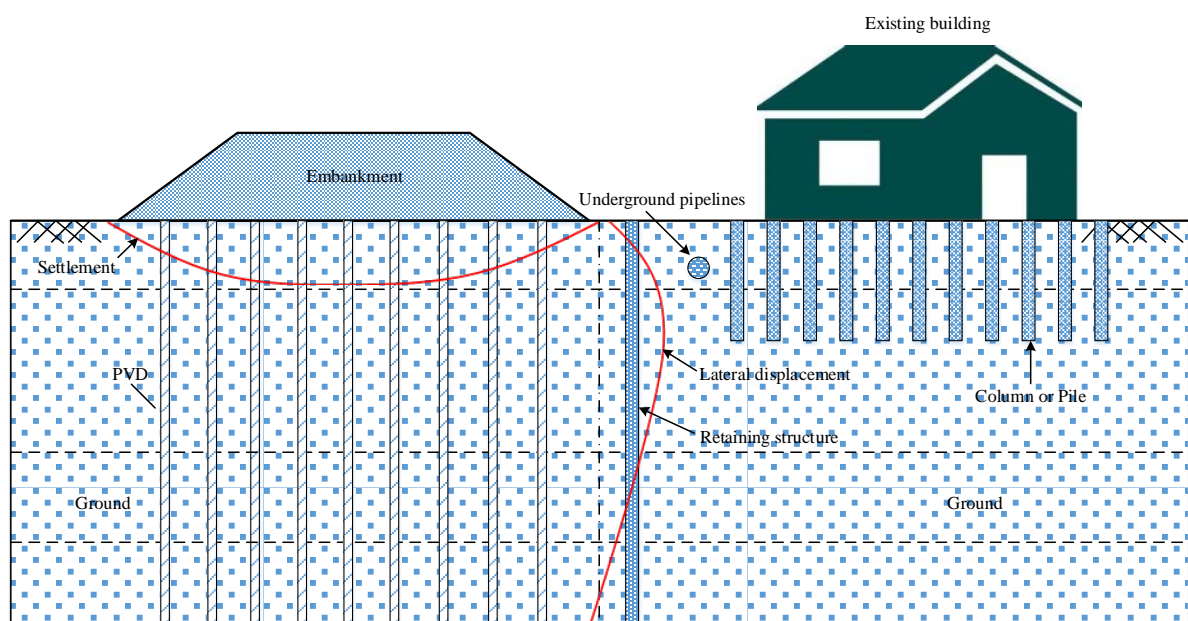
Fig. 2.2 Diagram of retaining structure used to reduce lateral displacement

For PVD-improved ground, the preloading pressure can be embankment load, vacuum pressure, or combined vacuum pressure and embankment load. Method of predicting settlement has been well established (e.g. Devata and Darch 1973; Asaoka 1978; Tan 1995; Cascone and Biodi 2013; Hu *et al*. 2014), whereas the prediction of lateral displacement remains as a difficult task.

2.2   PVD Induced Consolidation

2.2.1 Drainage properties of PVD

(1) Equivalent diameter of PVD

Usually a PVD has a rectangular cross-section, but most of the analytical solutions for PVD induced consolidation assume a cylindrical soil column with a circular drain in the center (unit cell). With this assumption, the rectangular cross-section of PVD needs to be converted into an equivalent circular one.

Based on the assumption of equal drainage periphery, Hansbo (1979) proposed an equivalent diameter of PVD as:

$$d_{\mathrm{w}} = \frac{2(a+b)}{\pi} \tag{2.1}$$

where a and b = width and thickness of a PVD, respectively; and d_{w} = equivalent diameter of PVD.

Fellenius and Castonguay (1985) proposed another equation by assuming PVD has the same cross-section area before and after conversion. Their equation is expressed as:

$$d_{\mathrm{w}} = \sqrt{\frac{4ab}{\pi}} \tag{2.2}$$

In fact the pore water in the soil flows into the PVD mainly through its perimeter, so Hansbo (1979)'s equation may be more proper than Fellenius and Castonguay (1985)'s equation.

Based on finite element analysis, Rixner *et al*. (1986) indicated that due to the corner effect, the equivalent drain diameter is less than the evaluation from equal perimeter assumption, and they proposed a new equation as:

$$d_\mathrm{w} = \frac{a+b}{2} \tag{2.3}$$

Now, this equation is widely used.

(2) Discharge capacity of PVD

The PVD gives a channel for the pore water to flow out from the soil. However, PVD is not a perfectly pervious boundary. Its discharge capacity (q_w) is finite and sometimes influences the rate of consolidation. This phenomenon is termed as well resistance of PVD.

Holtz *et al*. (1991) indicated that the main factors affecting discharge capacity of a PVD are as follows:

(1) The cross-section area of the plastic core for water flow;

(2) The effect of lateral earth pressure;

(3) Folding, bending, and crimping of the PVD;

(4) Infiltration of fine soil particles through the filter.

Chai and Miura (1999) further pointed out that air bubbles trapped in the drainage channels of the drain and creep of the filter also reduce the discharge capacity of PVD.

Holtz *et al*. (1991) reported that the discharge capacity of PVD could vary from 100-800 m^3/year, and if under significant vertical compression and high lateral pressure, values of q_w may reduce to 25-100 m^3/year. Chai and Miura (1999) conducted long-term discharge capacity tests of PVD confined in clay, and they found that the q_w of PVD may reduce from an initial value of more than 200 m^3/year to less than 50 m^3/year with time elapsed. Indraratna and Redana (2000) reported that long term q_w of PVD can be reduced in the range of 40-60 m^3/year.

Holtz *et al*. (1988) suggested that if the value of q_w is higher than 150 m^3/year after PVD installation, the well resistance of the drain does not have significant effect on the consolidation rate of the surrounding soil. Chai *et al*. (2001) recommended that if without laboratory test, a value of 100 m^3/ year for q_w can be used in preliminary design.

(3) Smear zone caused by installation of PVD

Usually, the PVD is installed in a soft deposit using a mandrel. After the PVD reached the designed inserting depth, the mandrel will be withdrawn and the PVD will be left in the

ground. This installation procedure causes significant remolding of the subsoil adjacent to the mandrel, and the disturbed/remolded zone is called smear zone.

The size of the smear zone is related to the cross-section area of the mandrel used. According to the study of Holtz and Holm (1973) and Akagi (1977), the size of the smear zone (d_s) is:

$$d_s = 2d_m \tag{2.4}$$

where d_m = diameter of the cross-section of mandrel.

Jamiolkowski and Lancellota (1981) suggested that the smear zone can be estimated as:

$$d_s = (2.5 \sim 3)d_m \tag{2.5}$$

Hansbo (1981) proposed another relationship as:

$$d_s = (1.5 \sim 3)d_m \tag{2.6}$$

Based on laboratory test, Sathananthan and Indraratna et al. (2006) stated that:

$$d_s = (2 \sim 3)d_m \tag{2.7}$$

From the above studies, it can be concluded that the smear zone is commonly suggested as 1.5 to 3 times of the cross-section of the mandrel.

Except the size of the smear zone, the permeability of the smear zone is another main parameter affecting the consolidation rate of PVD-improved ground. In the commonly used radial consolidation theory (Barron 1948; Hansbo 1981), the soil inside the smear zone is assumed entirely remolded and the hydraulic conductivity of the smear zone (k_s) is small than that of the intact zone. Because of the anisotropy of the subsoil formed by the process of sedimentation, usually, the hydraulic conductivity of the soil in the horizontal direction (k_h) is higher than that in the vertical direction. Hansbo (1987) reported that the hydraulic conductivity of the smear zone (k_s) can be estimated the same as the corresponding vertical hydraulic conductivity of the intact soil (k_v).

The ratio of k_h/k_s (or k_h/k_v) plays an important role in the radial consolidation theory of PVD-improvement. The value of k_h/k_v for intact soil can vary from 1 to 15 (Jamiokowski et al. 1983; Tavenas et al. 1983; Leroueil et al. 1990; Bergado et al. 1991; Bergado et al. 1993;Hansbo 1997; Indraratna and Redana, 1998; Hird et al. 2000; Chai et al. 2001; Bo et al. 2003; Sathananthan et al. 2008; Chai et al. 2013; Vu 2014;).

(4) Diameter of an unit cell

PVDs are normally installed in a square or triangular pattern, as shown in Fig. 2.3.
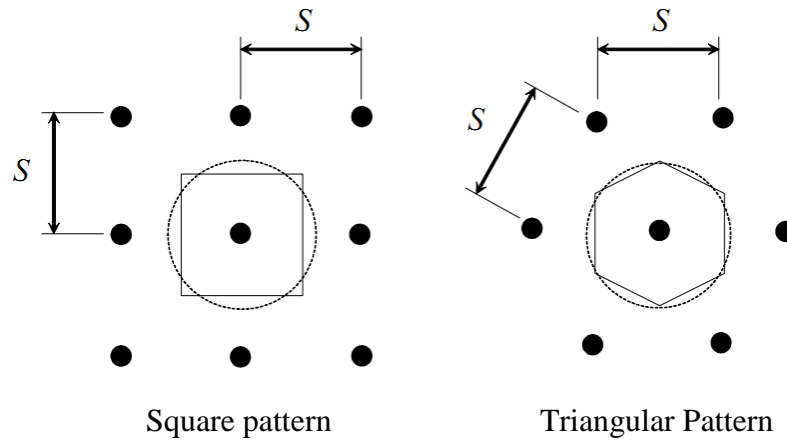
Fig. 2.3 Installation parttens of PVD (after Walker 2006)

Based on the equal area assumption, the improved square prism or hexagonal prism of each PVD is converted into a cylindrical column (unit cell). The diameter of the unit cell is calculated as follows:

$$D_e = 1.13S \text{ , for squire pattern} \tag{2.8}$$

$$D_e = 1.05S \text{ , for triangular pattern} \tag{2.9}$$

where D_e = diameter of unit cell; and S = spacing of PVD.

(5) Summary and Comments

The consolidation parameters related to PVD-improvement are equivalent diameter of PVD, discharge capacity of PVD, diameter of smear zone due to installation of PVD, the ratio of the horizontal hydraulic conductivity of smear zone to that of intact zone, and the diameter of unit cell of a PVD.

2.2.2 Theories for PVD induced consolidation

For a PVD-improved deposit, the subsoil not only consolidates in the vertical direction but also in the radial direction. To analyze the ground deformation, the effects of both the vertical and radial drainages have to be considered.

(1) Vertical consolidation theory

Terzaghi's one-dimensional (1D) consolidation theory (Terzaghi 1925) is commonly used to calculate the average degree of consolidation of the ground in the vertical direction (U_v) or to predict the dissipation of the excess pore water pressure induced by external load. The basic assumptions of this theory are as follows:

(1) The soil is homogeneous and fully saturated;

(2) The soil particles and the pore water are incompressible;

(3) The flow of the pore water is only in the vertical direction;

(4) Darcy's law is valid;

(5) The strains are small.

The basic differential equation of Terzaghi's 1D consolidation theory is:

$$\frac{\partial^2 u}{\partial z^2} = c_v \frac{\partial u}{\partial t} \tag{2.10}$$

where u = excess pore water pressure caused by increase of stress; c_v = coefficient of consolidation of the soil in the vertical direction; z = depth; and t = time.

The solution of Eq. (2.10) yields:

$$u = \sum_{g=0}^{g=\infty} \left[\frac{2u_0}{G} \sin\left(\frac{Gz}{H_d} \right) \right] e^{-G^2 T_v} \tag{2.11}$$

where g = an integer; u_0 = initial excess pore water pressure; $G = (2g+1)\pi/2$; H_d = length of drainage path; and T_v = time factor for vertical consolidation which is express as:

$$T_v = \frac{c_v t}{H_d^2} \tag{2.12}$$

According to Eq. (2.11), the average degree of consolidation can be derived as:

$$U_v = 1 - \sum_{g=0}^{g=\infty} \frac{2}{G^2} e^{-G^2 T_v} \tag{2.13}$$

(2) Radial consolidation theory

Fig. 2.4 presents the schematic diagram of the unit cell of a PVD. Barron (1948) derived a rigorous solution of vertical drain using 'free strain hypothesis' and an approximate solution using 'equal strain hypothesis'. For both of the two hypothesis the smear effect and the well resistance can be involved in the solutions. The difference between the rigorous solution and the approximate one is quite small, so the approximate solution is more often used due to its simplicity.
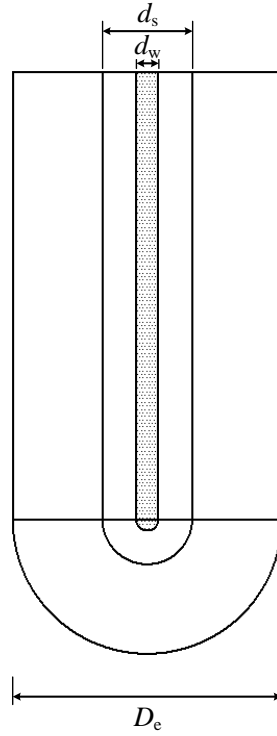
Fig. 2.4 Unit cell of a PVD

Besides, based on 'equal strain hypothesis' and considering well resistance and both vertical and radial flows of pore water, Yoshikuni and Nakanodo (1974) derived a rigorous solution for vertical drain and gave the results in graphs forms. Hansbo (1981) presented a simple solution assuming the volume of pore water flow into the inner boundary of a soil hollow cylinder equals to the change in the volume of the hollow cylinder based on 'equal strain hypothesis'. By assuming the compressibility of the soil inside and outside the smear zone are different, Onoue (1988) presented a rigorous solution for consolidation with vertical drains based on 'free strain hypothesis'. Basu *et al.* (2006) obtained analytical solutions of the consolidation of vertical drain considering the variation of soil hydraulic conductivity in the radial direction. Deng *et al.* (2013) analyzed the effect of variation of discharge capacity with depth and time on the consolidation of vertical drain. Lu *et al.* (2015) developed a solution for vertical drain with coupled radial-vertical flow considering well resistance. In all of these solutions of radial consolidation due to vertical drain, Hansbo (1981)'s solution is widely used for its simplicity. Here, only Hansbo (1981)'s solution is given in detail.

The governing equation of the average excess pore water pressure ($\bar{u}$) is as:

$$\frac{\partial \bar{u}}{\partial t} = c_h \left(\frac{1}{r} \frac{\partial u}{\partial r} + \frac{\partial^2 u}{\partial r^2} \right) \tag{2.14}$$

where c_h = coefficient of consolidation of the soil in the horizontal direction; and r = radial coordinates.

Hansbo (1981) derived a simple solution for Eq. (2.14) which considers the smear effect and well resistance under equal vertical strain assumption. The solution is as follows:

$$\bar{u} = \bar{u}_0 \exp\left(\frac{-8T_h}{\mu}\right)$$ (2.15)

$$U_h = \exp\left(\frac{-8T_h}{\mu}\right)$$ (2.16)

where $\bar{u}_0$ = initial average excess pore water pressure; and T_h = time factor for radial consolidation which is calculated as:

$$T_h = \frac{c_h t}{D_e^2}$$ (2.17)

and μ is express as:

$$\mu = \ln\frac{n}{s} + \frac{k_h}{k_s}\ln(s) - \frac{3}{4} + \frac{2\pi l^2 k_h}{3q_w}$$ (2.18)

where $n = D_e/d_w$; $s = d_s/d_w$; k_h and k_s = hydraulic conductivity in the horizontal direction for intact zone and smear zone, respectively; l = drainage length of PVD; and q_w = discharge capacity of a PVD.

(3) Consolidation of clayey deposit with partially penetrated PVD

In engineering practice, for cost consideration or avoidance of vacuum pressure leakage from the bottom drainage boundary in the case of vacuum preloading, sometimes PVDs are partially penetrated in the subsoil layers (e.g. Runesson *et al*. 1985; Chai *et al*. 2005; Chai *et al*. 2009; Geng *et al*. 2011). For the consolidation of a soft deposit with partially penetrated PVDs, the degree of consolidation of the bottom layer without PVD improvement is also need to be calculated. There are some approximate or semi-analytical solutions for this kind of situation (e.g. Hart *et al*. 1958; Zeng and Xie 1989; Tang and Onitsuka 1998; Zhang *et al*. 2005; Ong *et al*. 2012). Here, the simple and easy for using one proposed by Ong *et al*. (2012) is briefly described.

For the bottom layer without PVD, only vertical drainage needs to be considered, and the average degree of consolidation of this layer (U_2) is expressed as:

13

$$U_2 = \alpha_2 U_T \tag{2.19}$$

where U_T is the degree of the consolidation of the layer calculated by Terzaghi's one-dimensional consolidation theory under one-way drainage conditions for the case where the bottom boundary of the layer is impermeable and under two-way drainage conditions for the case where the bottom boundary of the layer is permeable, and α_2 is a multiplier, which can be calculated as:

For one-way drainage,

$$\alpha_2 = \left(0.33 U_p^2 + 0.20 U_p + 0.1\right)\left(\frac{k_h/k_s}{2}\right)^{0.07}\left(\frac{D_0}{D_e}\right) \tag{2.20}$$

For two-way drainage,

$$\alpha_2 = \left(0.05 U_p^2 + 0.48 U_p + 0.3\right)\left(\frac{k_h/k_s}{2}\right)^{0.07} \tag{2.21}$$

where U_p = the average degree of consolidation of the layer with PVDs located above the bottom layer; and D_0 = a constant (= 1.5 m).

(4) Combination of vertical and radial consolidation

With PVD-improvement, the soft ground consolidates in both the vertical and radial directions. Carrillo (1942) proved that the vertical consolidation and the radial consolidation can be combined, and the overall average degree of consolidation (U_{av}) can be calculated as:

$$U_{av} = 1 - \left[\left(1 - U_v\right)\cdot\left(1 - U_h\right)\right] \tag{2.22}$$

(5) Consolidation under time-dependent loading

Terzaghi (1925)'s 1D consolidation theory as well as Hansbo (1981)'s solution for radial consolidation are for the case of instantaneous loading. In engineering practice, embankment load gradually increases with time during the construction process. There have been some analytical solutions or design charts for considering the time-dependent embankment loading induced consolidation of the ground (e.g. Olson 1977; Lekha *et al*. 1998; Tang and Onitsuka 2000; Zhu and Yin 2001; Zhu and Yin 2004; Conte and

Troncone 2009; Jimenez *et al.* 2009; Geng *et al.* 2012; Lu *et al.* 2014). However, due to the complexities, these methods are not easy for use.

According to the fact that the effective stress in a soft clayey deposit continuously increases during the loading process, Chai and Miura (2002) proposed an empirical method to calculate the degree of consolidation due to time-dependent loading as follows:

(1) Approximate the time-dependent loading process by stepwise loads (Fig. 2.5).
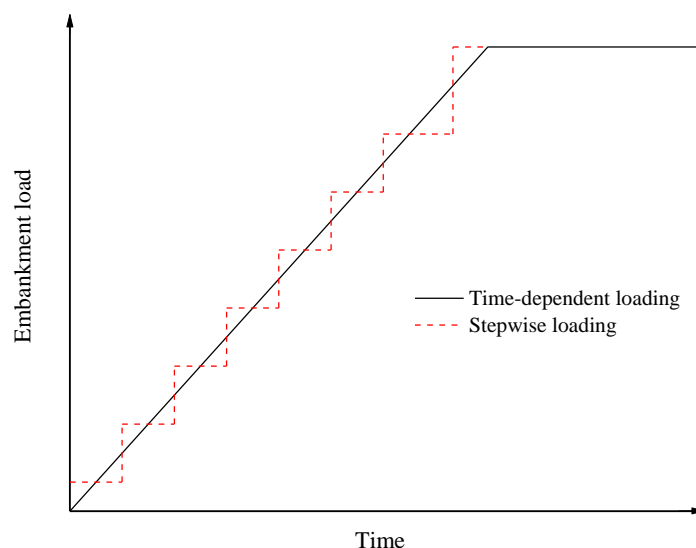
Fig. 2.5 Assumed loading procedure of Chai and Miura (2002)

(2) Suppose at time t_i the applied load is p_i, and the degree of consolidation corresponding to p_i is U_i. A load increment Δp_j is applied instantaneously at time t_i, and the degree of consolidation (U_j) associated with $p_j = p_i + \Delta p_j$ at time t_i is:

$$U_j = \frac{U_i p_i}{p_j} \tag{2.23}$$

(3) With U_j known, an imaginary time t_{j0} can be obtained from the corresponding consolidation theory.

(4) Under the loading p_j, at time $t_i + \Delta t$, the degree of consolidation is calculated using a time of $t_{j0} + \Delta t$.

(6) Summary and Comments

For PVD-improved deposit, the degree of consolidation due to vertical flow and radial flow can be calculated using Terzaghi's one dimensional consolidation theory and Hansbo

(1981)'s solution, respectively. The average degree of consolidation combined vertical and radial flow can be evaluated using Carrillo (1942)'s equation.

2.3 Consolidation Settlement

2.3.1 One-dimensional (1D) compression theory

The settlement of the soft ground under load consists of 3 parts, i.e. immediate settlement, primary consolidation settlement and secondary consolidation settlement. Under one-dimensional deformation condition, the immediate settlement is negligible. The primary consolidation settlement takes place during the process of pore water being squeezed out, and it is the largest part of the ground settlement. The secondary consolidation settlement is resulted by the adjustment of the soil fabrics under a constant load, and usually it is relatively small comparing with the primary consolidation settlement.

The consolidation settlement is usually calculated using Terzaghi's one-dimensional compression theory using linear e-log (σ'_v) assumption (Fig. 2.6).
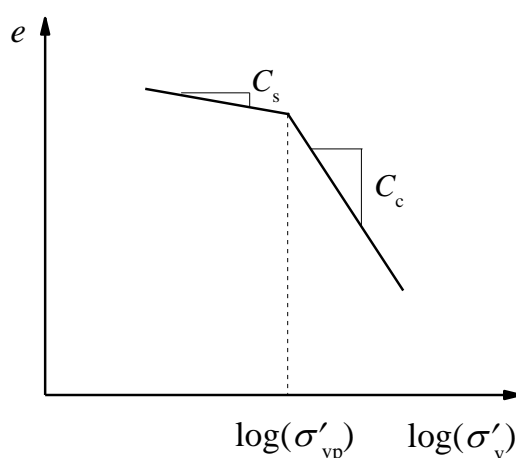
e = void ratio; σ'_v = vertical effective stress; σ'_{vp} = pre-consolidation pressure;

C_s = swelling index; and C_c = compression index

Fig. 2.6 One-dimensional compression of soil in e-lg(σ'_v) plot.

If both the initial vertical effective stress (σ'_{v0}) and the vertical effective stress after loading ($\sigma'_{v0}+\Delta\sigma'_v$) are located in the overconsolidated range, the consolidation settlement is calculated as:

$$S_c = \frac{HC_s}{1+e_0}\log\left(\frac{\sigma'_{v0}+\Delta\sigma'_v}{\sigma'_{v0}}\right) \tag{2.24}$$

where S_c = consolidation settlement; H = thickness of the soil layer; e_0 = initial void ratio; and $\Delta\sigma'_v$ = increment of vertical effective stress due to loading.

If both σ'_{v0} and ($\sigma'_{v0}+\Delta\sigma'_v$) are located in the normally consolidated range, the consolidation settlement is:

$$S_c = \frac{HC_c}{1+e_0}\log\left(\frac{\sigma'_{v0}+\Delta\sigma'_v}{\sigma'_{v0}}\right) \tag{2.25}$$

If σ'_{v0} is less than σ'_{vp} and ($\sigma'_{v0}+\Delta\sigma'_v$) is larger than σ'_{vp}, the consolidation settlement is:

$$S_c = \frac{H}{1+e_0}\left[C_c\log\left(\frac{\sigma'_{v0}+\Delta\sigma'_v}{\sigma'_{v0}}\right)-(C_c-C_s)\log(OCR)\right] \tag{2.26}$$

where OCR = overconsolidation ratio, defined as:

$$OCR = \frac{\sigma'_{vp}}{\sigma'_{v0}} \tag{2.27}$$

2.3.2 Vertical stress induced by embankment load
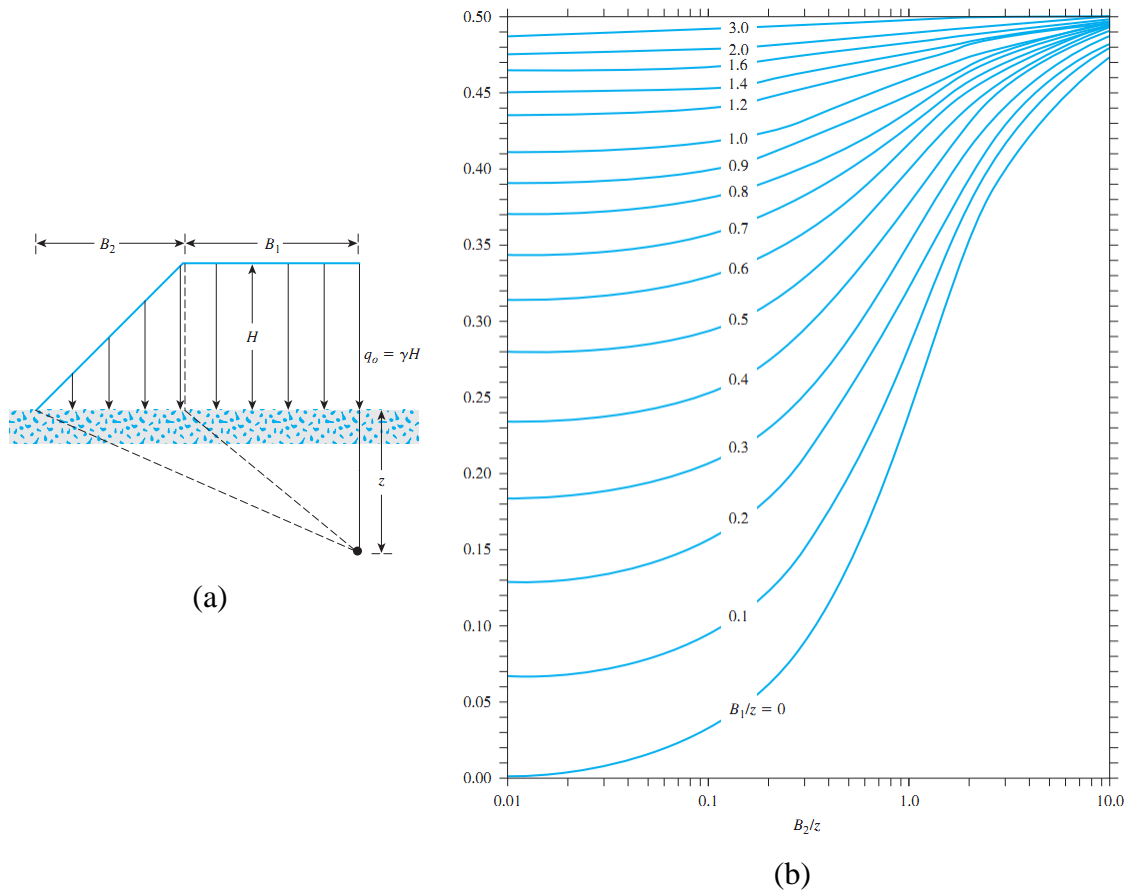
Fig. 2.7 Osterberg's chart for determing increase of vertical stress due to an embankment load (after Das and Sobhan 2010)

17

To calculate the settlement of soft deposit, the increase of vertical stress in the soil mass due to an embankment load is required. Based on Boussinesq (1985)'s solution of the vertical stress caused by a point load acting perpendicular to the ground surface, Osterberg (1957) developed an chart (Fig. 2.7) for calculating increment of vertical stress ($\Delta\sigma_z$) under a plane strain embankment load, as:

$$\Delta\sigma_z = p_{em}I \qquad (2.28)$$

where $p_{em} = \gamma_{em}H$; γ_{em} = unit weight of embankment fill; H_{em} = embankment height; and I = a function of B_1/z and B_2/z . The meanings of B_1 and B_2 are illustrated in Fig. 2.7 (a), and the value of I is determined using Fig. 2.7 (b).

2.3.3 Summary and comments

The ground settlement induced by embankment load can be calculated using Terzaghi's one dimensional compression theory together with consideration of vertical stress spreading of embankment load by Osterberg (1957)'s chart.

2.4 Lateral Displacement of Natural Deposit

2.4.1 Deformation characteristics of the ground

Embankment load not only induces consolidation stress but also shear stress in the soft subsoil, which results in vertical settlement and outward lateral displacement of the ground (Fig. 2.8). The lateral displacement is mainly caused by the embankment load induced shear stress.

2.4.2 Prediction of lateral displacement

Poulus (1972) conducted finite element analysis (FEA) of several embankments constructed on natural deposit, in which he stated that even though the agreement between measured and predicted settlements was quite good, the discrepancy between the measured and predicted values of lateral displacement was still large. According to Poulus's viewpoint, the reasons for the poor predictions of lateral displacement are:
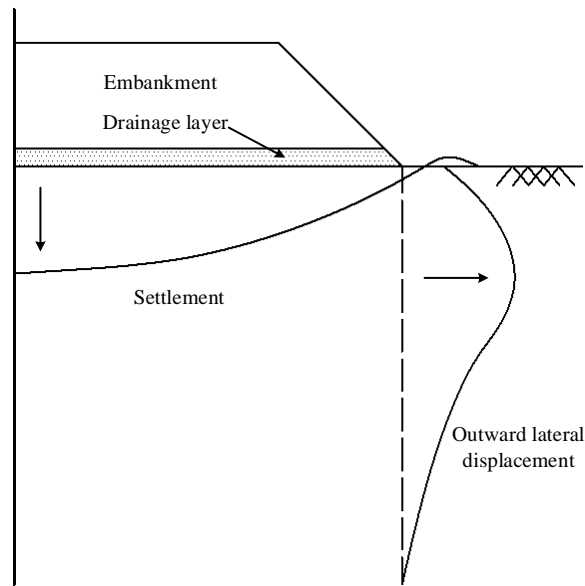
Fig. 2.8 Ground deformation of natural deposit due to embankment load

(1) The difficulty of estimating Poisson's ratio of the soil;

(2) Anisotropy of the soil;

(3) Nonlinear stress-strain behavior of soil;

(4) Nonhomogeneity of soil;

(5) Neglect of certain factors in specific cases such as the effect of embankment stiffness, or more generally, incorrect assumptions made regarding the stresses applied to the ground by an embankment.

Due to these difficulties, there were other researchers tried to develop empirical methods to predict the maximum lateral displacement under embankment load.

Tavenas *et al*. (1979) stated that taking the whole construction stage of an embankment as an entirely undrained loading process to predict ground lateral displacement might be questionable. They pointed out that sufficient drainage occurs in the initial construction stage of an embankment on overconsolidated clayey deposit, and the Poisson's ratio (v) of the subsoil during this stage should be much less than 0.5, therefore less lateral displacement would be induced. When the subsoil layers become normally consolidated, the ground roughly corresponds to an undrained loading stage with $v \approx 0.5$, and much more lateral displacement would be developed.

Tavenas and Leroueil (1980) made a statistic analysis of the lateral displacements observed in 21 embankments on soft clayey deposits. Their results are shown in Fig. 2.9.

During embankment construction, when the subsoil layers are overconsolidated, the maximum lateral displacement is predicted as:

19

$$\Delta\delta_\mathrm{m} = \left(0.18 \pm 0.09\right)\Delta S_\mathrm{f} \tag{2.29}$$

where $\Delta\delta_\mathrm{m}$ = increment of maximum lateral displacement under the toe of embankment; and ΔS_f = increment of ground surface settlement on the embankment centerline.
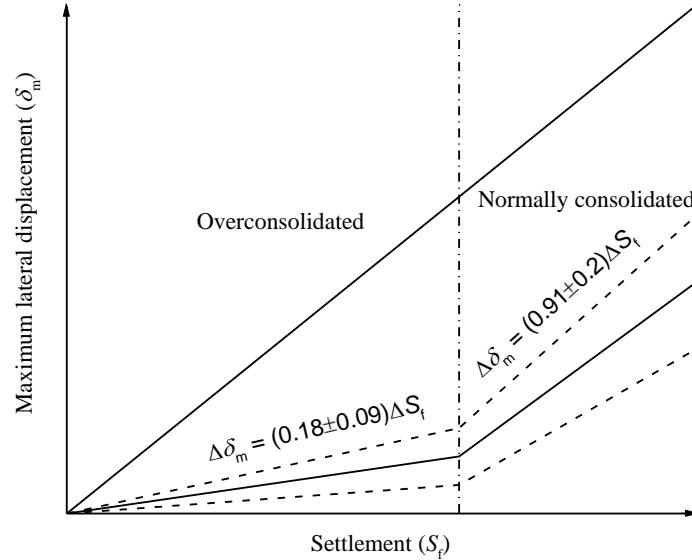
Fig. 2.9 Average correlation between δ_m and S_f during embankment construction (after Tavenas and Leroueil 1980)

When the subsoil layers are normally consolidated, the value of $\Delta\delta_\mathrm{m}$ is predicted as

$$\Delta\delta_\mathrm{m} = \left(0.91 \pm 0.2\right)\Delta S_\mathrm{f} \tag{2.30}$$

After embankment construction, the long-term lateral displacement during consolidation stage is predicted as:

$$\Delta\delta_\mathrm{m} = \left(0.16 \pm 0.02\right)\Delta S_\mathrm{f} \tag{2.31}$$

Suzuki (1988) analyzed the measured data of lateral displacements of 11 field cases, and found out that the maximum lateral displacement (δ_m) under the toe of an embankment has a good relationship with the settlement and the total embankment load, and the depth of δ_m is related to the width of embankment. Similar prediction equations as Tavenas and Leroueil (1980) were also proposed by Akai *et al.* (1974), Suzuki (1988) and Ma (1995). Loganathan *et al.* (1993) proposed a methodology to analyze the deformation of a deposit under embankment load, and stated that the maximum lateral deformation beneath the toe of the embankment is approximately 0.28 times the ground surface settlement observed at the centerline of the embankment at the end of the embankment construction.

Besides the above empirical prediction methods, there have been some studies about the characteristics of lateral displacement of a deposit under embankment load. Tominaga *et al*. (1973; 1974) stated that the influencing distance of lateral displacement from the toe of embankment nearly equals to the embankment width. Mochizuki *et al*. (1980) pointed out that most of the lateral displacement is developed during the construction process of an embankment. Marche and Chapuis (1974), Tavenas *et al*. (1979) and Yamaguchi *et al*. (1981) mentioned that lateral displacement can be taken as a good indicator of the stability of embankment system, i.e. lateral displacement increase rapidly when the factor of safety of the system is less than 1.3 (Tavenas *et al*. 1979) or 1.5 (Yamaguchi *et al*. 1981). Shibata *et al*. (1982) stated that the maximum lateral displacement occurs at a depth of 1/3 of the total thickness of soft subsoil layers.

2.4.3 Summary and comments

It is difficult to predict the lateral displacement of natural deposit under embankment loading. To date, the available methods are simply empirical statistics of the measured data from filed case histories and the maximum lateral displacement is predicted as a percentage of ground surface settlement.

2.5 Lateral Displacement of PVD-Improved Deposit

2.5.1 Vacuum preloading

(1) Deformation characteristics of the ground

The vacuum preloading method for PVD-improved deposit was first introduced in Sweden by Kjellman (1952). Since then, it has been used in many engineering practices (e.g. Bergado *et al*. 1998; Chu *et al*. 2000; Tang and Shang 2000; Tran and Mitachi 2008). The improvement mechanism of a vacuum pressure is different from a surcharge load. Vacuum pressure is an isotropic consolidation stress and generates negative pore water pressures inside the subsoil layers, and the effective stress of the soil increases while the total stress remains unchanged. Therefore, a vacuum pressure tends to results in vertical settlement and inward lateral displacement of the ground (Fig. 2.10) and can cause cracks

21

around the perimeter of the vacuum treated area (Shang *et al.* 1998; Chu *et al.* 2000; Chai *et al.* 2005). The inward lateral displacement has a maximum value at the ground surface and gradually reduces with increase of depth.
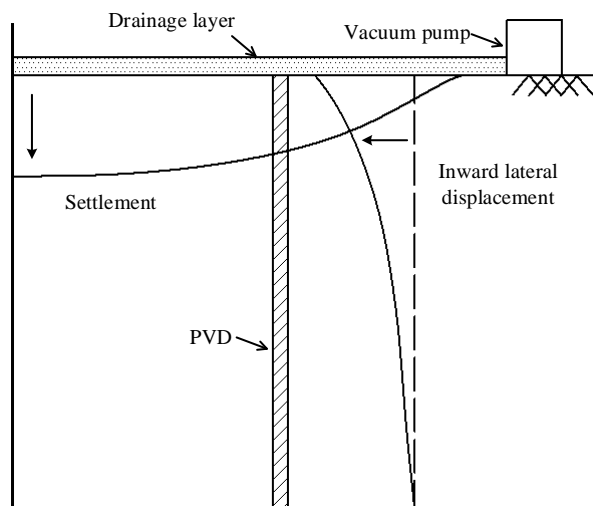
Fig. 2.10 Ground deformation due to vacuum preloading

(2) Prediction of lateral displacement

Based on a series of laboratory oedometer tests with one way drainage condition using vacuum pressure for samples with different initial vertical effective stress, Chai *et al.* (2005) stated that inward lateral displacement occurs when the vacuum pressure is larger than the stress required to maintain a K_0 condition. The condition for inward lateral displacement to occur is expressed as:

$$\Delta\sigma_{\text{vac}} > \frac{K_0 \cdot \sigma'_{v0}}{1-k_0} \tag{2.32}$$

where $\Delta\sigma_{\text{vac}}$ = increment of vacuum pressure; K_0 = at-rest earth pressure coefficient; and σ'_{v0} = initial vertical effective stress.

In field conditions, the vacuum pressure induced inward lateral displacement may cause tension cracks with a depth of z_c (Fig. 2.11). According to Rankine earth pressure theory, by assuming the groundwater level is z_w below the ground surface, the depth of cracking z_c can be expressed as:

$$z_c = \frac{2c'}{\gamma_t\sqrt{K_a}}, \text{ for } z_c < z_w \tag{2.33}$$

22

$$z_c = \frac{1}{(\gamma_t - \gamma_w)} \left(\frac{2c'}{\sqrt{K_a}} - \gamma_w z_w \right), \text{ for } z_c > z_w \qquad (2.34)$$

$$K_a = \tan^2 \left(45 - \frac{\phi'}{2} \right) \qquad (2.35)$$

where γ_t = total unit weight of soil; γ_w = unit weight of water; c' and ϕ' = effective cohesion stress and friction angle of the soil, respectively; and K_a = Rankine active earth pressure coefficient.
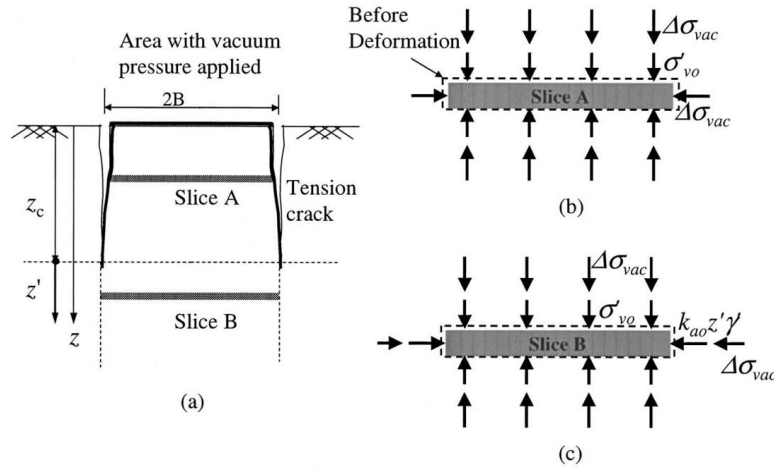
Fig. 2.11 Stress state and deformation pattern of soil slices in the ground under vacuum consolidation; (a) location of soil slices; (b) above the depth of tension crack; (c) below the depth of tension crack (after Chai *et al*. 2005)

Below depth z_c, there is a location at depth $z_L = z_c + z'$ (Fig. 2.10) where no lateral displacement occurs. z' is determined by the following equation:

$$\Delta \sigma_{vac} = \frac{K_0 \cdot \sigma'_v - K_a z' \gamma'}{1 - K_0} \qquad (2.36)$$

where γ' = effective unit weight of soil, equal to γ_t above the ground water level and $(\gamma_t - \gamma_w)$ below the groundwater level.

Chai *et al*. (2005) assumed that the volumetric strain (ε_{vol}) under vacuum consolidation is the same as that under 1D compression (Eq. (2.37)) and the vertical strain (ε_{vv}) under vacuum consolidation is a portion of the vertical strain under 1D compression (Eq. (2.38)).

$$\varepsilon_{vol} = \frac{\lambda}{1 + e_0} \ln \left(1 + \frac{\Delta \sigma_{vac}}{\sigma'_{v0}} \right) \qquad (2.37)$$

$$\varepsilon_{vv} = \alpha \frac{\lambda}{1+e_0} \ln\left(1 + \frac{\Delta\sigma_{vac}}{\sigma'_{v0}}\right) \tag{2.38}$$

where e_0 = initial void ratio, λ = the slope of virgin compression line in e-$\ln(p')$ plot, p' = effective mean stress and α = a multiplying factor with a minimum value less than 1 at the ground surface and gradually increases to 1 when $z > z_L$. Assuming a linear variation of α with depth, the expression for α is derived as:

$$\alpha = \alpha_{min} + \frac{1-\alpha_{min}}{\Delta\sigma_{vac}}\left(\frac{K_0 \cdot \sigma'_{v0} - K_a z'\gamma'}{1-K_0}\right), \text{ for } \Delta\sigma_{vac} \geq \frac{K_0 \cdot \sigma'_{v0} - K_a z'\gamma'}{1-K_0} \tag{2.39}$$

where α_{min} = 0.8 for triaxial stress conditions and 0.85 for plane strain conditions.

With known values of volumetric and vertical strains, the average inward lateral strain (ε_h) can be expressed as:

$$\varepsilon_h = \frac{1}{2}\left(\varepsilon_{vol} - \varepsilon_{vv}\right), \text{ for triaxial stress conditions} \tag{2.40}$$

$$\varepsilon_h = \left(\varepsilon_{vol} - \varepsilon_{vv}\right), \text{ for plane strain conditions} \tag{2.41}$$

Then, the lateral displacement (δ) is evaluated as:

$$\delta = B \cdot \varepsilon_h \tag{2.42}$$

where B = half width of the vacuum preloading treated aera.

(3) Summary and comments

Vacuum preloading with PVD-improvement has been extensively used in engineering practice after 1980s. The isotropic vacuum pressure results in inward lateral displacement of a deposit, and may cause tension crack around the periphery of the improved area. Chai *et al*. (2005) proposed a method to predict the lateral displacement of PVD-improved ground under vacuum preloading, in which the depth of cracking, the influencing depth of lateral displacement as well as the magnitudes of lateral displacement can be predicted.

2.5.2 Combined embankment load and vacuum pressure

(1) Deformation characteristics of the ground

The combination of embankment load and vacuum pressure has been used more and more to enhance the efficiency of preloading. Usually, an embankment load results in

outward lateral displacement, whereas a vacuum pressure generally induces inward lateral displacement. Therefore, ideally combination of both the loads can reduce the overall lateral displacement of the ground, and there may be three patterns of lateral displacement profile, i.e. overall outward lateral displacement (①), overall inward lateral displacement (②), and inward lateral displacement adjacent to the ground surface and outward lateral displacement below a certain depth (③), as shown in Fig. 2.12.
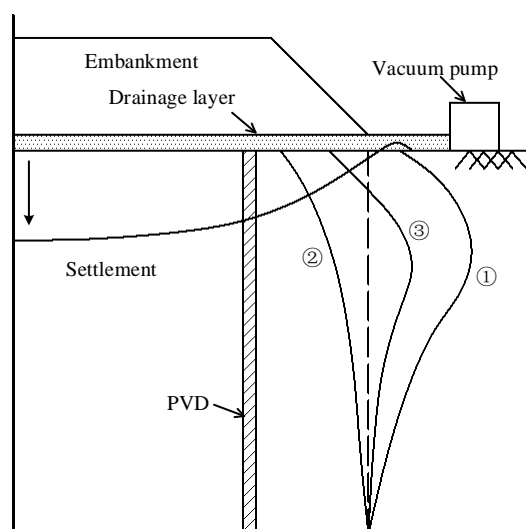
Fig. 2.12 Ground deformation due to combined embankment load and vacuum pressure

(2) Prediction of lateral displacement

Ong and Chai (2011) and Chai *et al*. (2013) reported that the main factors affecting lateral displacement of a PVD-improved deposit under the combination of embankment load and vacuum pressure are the magnitudes of embankment load and vacuum pressure, loading rate of embankment load, and strength, consolidation and compression properties of the soft subsoil.

The possible three patterns of lateral displacement increases the difficulties of predicting the maximum lateral displacement. A displacement ratio (*DR*) of average lateral displacement (δ_{av}) to ground surface settlement at the embankment centerline (S_f) was proposed to make a preliminary prediction by Ong and Chai (2011). The expression of *DR* is as follows:

$$DR = \frac{\delta_{av}}{S_f} \tag{2.43}$$

$$\delta_{\mathrm{av}} = \frac{A_1 + A_2}{H_{\mathrm{L}}} \qquad (2.44)$$

The meanings of A_1, A_2 and H_{L} are shown in Fig. 2.13. A_1 and A_2 are defined as the area enclosed by the horizontal and vertical axes through the toe of embankment and the lateral displacement profile under the toe. A_1 represents the inward lateral displacement and negative value should be adopted. A_2 represents outward lateral displacement and positive value should be adopted. H_{L} is the ground thickness of PVD improved zone.
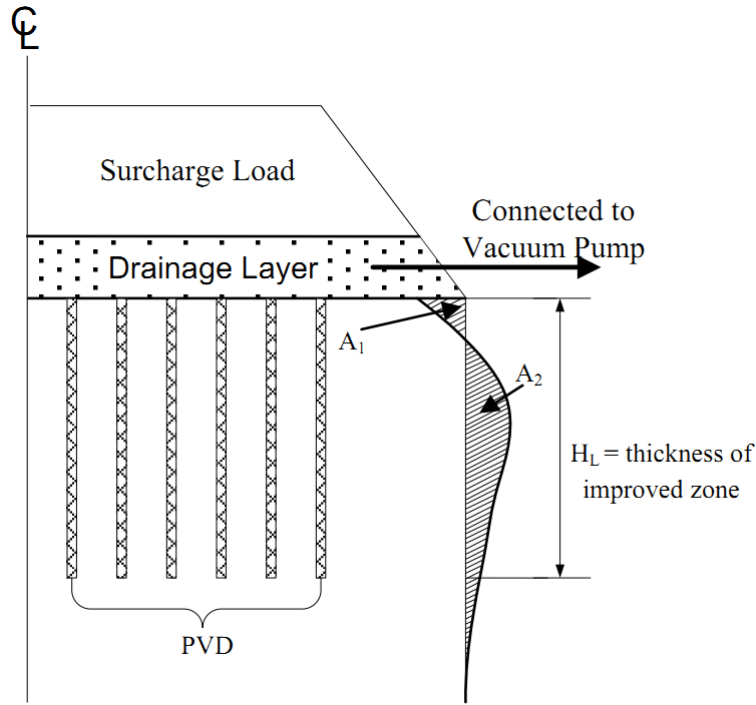
Fig. 2.13 Definition of A_1, A_2 and H_{L} (after Ong and Chai 2011)

Ong (2011) proposed a new parameter, a ratio of load to undrained shear strength (*RLS*), to make a correlation with *DR*. The definition of *RLS* is as follows:

$$RLS = \frac{p_{\mathrm{n}}}{s_{\mathrm{u}}} \qquad (2.45)$$

$$p_{\mathrm{n}} = p_{\mathrm{em}} - \left(\left| p_{\mathrm{vac}} \right| + p_{\mathrm{em}} \right) U \qquad (2.46)$$

where s_{u} = representative undrained shear strength of the subsoil; p_{n} = an index pressure; p_{em} = maximum value of embankment load; p_{vac} = vacuum pressure applied; and U = average degree of consolidation of the PVD-improved zone at the end of embankment construction.

Based on the results of model tests and numerical simulations, Ong (2011) proposed a relationship between *DR* and *RLS* to predict the average lateral displacement as depicted in Fig. 2.14, in which *DR* is expressed as:

$$DR = 0.09RLS + 0.12 \tag{2.47}$$
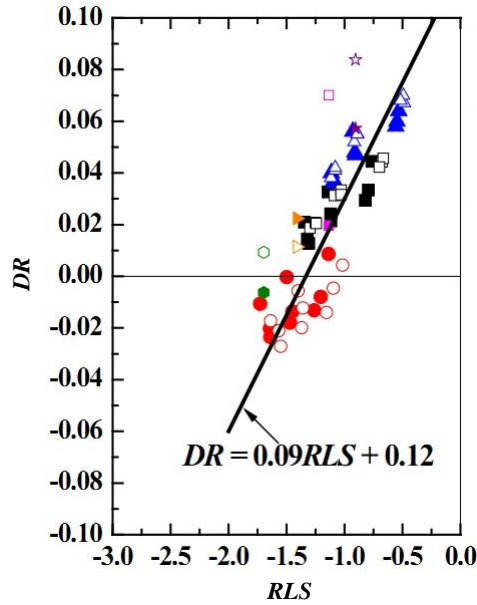
Fig. 2.14 Relationship between *DR* and *RLS* (after Ong 2011)

In engineering practice, the maximum lateral displacement is more important than the average lateral displacement. Chai *et al*. (2013) modified Ong (2011)'s method to predict the maximum net lateral displacement (δ_{nm}). The definition of δ_{nm} is as:

$$\delta_{nm} = \delta_{mo} - |\delta_{mi}| \tag{2.48}$$

where δ_{mo} = maximum outward lateral displacement, and δ_{mi} = maximum inward lateral displacement.

The ratio between δ_{nm} and S_f has been designated as normalised lateral displacement (*NLD*), and expressed as:

$$NLD = \frac{\delta_{nm}}{S_f} \tag{2.49}$$

Based on the results analyzed from 18 field case histories, Chai *et al*. (2013) proposed a linear range for predicting the maximum net lateral displacement (Fig. 2.15). The *NLD-RLS* relationship is as:

$$NLD = 0.168RLS + 0.05 \pm 0.05 \tag{2.50}$$

27
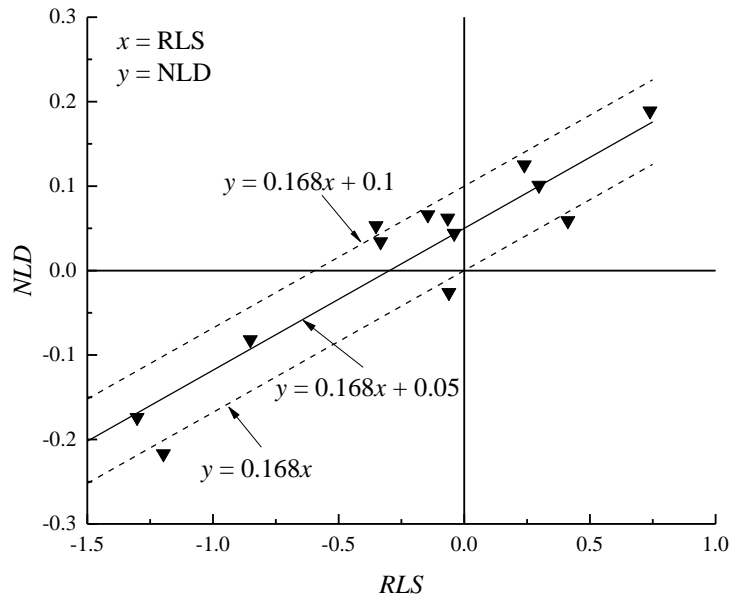
Fig. 2.15 Relationship between *NLD* and *RLS* (after Chai *et al*. 2013)

It should be noted that in the calculations of the values of p_n, U and s_u using both Ong (2011)'s and Chai *et al*. (2013)'s methods, the effects of the main factors affecting lateral displacement are involved.

(3) Summary and Comments

Preloading with installation of PVD under combined embankment load and vacuum pressure is an efficient way to improve soft deposit. The ground lateral displacement profile under this kind of loading manner may have 3 patterns, i.e. overall outward lateral displacement, overall inward lateral displacement, and inward lateral displacement near the ground surface and outward lateral displacement below a certain depth. Chai *et al*. (2013) proposed an empirical method to predict the maximum net lateral displacement. This empirical method considers the effects of the main influencing factors on lateral displacement.

2.6 Summary and Remarks

In some regions, especially in urban areas, the maximum lateral displacement at the property boundary of a highway or railway embankment is sometimes required to be a

small value, such as to be less than ±50 mm in Saga, Japan (Chai and Carter 2011). Therefore, predicting the maximum lateral displacement under an embankment loading is an essential design requirement.

To date, there is not a study specifically aiming at predicting lateral displacement of PVD-improved deposit under embankment load.

The PVDs installed in the soft deposit accelerates the consolidation process and increases the rate of strength gain of the soft subsoil. Therefore, less lateral displacement will be induced comparing with the case of embankment constructed on natural soft ground (Fig. 2.16).
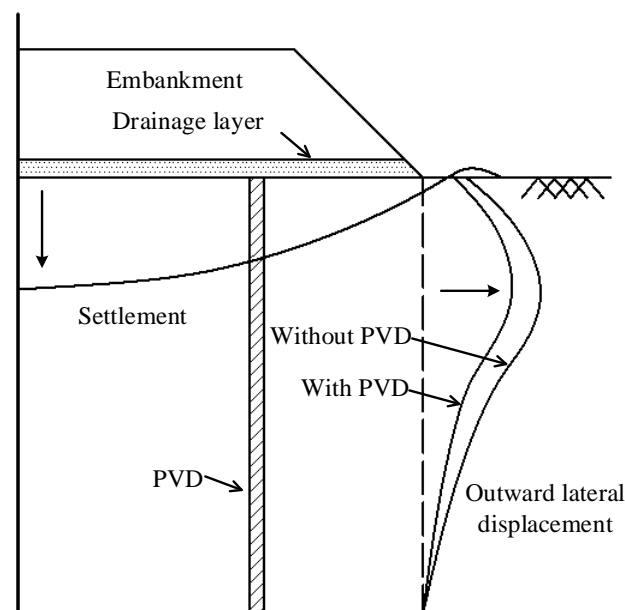
Fig. 2.16 Ground deformation of PVD-improved deposit due to embankment load

In this study, the behavior of lateral displacement of PVD improved deposit under embankment load has been investigated by a series of large-scale laboratory model tests and a number of field case histories. Based on the test and analysis results, an empirical method has been proposed to predict the lateral displacement.

CHAPTER THREE
INVESTIGATION BY LABORATORY MODEL TESTS

3.1 Introduction

For a specific embankment, the ground deformation, especially lateral displacement, is not only influenced by the magnitude of the embankment load but also the loading rate. A series of large-scale laboratory model tests were conducted focusing on the effect of loading rate on ground deformation. The test device and materials, test procedures, case tested and test results are described in this chapter.

3.2 Test Device and Materials

The test devices used are illustrated in Figs. 3.1(a) and (b). It mainly consists of a metal box with inner dimensions of 1.50 m in length, 0.62 m in width and 0.85 m in height. The front and back walls of the box are made of transparent acrylic glass, which facilitated the direct observation of lateral displacement from outside. The model ground was divided into two parts by a 15 mm thick acrylic glass plate fixed at the center of the model box along the longitudinal direction. The surcharge (embankment) load was applied by air pressure through three Bellofram cylinders (diameter: 100 mm; maximum elongation: 140 mm) together with three metal loading plates with dimensions of 0.29 m in length, 0.166 m in width and 0.02 m in thickness (Fig. 3.1(a)). The soil used was remolded Ariake clay with liquid limit, w_L = 114.0%, plastic limit, w_P = 60.6%. The Mini-PVDs used to accelerate the consolidation process of the model ground were made of nonwoven geotextiles with a cross-section of 0.03 m $\times$ 0.01 m (Fig. 3.2). And two piezometers (P_1 and P_2) were installed in the model ground to monitor the variations of the excess pore water pressure inside the model ground and their depths are indicated in Fig. 1(a). The

settlements and pore water pressures were recorded using a computer linked to a data logger. Fig. 3.3 presents the photograph of the model test.

(a)

(b)
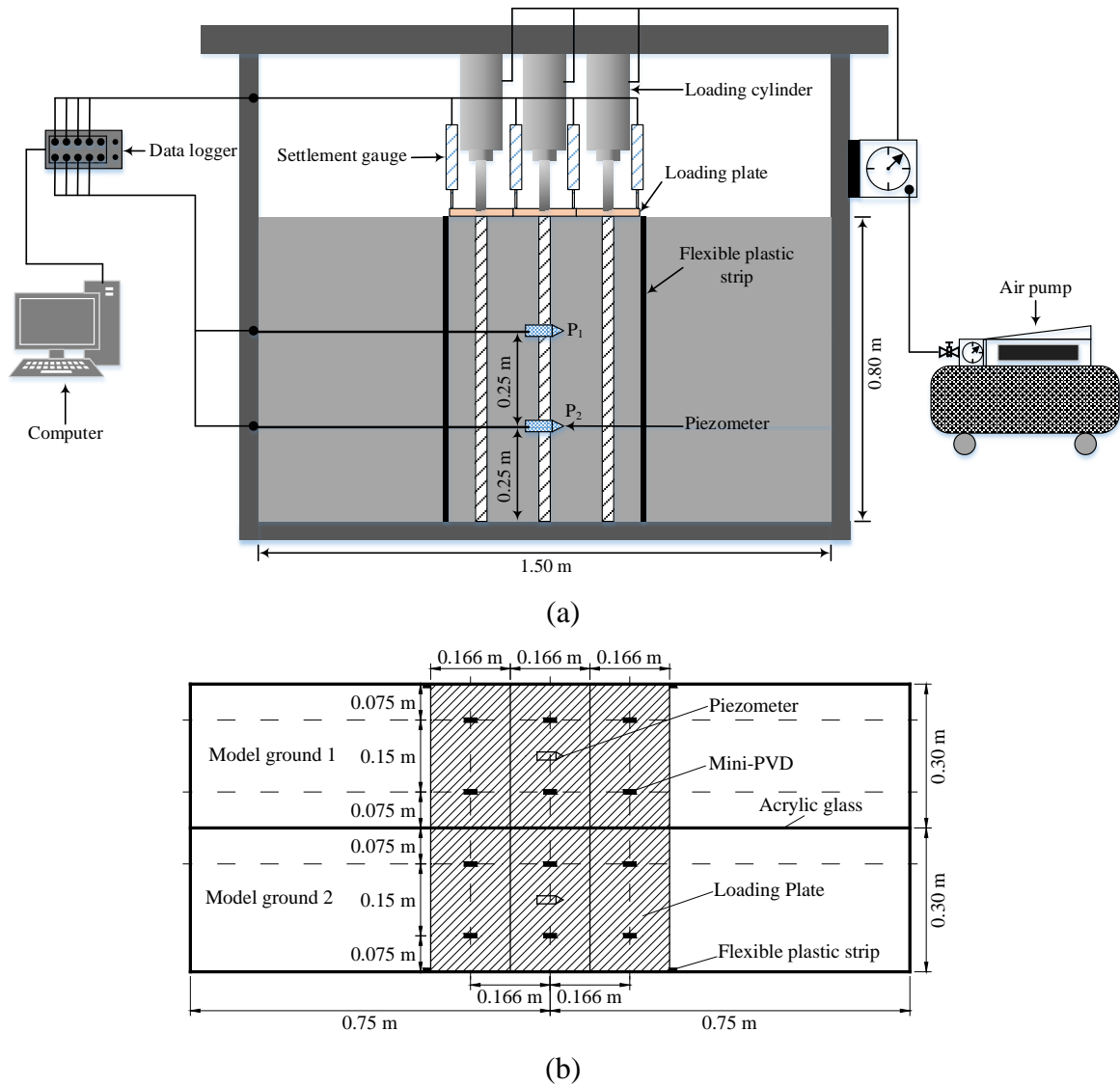
Fig. 3.1 Illustration of laboratory model test: (a) cross section; (b) plan view

Fig. 3.2 Picture of mini-PVD
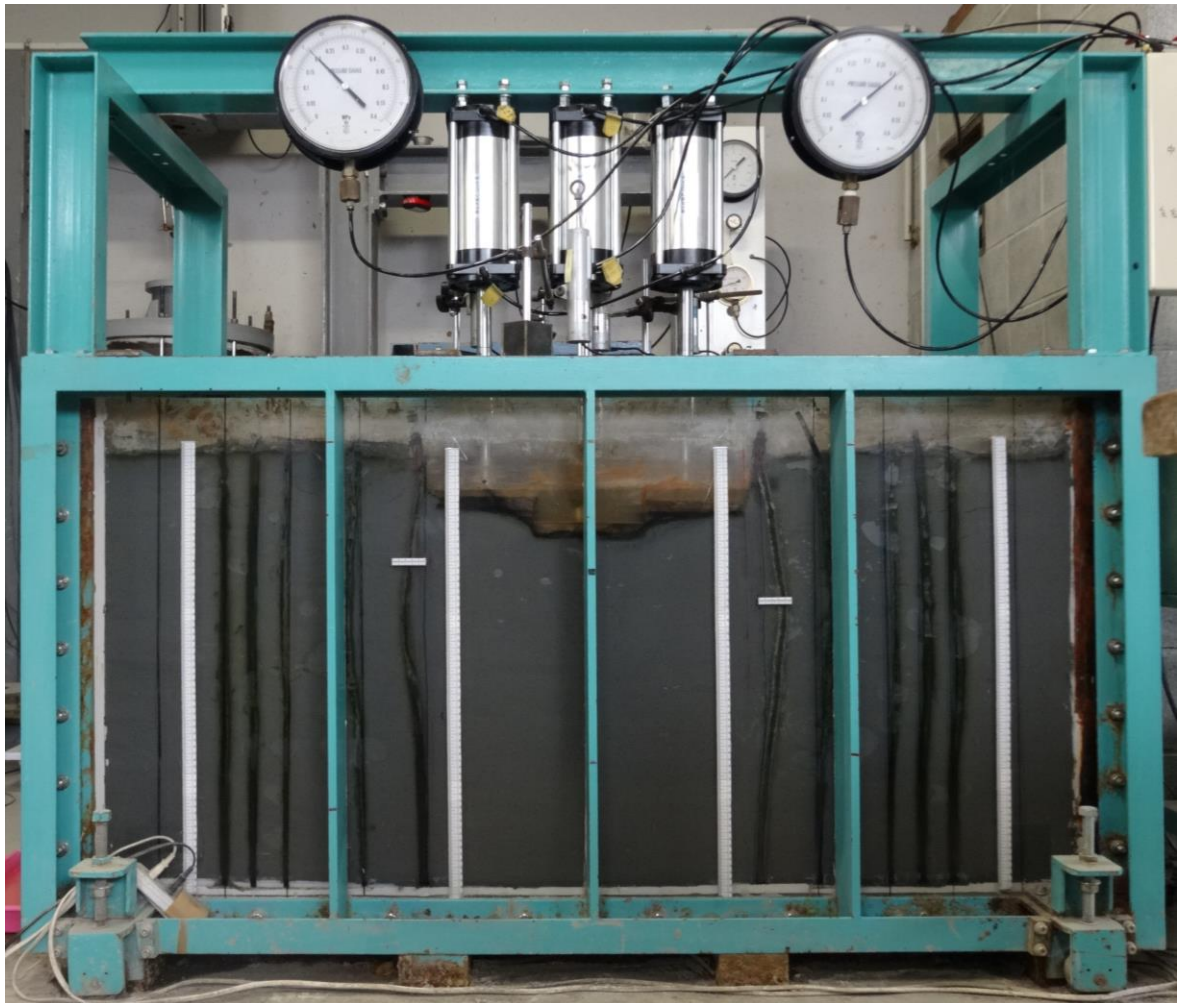
Fig. 3.3 Photograph of laboratory mode test

3.3 Test Procedures

3.3.1 Preparation of model ground

Three layers of nonwoven geotextiles (thickness: 3 mm; weight: 130 g/m^2) were first placed at the bottom of the model box functioned as a bottom drainage layer. Then four flexible plastic strips for measuring the lateral displacement were lined vertically on the inner face of the front and back transparent acrylic glass walls. Initially several pieces of adhesive tape were applied to keep the plastic strips attached on the acrylic glass walls. Then thoroughly remoulded Ariake clay slurry with water content of about 125%-145% (about 1.1-1.3 w_L) was filled in the model box layer by layer to reach a total thickness of about 0.8 m. When the surface of the soil reached the level where the adhesive tape used to

fix the flexible plastic strips, the adhesive tapes were removed to allow the plastic strips to move with the soil. During the filling process, two piezometers were installed at 0.25 m and 0.50 m from the bottom of the model ground. Finally, another three layers of nonwoven geotextiles were placed at the top surface of the model ground to act as a surface drainage layer.

The soft model ground was first pre-consolidated under a uniform pressure of 10 kPa by dead load under two-way drainage conditions for a duration of more 60 days to reach a degree of consolidation of about 90%. After pre-consolidation the model ground was about 0.65 m thick. Then, the dead load was removed and two independent model grounds (length: 1.50 m; width: 0.30 m; thickness: 0.65 m) were formed. For each model ground two soil samples were taken from the soil near the ends of the model box in longitudinal direction to conduct conventional oedometer tests.

3.3.2 Installation of mini-PVDs

Six mini-PVDs were driven into the model ground by a steel rod and were arranged in a rectangular pattern of 0.166 m × 0.15 m as shown in Fig. 3.1(b). After the mini-PVDs fully penetrated the model ground the steel rod was withdrawn and the mini-PVDs were left in the model ground.
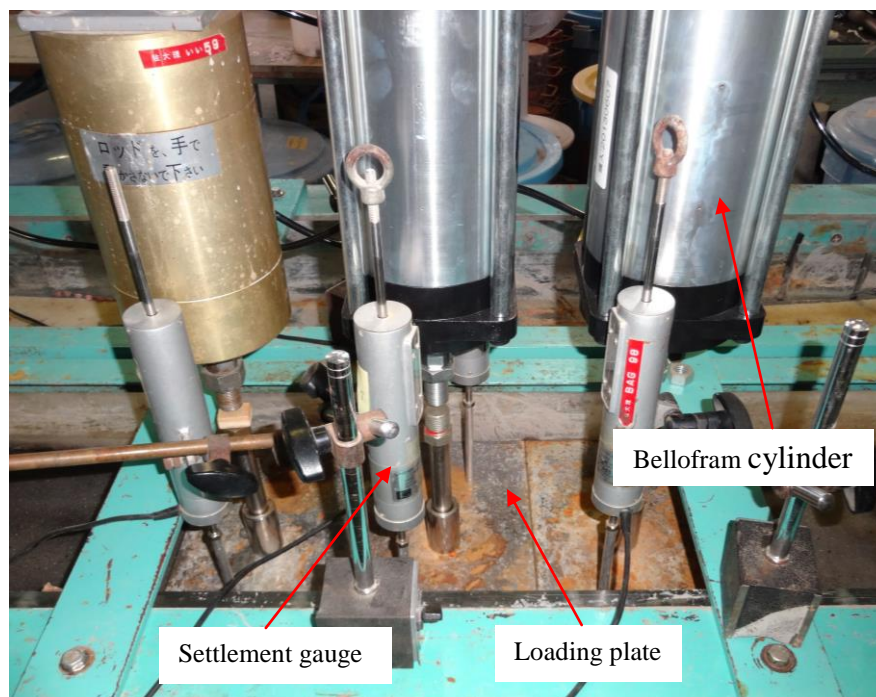
Fig. 3.4 Arrangement of loading plates and settlement gauges

3.3.3 Application of surcharge (embankment) load

Before applying the surcharge (embankment) load, four settlement gauges were settled on the loading plates. One on each loading plate at the two sides and two on the central loading plate (as shown in Fig. 3.4) to measure the ground surface settlement. To simulate the embankment load, the pressure applied on the loading plates at the two sides was half of the value applied on the central one. The load was applied in a stepwise manner, i.e. increment loads were instantly applied with pre-determined time interval.

3.3.4 Measuring undrained shear strength

After the test completed, soil samples at different depth were taken at the longitudinal centerline and the left and right ends of the model box alone the longitudinal direction, and their undrained shear strengths were measured by laboratory mini-vane shear tests.
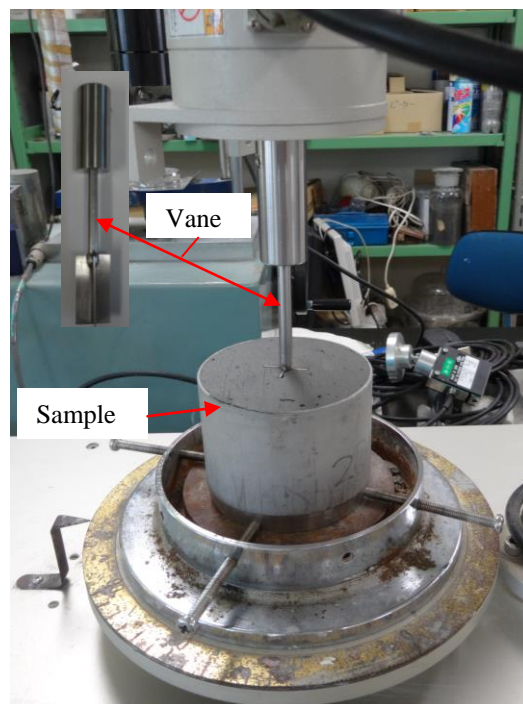
Fig. 3.5 Illustration of mini-vane shear test

The undrained shear strength of the soil samples taken at two sides of the model box (away from the loading area) can be considered as the initial strength of the model ground before application of surcharge load. The mini-vane used was 20 mm in diameter and 40 mm in height (Fig. 3.5), and the shearing speed was 6 degrees/min. During the test, the top

of the blade was not in the soil sample (Fig. 3.5), therefore only the resistance of the bottom and perimeter surfaces of the cylinder were mobilized. As a result, the undrained shear strength of the soil sample (s_u) is calculated as:

$$s_u = \frac{12T_{max}}{13\pi D^3}$$

(3.1)

where T_{max} = measured maximum torque, and D = diameter of the mini-vane.

3.4 Case Tested

The cases tested are summarized in Table 1. For all of the cases, the total applied surcharge load was the same of 60 kPa, while the loading rate was different. After the surcharge load reached the designed value of 60 kPa, it was maintained for a period of about two weeks before terminating the tests.

Table 3.1 Cases tested

Case	Surcharge load (kPa)	Loading rate (kPa/day)	w_n (%)
1	60	2	
2	60	4	145
3	60	5	
4	60	7	
5	60	6	125
6	60	8	

Note: w_n is the initial water content of the clay slurry used

3.5 Test Results

First, the initial undrained shear strength and settlements of the model ground as well as the measured excess pore water pressure variations are described. Then, the measured lateral displacements are presented and discussed.

3.5.1 Initial undrained shear strength of the model ground

The initial undrained shear strength profiles of the model grounds are presented in Fig. 3.6. For Cases 5 and 6, the model grounds yielded higher values of s_u comparing with Cases 1 to 4; the reason is that the clay slurry used to fill the model grounds of Cases 5 and 6 had a lower water content and therefore formed stiffer model grounds. For soft clayey

soil, the initial water content has an obvious influence on its consolidation behavior (Hong *et al.* 2013). For Cases 1 to 4, although the water contents of the clay slurry used were the same, the values of s_u of Cases 3 and 4 were smaller than that of Cases 1 and 2 and the reason is not clear. However, it indicated that the model grounds of Cases 3 and 4 were softer than that of Cases 1 and 2.
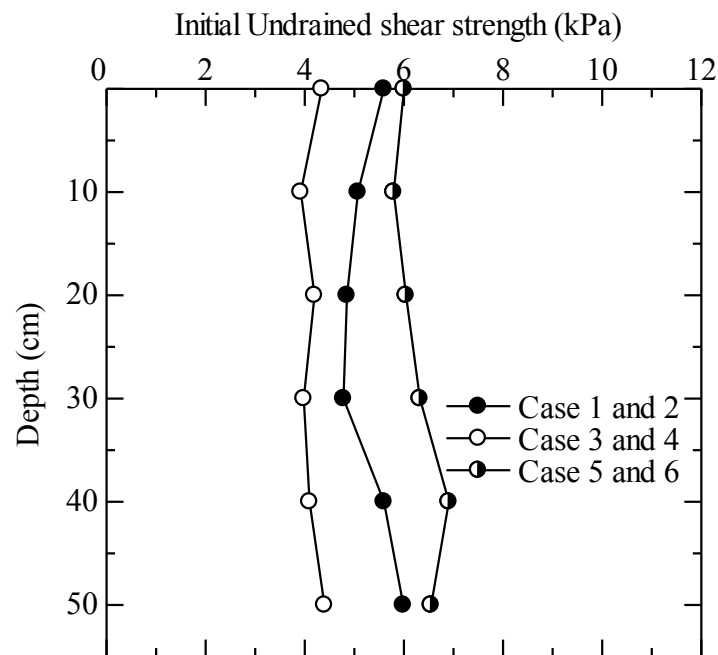
Fig. 3.6 Initial undrained shear strength of model ground

3.5.2 Settlement-time curves

The ground surface settlement curves measured at the central loading plate of Cases 1 and 2, Cases 3 and 4, Cases 5 and 6 are shown in Figs. 3.7-3.9, respectively. As expected, it clearly shows that for the similar model grounds the settlement rate increases with the increase of loading rate during the application of surcharge load.

For Case 1, at about 33 days (3 days after the end of surcharge loading) of total elapsed time, there was an increase of the settlement rate, it was because before that time, the piston of the central Bellofram cylinder reached its maximum elongation. The problem was solved by adding a metal block on the loading plate, which caused temporary unloading, and the settlement rate increased immediately after that. For Case 4, the same issue as Case 1 was occurred at about 6 days of total elapsed time.
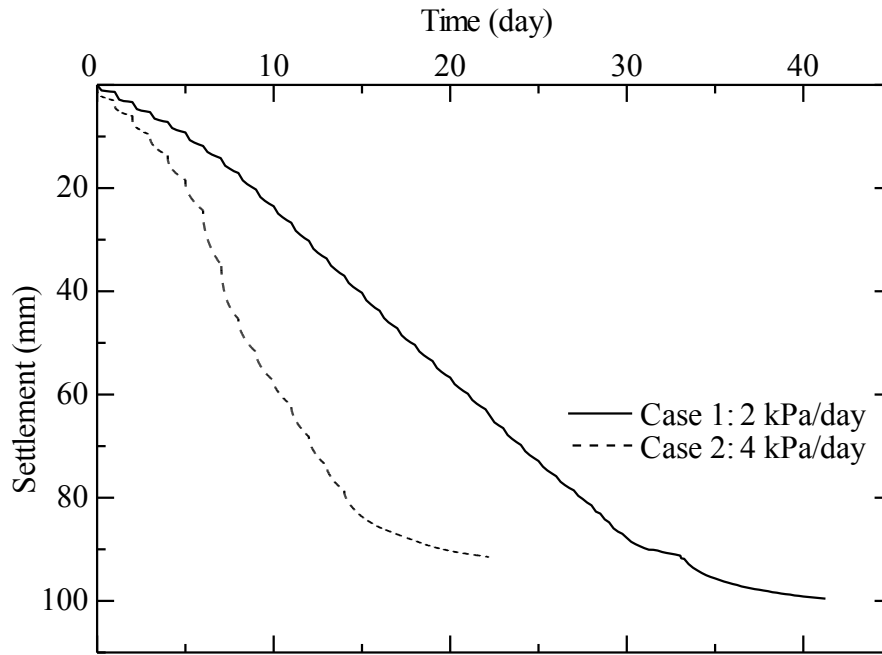
Fig. 3.7 Ground surface settlements of Cases 1 and 2
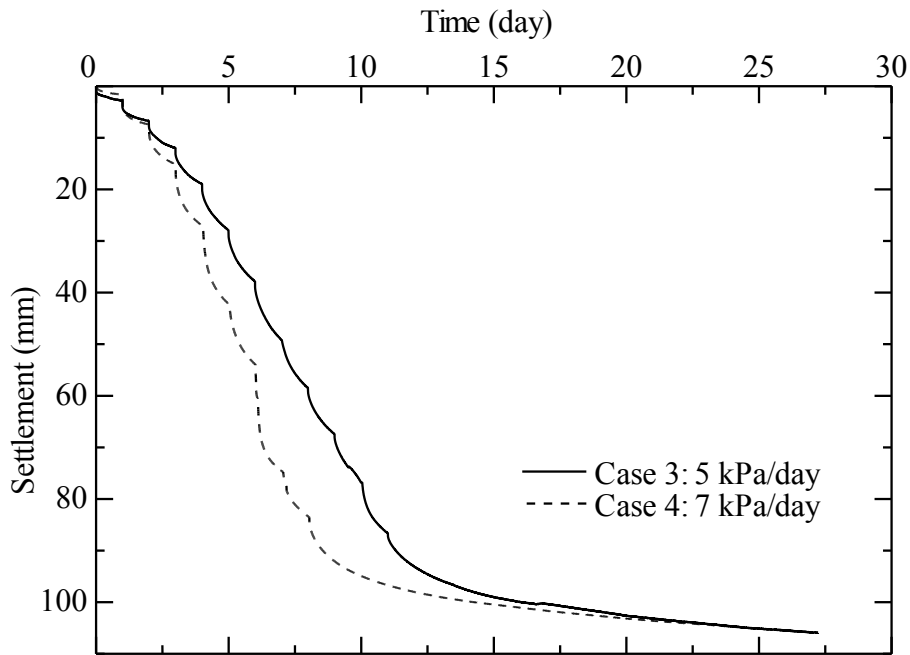
Fig. 3.8 Ground surface settlements of Cases 3 and 4

Comparing the undrained shear strength of the model grounds presented in Fig. 3.6, it is observed that the stronger the model ground was, the less ground settlement was induced. Case 6 had larger settlement than that of Case 5. This difference was due to the faster loading rate of Case 6 induced larger lateral displacement of the model ground and it will be presented later on. Generally, most of the lateral displacements are due to the undrained

shear deformation. Under undrained condition, there is almost no volume change of the saturated subsoil, which implies that the settlement volume is almost equal to the lateral displacement volume in this stage. Therefore, the larger lateral displacement results in more ground settlement.
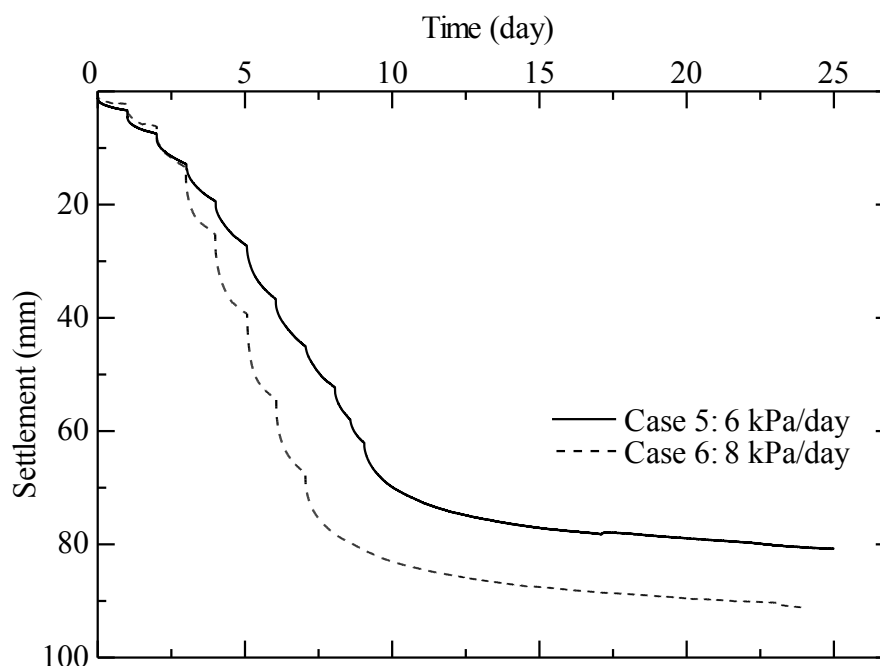
Fig. 3.9 Ground surface settlements of Cases 5 and 6

3.5.3 Variations of excess pore water pressure

Figs. 3.10-3.13 present the variations of excess pore water pressure for Cases 3-6, respectively. For Cases 3, 4 and 6, P_2 was malfunctioned, and the measurements were excluded. There is a clear trend of excess pore water pressure increased when applying load increment and dissipated during the consolidation period. At the initial stage of applying surcharge load (about 3 days of the total elapsed time) as well as the final stage, the measured excess pore water pressure was negative. There are two possible reasons. One is that the Mini-PVDs were dry before inserting them into the model grounds, and after inserted they would absorb water from the surrounding soil, therefore induced an initial suction pressure around the Mini-PVDs. The other one is that the bottom of the model ground was drained and the water pressure was zero which was less than the static water pressure, i.e. about 6 kPa suction pressure was applied at the bottom boundary.

The loading rate of Case 6 was larger than that of Cases 3-5, however the measured maximum excess pore water pressure was less than that of Cases 3-5. The exact reason is not clear, possibly the piezometers were installed closer to the inserted Mini-PVDs for Case 6.
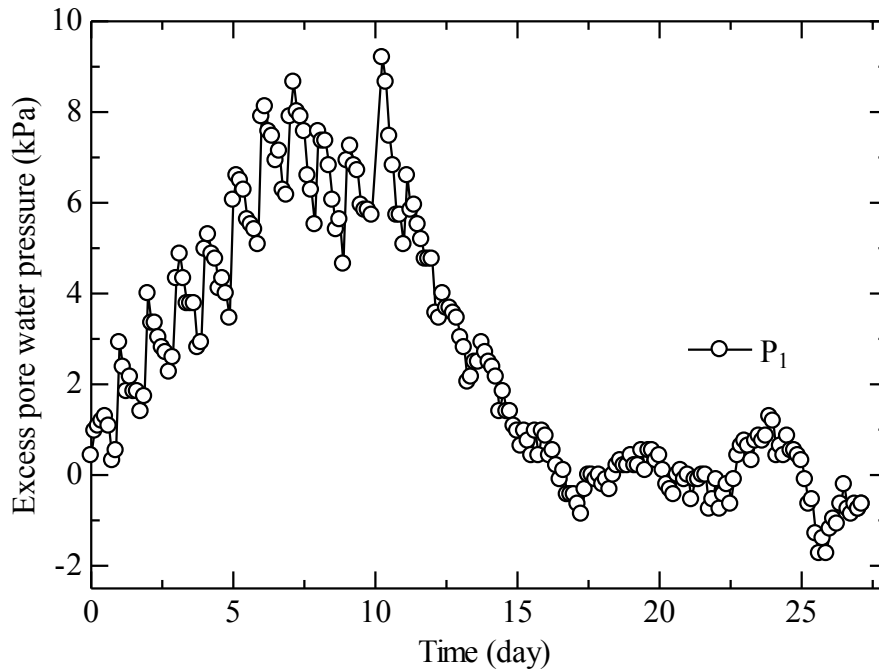
Fig. 3.10 Excess pore water pressure of Case 3 (5 kPa/day)
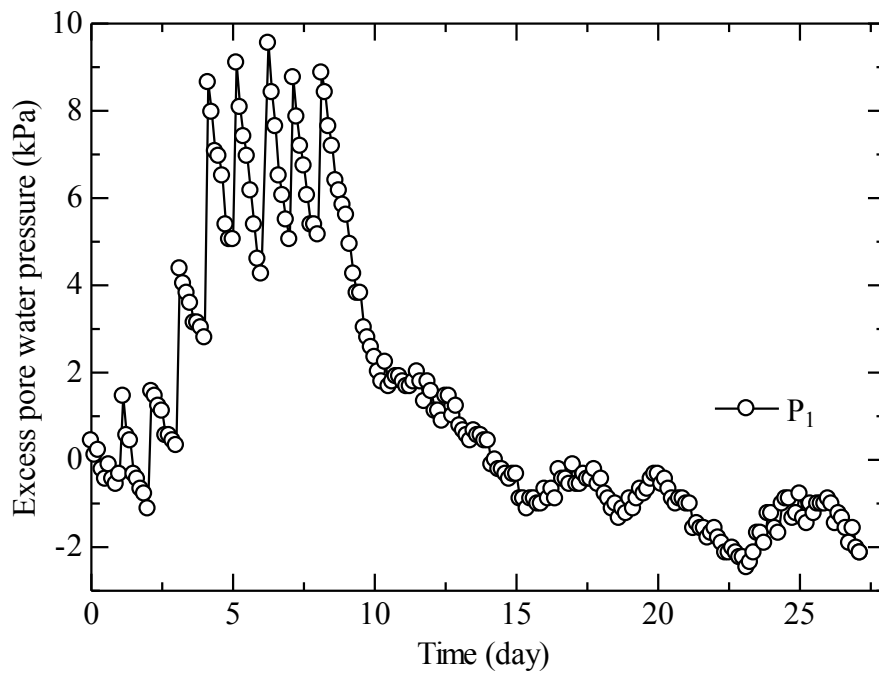
Fig. 3.11 Excess pore water pressure of Case 4 (7 kPa/day)
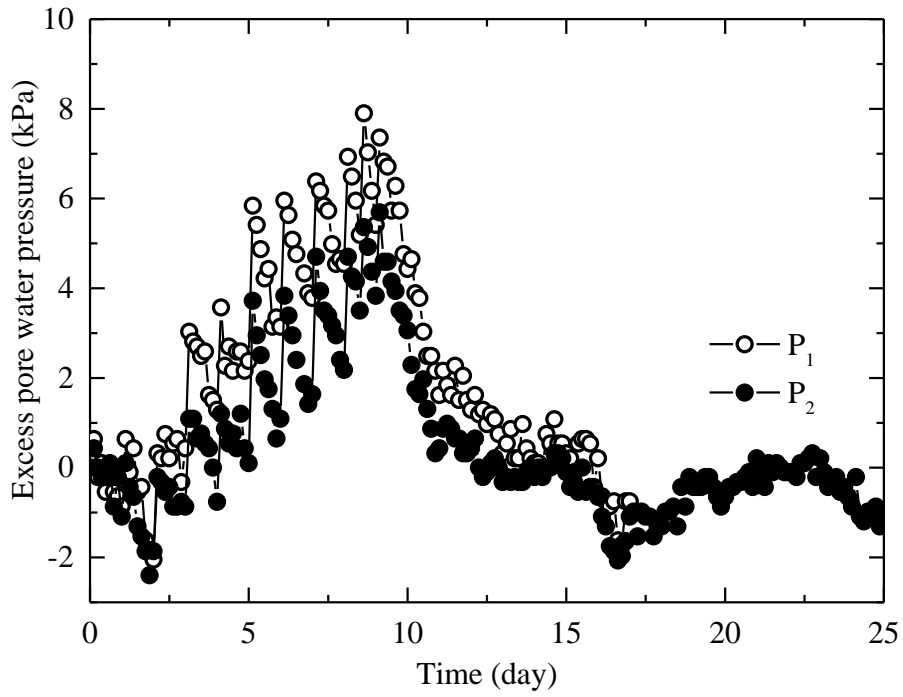
Fig. 3.12 Excess pore water pressure of Case 5 (6 kPa/day)
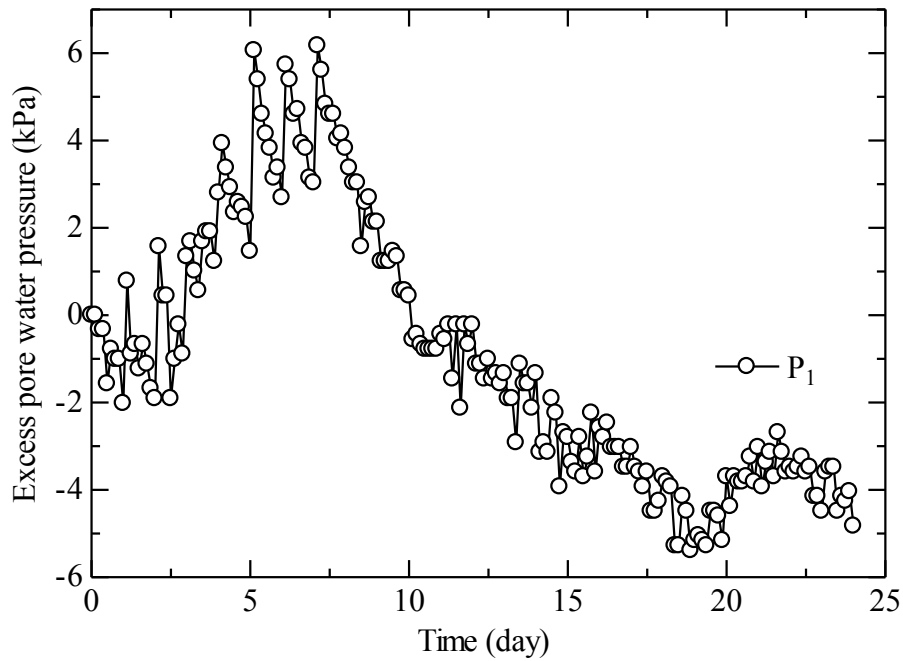
Fig. 3.13 Excess pore water pressure of Case 6 (8 kPa/day)

3.5.4 Lateral displacements

(1) Measured data

The final measured lateral displacements profiles under the edge of the surcharge loading area are plotted in Figs. 3.14-3.19 for Cases 1-6, respectively. For the same case, the measured lateral displacements at two sides of the surcharge loading area are not exactly identical. The similar phenomenon was reported for field cases, such as Cowland and Wong (1993) and Kelln *et al*. (2007).
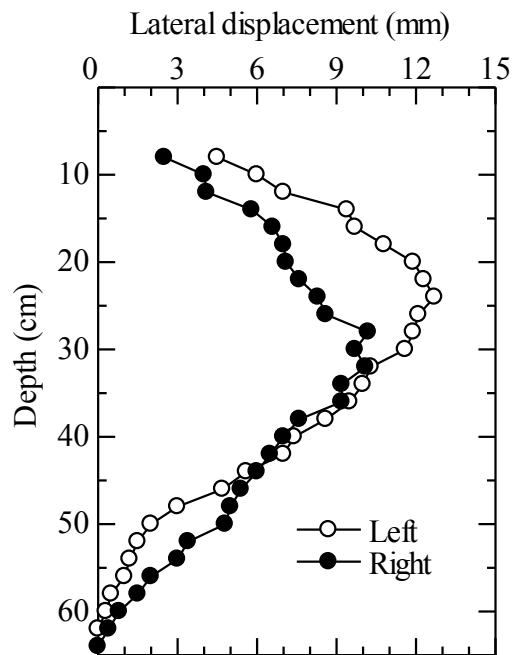
Fig. 3.14 Lateral displacement profile of Case 1 (2 kPa/day)
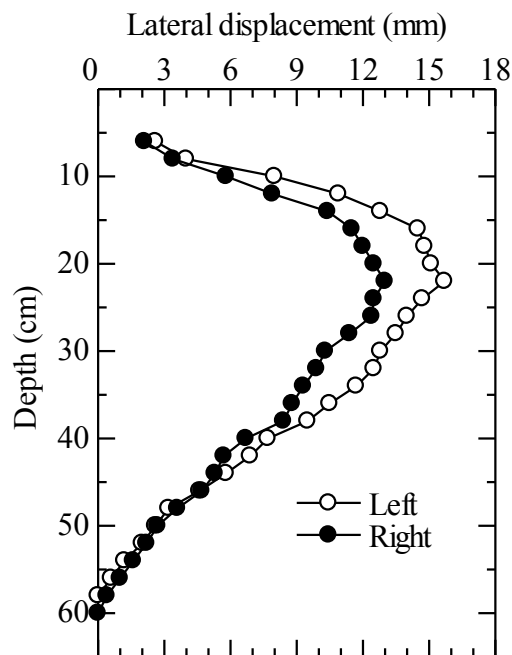
Fig. 3.15 Lateral displacement profile of Case 2 (4 kPa/day)
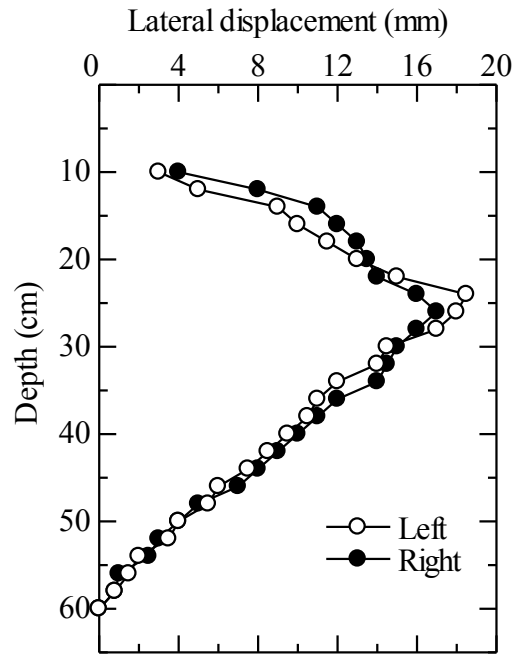
Fig. 3.16 Lateral displacement profile of Case 3 (5 kPa/day)
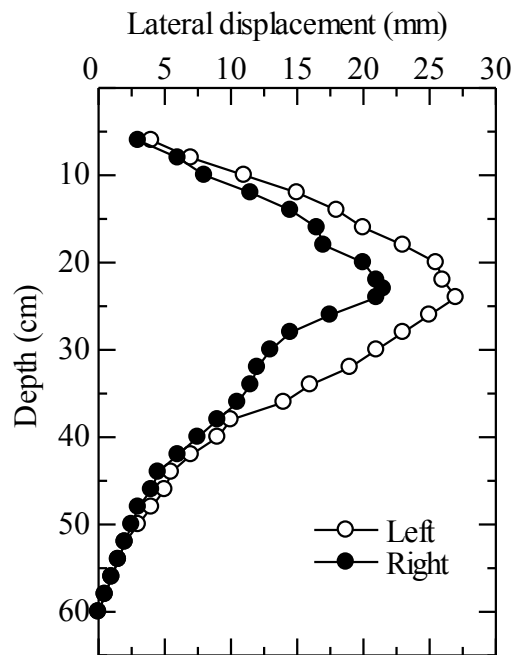
Fig. 3.17 Lateral displacement profile of Case 4 (7 kPa/day)

Model grounds of Cases 5 and 6 had lower initial water content, but due to the higher loading rate, the measured maximum lateral displacements were larger than that of Cases 1 and 2. Another interesting point is that comparing with Cases 1 and 2, the level where the maximum lateral displacement occurred was shallower for Cases 5 and 6. Although the exact reason is not clear, one possible reason is that with larger loading rate, the stiffer

surface layer due to the vertical drainage was thinner. For the consolidation due to vertical drainage, the soil just below the ground surface (drained boundary) consolidates much faster and gets stiffer than the soil locates at a certain depth below the ground surface. With increase of elapsed time, the effect of vertical consolidation will propagate into a deeper soil layer. For a faster load application, the thickness of the surface layer affected by the vertical drainage will be thinner.
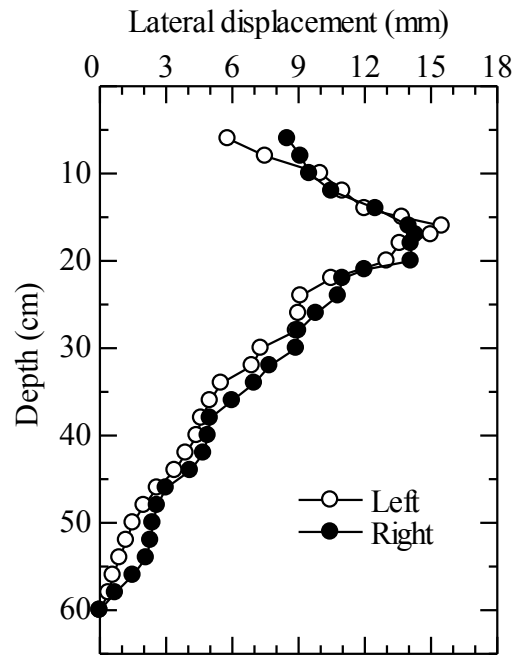
Fig. 3.18 Lateral displacement profile of Case 5 (6 kPa/day)
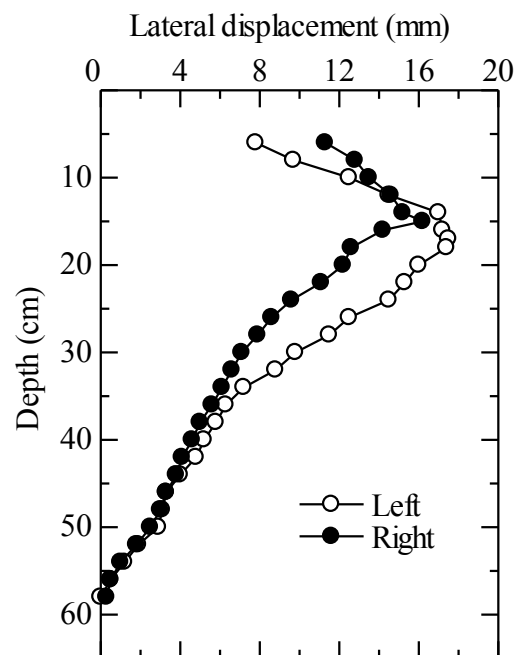
Fig. 3.19 Lateral displacement profile of Case 6 (8 kPa/day)

43

(2) Effect of loading rate and undrained shear strength of the ground on lateral displacement

The measured maximum ground lateral displacement and final ground surface settlement of the six (6) cases tested are summarized in Table 3.2.

Table 3.2 Measured lateral displacements and settlements

Case	LR (kPa/day)	S_f (mm)	δ_{mL} (mm)	δ_{mR} (mm)	NLD-L	NLD-R
1	2	99.5	12.7	10.2	0.128	0.103
2	4	91.5	15.7	13.0	0.172	0.142
3	5	105.9	18.5	17.0	0.175	0.161
4	7	106.0	27.0	21.5	0.255	0.203
5	6	80.8	15.5	14.3	0.192	0.177
6	8	90.3	17.5	16.2	0.194	0.179

Note: LR = loading rate; S_f = ground surface settlement at the centerline of the surcharge loading area; δ_{mL} and δ_{mR} = maximum lateral displacement measured at left and right side of the loading area, respectively; NLD-L and NLD-R = normalized lateral displacement at the left and right side sides of the loading area, respectively.

The relationship between the maximum lateral displacement and surcharge loading rate is presented in Fig. 3.20. It clearly shows that for the similar model grounds (initial undrained shear strength is the same), the maximum lateral displacement increases with increase of loading rate.
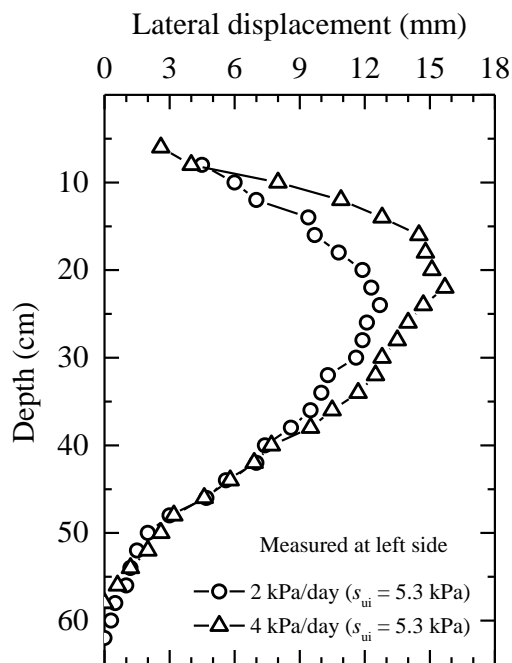
Fig. 3.20 Lateral displacement of similar model grounds under different loading rate

The values of the normalized maximum lateral displacement (*NLD*), i.e. a ratio of the maximum lateral displacement (δ_m) to the ground surface settlement at the embankment centerline (S_f) for the six (6) cases tested are also summarized in Table 3.2, and their relationship with surcharge loading rate is shown in Fig. 3.21. It is observed that for the similar model grounds the normalized maximum lateral displacement increases with the increase of loading rate. For the cases tested, within the range of loading rate of 2 to 7 kPa/day and excepting the normalized maximum lateral displacement at left side of the case of 7 kPa/day, *NLD* almost linearly increases with the increase of loading rate as depicted by the dash line in Fig. 3.21.
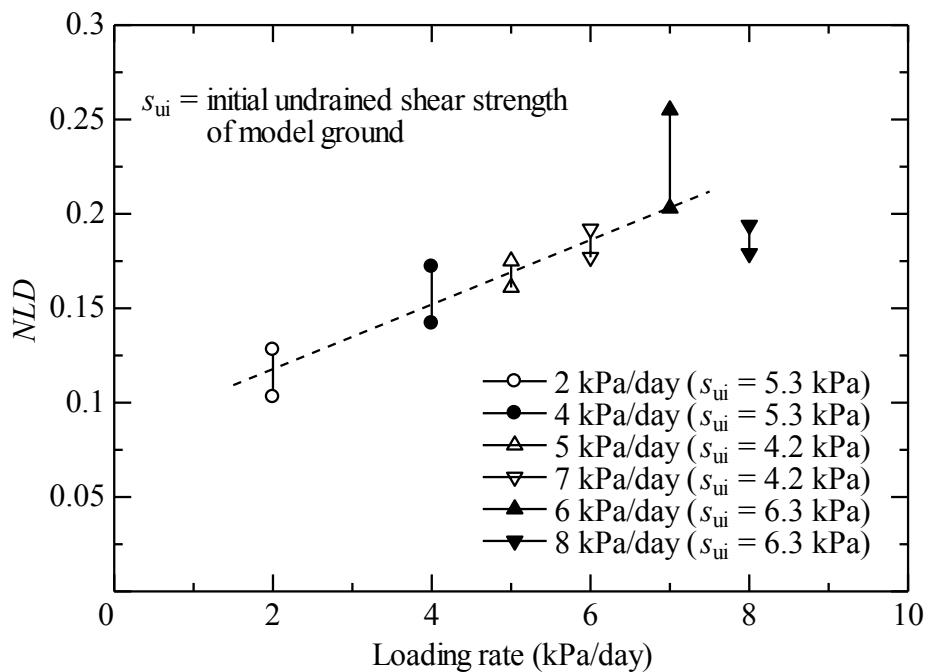
Fig. 3.21 Effect of loading rate on *NLD*

If the stiffness of the model grounds is different, a faster loading on a stiffer model ground may induce smaller lateral displacement than that induced by a slower loading on a softer model ground, for example the maximum lateral displacement of the case of 6 kPa/day (s_{ui} = 6.3 kPa) is smaller than that of the case of 5 kPa/day (s_{ui} = 4.2 kPa), as presented in Fig. 3.22. This indicated that the strength of the model ground is also an important influencing factor of lateral displacement. And if the loading condition and ground conditions are the same, *NLD* will reduce with increase of s_u.
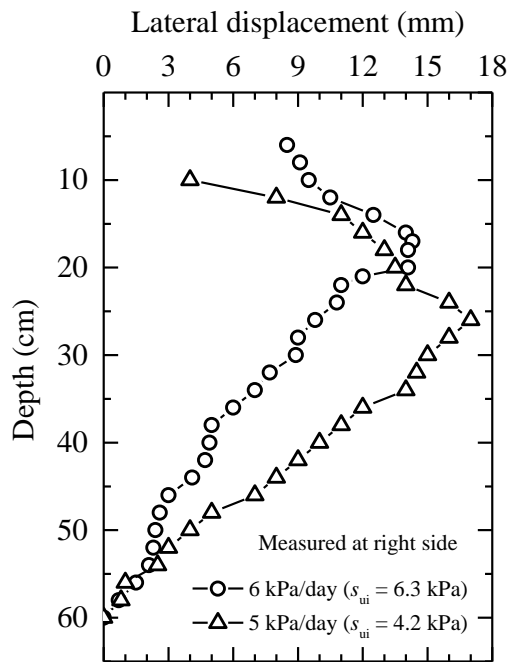
Fig. 3.22 Lateral displacement of model grounds with different
strength under different loading rate

3.6 Investigating Lateral Displacement with Considering Main Affecting Factors

Except the embankment loading rate and undrained shear strength of the ground, there are other main parameters having effects on the magnitude of lateral displacement, i.e. magnitude of embankment load and deformation and consolidation properties of the soft subsoil (Ong and Chai 2001; Chai *et al*. 2013). To consider all these influencing factors, a synthetic parameter termed as a ratio of an index load to the undrained shear strength of the ground (*RLS*) had been introduced by Chai *et al*. (2013). And it was considered as a key parameter to predict the value of *NLD*. However, the study of Chai *et al*. (2013) was based on the data from field case histories and only aiming at the cases of under combined embankment load and vacuum pressure. Generally, for different field cases they have different embankment geometries and different subsoil profiles, and these factors may lead to scatter of the value of *RLS*. Comparing with field cases, laboratory model tests can be conducted under controlled conditions and provide a base for assessing whether *RLS* is a control factor of lateral displacement or not. And also, the well controlled laboratory test results can be used to investigate the relationship between *NLD* and *RLS* for the case of PVD-improved deposits under only embankment load.

3.6.1 Ratio of load to undrained shear strength

The ground latral displacement can be taken as a good indicator of the stability of embankment system (e.g. Marche and Chapuis 1974; Tavenal *et al*. 1979 and Yamaguchi *et al*. 1981). Here, it is considered that the factor of safety (FS) at the end of embankment construction can be a major influencing factor for the value of *NLD*. For the case of embankment constructed on soft deposit, the ratio of embankment load (p_{em}) to the undrained shear strength of the soft subsoil, is somehow approximately inversely proportional to the value of FS. However, usually the PVD-improved ground consolidates much faster than the corresponding natural one, and the comsolidation of the ground has significant effects on the effective stress and undrained shear strenght of the subsoil. Therefore, it is further considered that the effects of consolidation of the ground should be involved in calculating the ratio of load to s_u. Considering these points and also the main influencing factors on lateral displacement, a synthetic parameter termed as a ratio of an index load (p_n) to the undrained shear strength of the ground (*RLS*) has been introduced. p_n is expressed as:

$$p_n = p_{em}\left(1 - U\right) \tag{3.2}$$

where p_{em} is the maximum value of the embankment load; and U is the average degree of consolidation of the PVD-improved zone corresponding to the end of embankment construction. The value of U can be calculated using Terzaghi's one-dimensional consolidation theory and Hansbo (1981)'s solution for radial drainage.

Then *RLS* is defined as:

$$RLS = \frac{p_n}{s_u} \tag{3.3}$$

where s_u is the representative undrained shear strength of the PVD-improved zone corresponding to the end of embankment construction. The reason for adopting values of U and s_u corresponding to the end of the embankment construction is that at that time the ground generally has the maximum applied load and a relatively small value of s_u, which leads to a lower factor of safety (FS) against foundation failure under the weight of the embankment. And there are many field cases showed that the maximum lateral displacement occurred at this time point.

3.6.2 Average degree of consoliation

To get the values of *RLS*, degree of consolidaiton of the ground needs to be calculated first. For PVD-improved subsoil, the value of *U* can be calculated by Terzaghi (1925)'s 1D consolidation theory and Hansbo (1981)'s solution. For the surface layer, both vertical and radial drainages need to be considered, and the average degree of consolidation is evaluated by Carrillo (1942)'s equation. Based on theoretical analysis, the thickness of the surface layer, for which both vertical and radial drainage need to be considered is approximately the same as the diameter of the unit cell of PVD-improvement (a PVD and its improvement area). Then, the weighted average degree of consolidation is calculated using the thickness of the subsoil layers in the PVD-improved zone.

3.6.3 Methods for considering time-dependent loading

(1) Existing methods

Terzaghi (1925)'s 1D consolidation theory and Hansbo's (1981) solution are for the condition of instantaneous loading. In engineering practice, the embankment load gradually increases with time during the construction process. There are some analytical solutions or design charts for considering the time-dependent embankment loading induced consolidation of the ground (e.g. Olson 1977; Lekha *et al.* 1998; Tang and Onitsuka 2000; Zhu and Yin 2001; Zhu and Yin 2004; Conte and Troncone 2009; Jimenez *et al.* 2009; Geng *et al.* 2012; Lu *et al.* 2014). However, due to the complexities, these methods are not easy for practical use. As a result, some approximate empirical methods have also been proposed to solve this problem (Terzaghi 1943; Olson 1998; Chai and Miura 2002).

Terzaghi (1943)'s method estimates the value of *U* at the end of a ramp loading (total loading time is T_1) is the same as the value of *U* due to the total pressure (p_{em}) instantaneously acting on the ground for a period of $T_1/2$ (Fig. 3.23(a)).

Olson (1998)'s method proposed that the value of *U* at any time during a time-dependent embankment loading can be calculated as a weighted average of the degree of consolidation of each loading step separately (Fig. 3.23(b)), i.e.

$$U = \sum_{i=1}^{N} \frac{\Delta p_i}{p_{em}} \cdot U_i \tag{3.4}$$

where Δp_i = load increment of *i*th step; and U_i = degree of consolidation for the *i*th step.
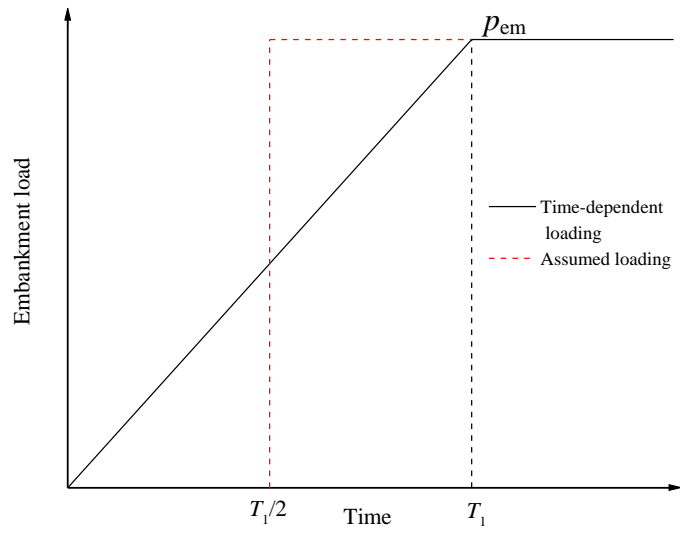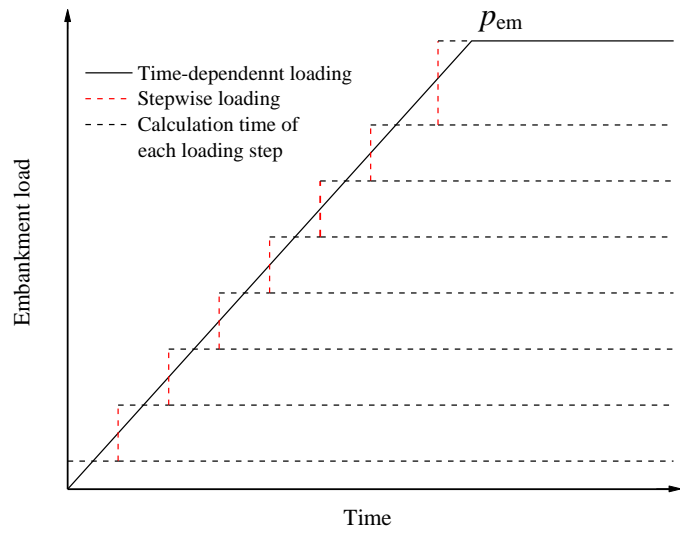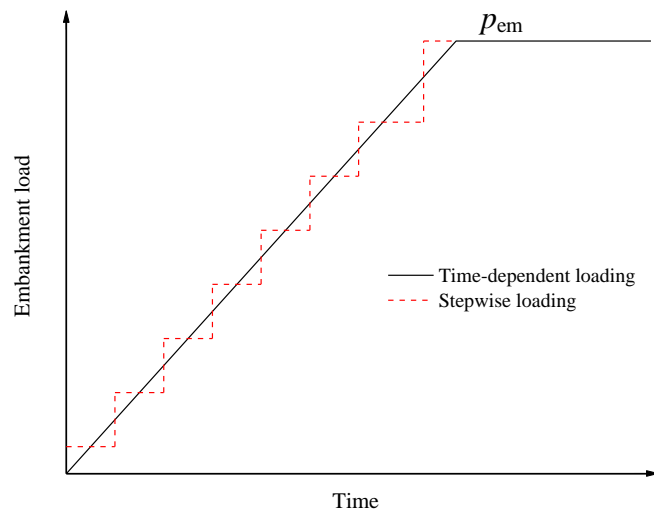
Fig. 3.23 Assumed loading procedure: (a) Terzaghi; (b) Olson; (c) Chai and Miura

Chai and Miura (2002) considering the fact that the effective stress in a soft clayey deposit is the same immediately before and after an incremental load application, and proposed to calculate the degree of consolidation under time-dependent loading as follows (Fig. 3.23(c)):

(a) Suppose at time t_i the applied load is p_i, and the degree of consolidation corresponding to p_i is U_i. A load increment Δp_j is applied instantaneously at time t_i, and the degree of consolidation (U_j) associated with $p_j = p_i + \Delta p_j$ at time t_i is

$$U_j = \frac{U_i p_i}{p_j} \tag{3.5}$$

(b) With U_j known, an imaginary time t_{j0} can be obtained from the corresponding consolidation theory.

(c) Under the loading p_j, at time $t_i + \Delta t$, the degree of consolidation is calculated using a time of $t_{j0} + \Delta t$.

The above empirical methods are simple and are easy for hand-calculating the value of U. However, the applicability of these methods for PVD-improved ground needs to be evaluated.

(2) Numerical investigation

Here, the applicability of the three approximate methods were investigated by a series of finite element analysis (FEA). The program used is Plaxis 2D (version 8.2). Two types of grounds were simulated; one consisted a uniform soil layer of 5.0 m thick (Fig. 3.24(a), termed as type A), the other one consisted two soil layers with thickness of each layer is 2.5 m (Fig. 3.24(b), termed as type B). Elastic models were adopted to the soil layers, and the soil properties used are listed in Table 3.3. The PVD was modeled by solid elements with the same properties as the soil (Table 3.3, layer 1) excepting hydraulic conductivity, and the drainage parameters of the PVD used is listed in Table 3.4. In the simulations, a uniformly distributed vertical load (maximum value is 80 kPa) was applied on the top surface of the ground but with different loading rate.

Table 3.3 Soil properties adopted for FEA

Soil layer	γ_t (kN/m^3)	E_s (MPa)	ν	k_v (m/day)	k_h/k_v
Layer 1	14.0	2.8	0.35	1.4×10^{-4}	2
Layer 2	14.0	1.4	0.35	1.4×10^{-4}	2

Table 3.4 Parameters of PVD adopted for FEA

D_e (m)	d_w (m)	d_s (m)	q_w (m^3/year)	k_h/k_s	l
1.5	0.052	0.13 m	100	2	5.0
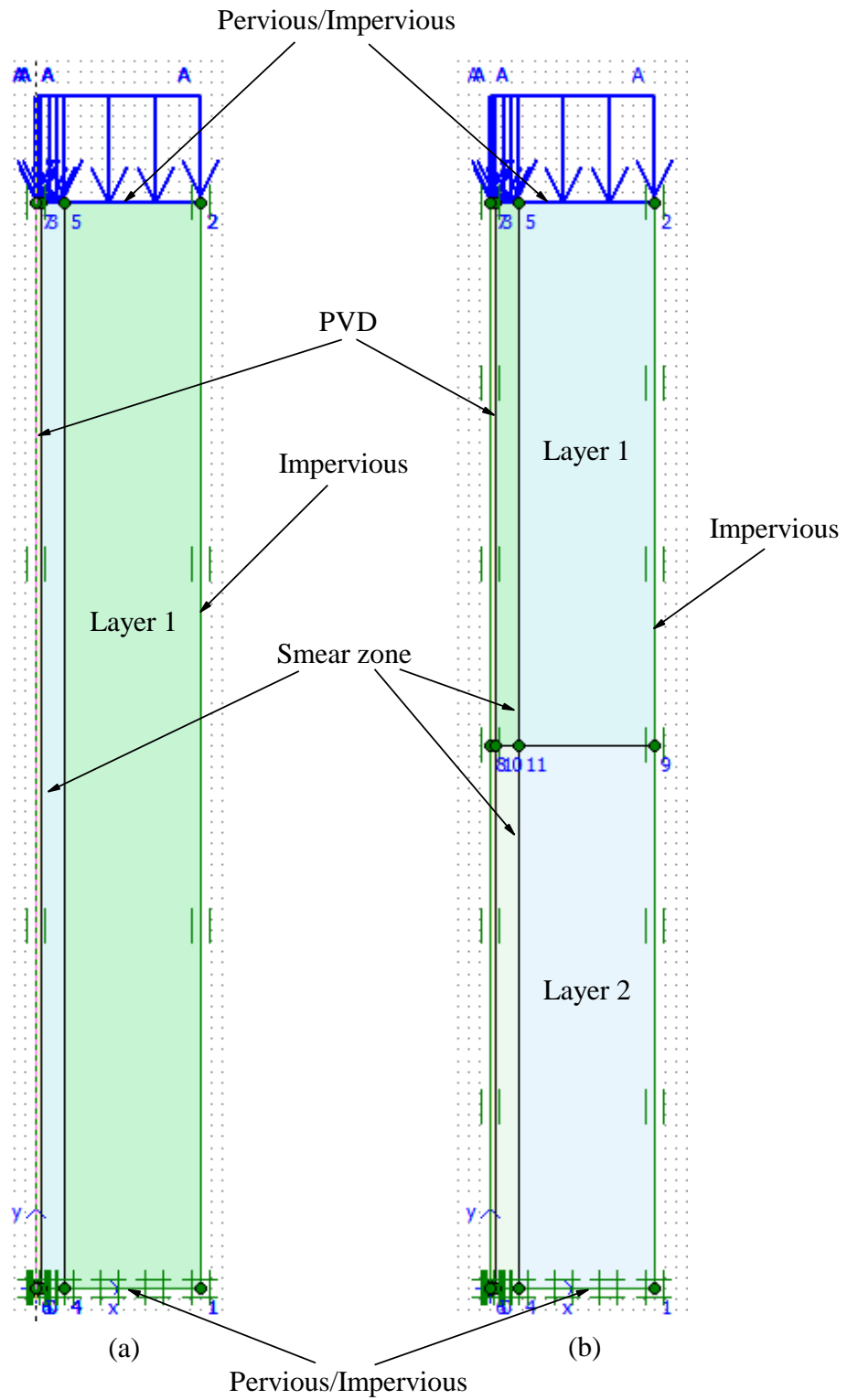
Fig. 3.24 Two types of grounds simulated: (a) one soil layer; (b) two soil layers

The analyzed values of *U* at the end of surcharge load application from FEA for different loading rate and different types of ground as well as the hand-calculated results using the approximate methods of Terzaghi (1943), Olson (1998) and Chai and Miura (2002) are summarized in Table 3.5. In the table, it is observed that there is no significant difference between the hand-calculated values of *U* by dividing the time-dependent loading into 4 steps and 8 steps using both the methods of Olson (1998) and Chai and Miura (2002).

Table 3.5 Values of *U* from FEA and different hand-calculation methods
at the end of load application (%)

Loading rate	Types	Boundary	FEA	Terzaghi	2 steps		4 steps		8 steps	
					Olson	Chai	Olson	Chai	Olson	Chai
10 kPa/day	A	H	39.9	35.1	33.3	33.3	33.0	33.0	33.0	33.0
		H + 1V	45.7	42.5	40.2	39.9	39.7	39.3	39.7	39.3
		H + 2V	51.5	50.0	47.2	46.5	46.3	45.6	46.2	45.5
	B	H	32.2	27.3	26.1	26.1	25.9	25.9	25.9	25.9
		H + 1V	38.1	34.7	33.0	32.7	32.6	32.2	32.5	32.2
		H + 2V	43.6	41.2	39.1	38.4	38.5	37.6	38.5	37.5
4 kPa/day	A	H	62.5	66.1	60.7	60.7	59.0	59.0	59.0	59.0
		H + 1V	67.3	72.2	66.7	66.8	64.7	65.1	64.5	65.0
		H + 2V	72.2	78.3	72.8	72.9	70.3	71.1	70.0	71.1
	B	H	53.0	53.9	49.9	49.9	48.9	48.9	48.9	48.9
		H + 1V	57.8	60.0	56.0	56.1	54.6	55.0	54.4	55.0
		H + 2V	63.8	67.5	63.0	62.8	61.2	61.4	61.0	61.3
1 kPa/day	A	H	88.8	98.7	95.8	95.8	90.8	90.8	88.7	88.7
		H + 1V	90.5	99.1	96.9	96.9	92.7	93.1	90.6	91.5
		H + 2V	92.2	99.4	98.0	98.0	94.6	95.4	92.5	94.3
	B	H	83.9	93.6	88.9	88.9	84.3	84.3	82.9	82.9
		H + 1V	85.6	94.0	90.0	90.0	86.2	86.6	84.8	85.7
		H + 2V	88.6	96.7	93.7	93.8	89.9	91.1	88.2	90.2

Note: H = only radial drainage; H + 1V = radial drainage and 1-way vertical drainage; H + 2V = radial drainage and 2-way vertical drainage; 2 steps, 4 steps and 8 steps = dividing the time-dependent ramp loading into stepwise loading of 2 steps, 4 steps and 8steps, respectively.

The relationships between the values of *U* from FEA and from the methods of Terzaghi (1943), Olson (1998) and Chai and Miura (2002) are presented in Figs. 3.25 to 3.27, respectively. For the latter two hand-calculation methods, the values of *U* are corresponding to the case of 8 steps loading. It is shown that the hand-calculated values of *U* are smaller than the values of *U* from the FEA when the hand-calculated values of *U* are less than about 52%, 88% and 85% for the methods of Terzaghi (1943), Olson (1998) and Chai and Miura (2002), respectively, and after that vice versa. Excepting the difference in

the approximation adopted for estimating consolidation time and load increment, another reason for the discrepancy of values of U is that the consolidation theory used in FEA is Biot (1941)'s coupled consolidation theory, while the hand-calculation methods use the theory of Terzaghi (1925) and the solution of Hansbo (1981). There are differences in basic assumptions adopted in each theory/solution.
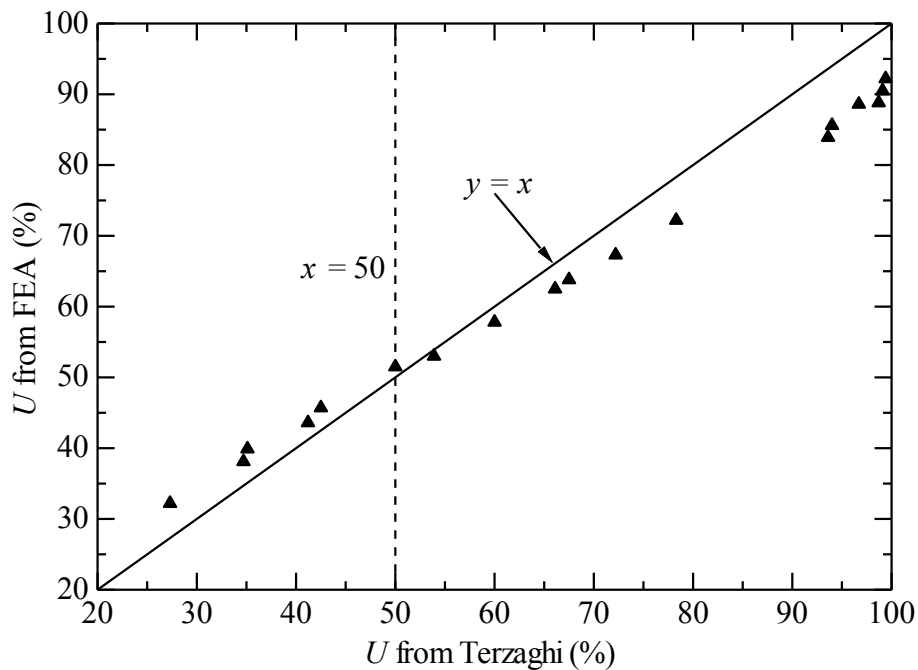
Fig. 3.25 Relationship between U from FEA and Terzaghi (1943)
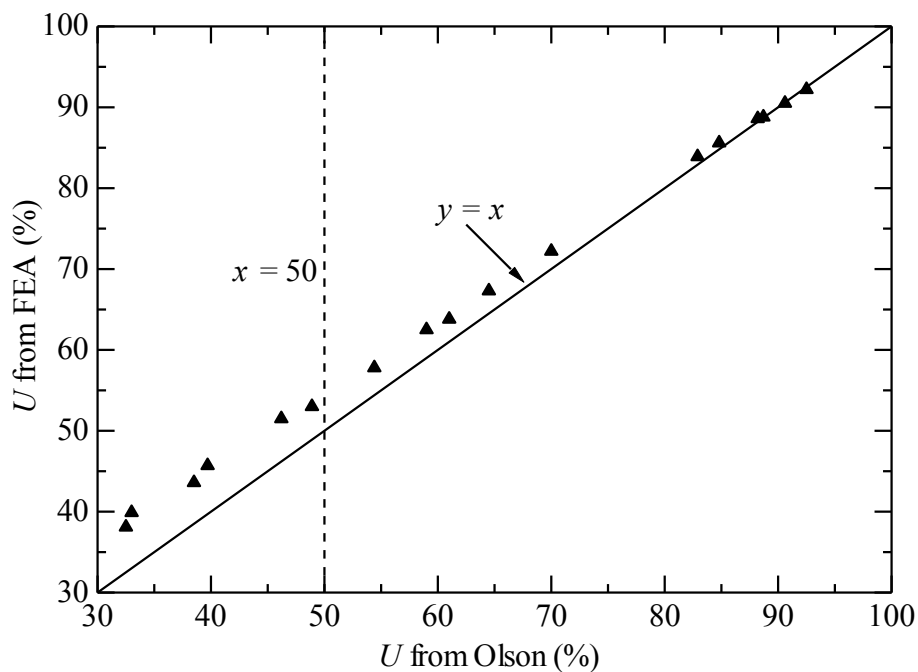
Fig. 3.26 Relationship between U from FEA and Olson (1998)
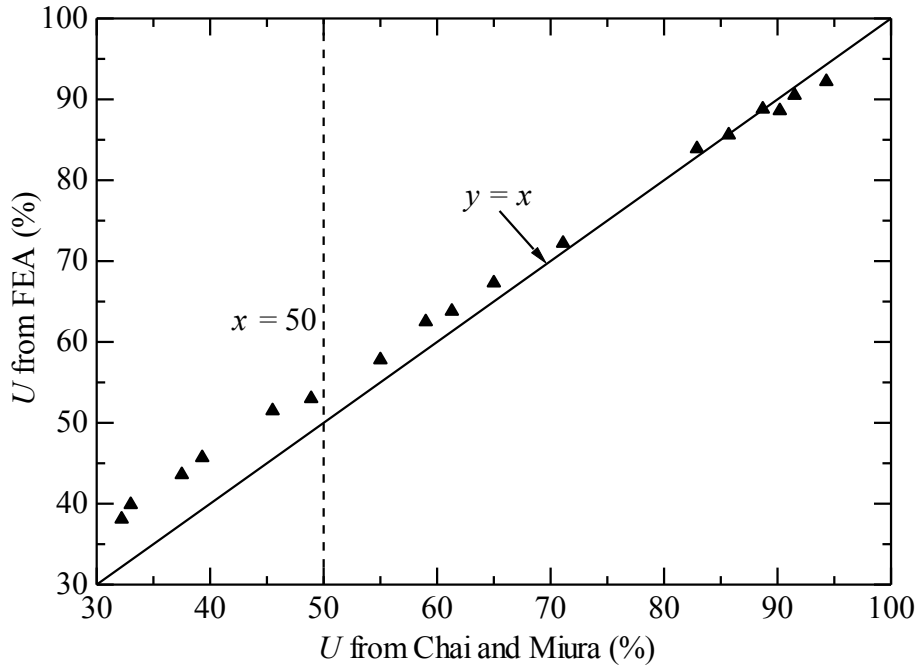
Fig. 3.27 Relationship between U from FEA and Chai and Miura (2002)

Another point is that when the degree of consolidation is less than about 50%, the values of U from Terzaghi (1943)'s method gives a better results. While, when the degree of consolidation is larger than 50%, Olson (1998)'s and Chai and Miura (2002)' method performances better.

Generally, the ground with PVD-improvement consolidates much faster than the corresponding natural one, and normally it can yields a degree of consolidation larger than 50% at the end of embankment construction, and for some field case histories the values were larger than 70% (Chai *et al.* 2013; Xu and Chai 2014). Therefore, it is suggested that the approximate methods of Olson (1998) and Chai and Miura (2002) are more applicable for calculating the degree of consolidation of PVD-improved deposits under time-dependent embankment loading. In this study, to analyze the model test results, the method of Chai and Miura (2002) was used due to its simplicity.

3.6.4 Representative undrained shear strength

It is suggested that the value of s_u of each soil layer can be estimated to sufficient accuracy by the empirical equation proposed by Ladd (1991), which is as follows:

$$s_u = S_1 \sigma'_v (\text{OCR})^m \tag{3.6}$$

54

where σ'_v is the representative vertical effective stress in a soil layer corresponding to the end of embankment construction, OCR is overconsolidation ratio, and S_1 and m are costants. For most of the field cases, at the end of embankment construction the soft clayey deposits will be either in or close to a normally consolidated state (i.e. OCR ≈ 1.0), so that the effect of m value will therefore be insignificant. As for the value of S_1, it is recommended that it can be back-calculated using measured initial values of s_u for the deposit. If no such initial values exist, a value of $S_1 = 0.25$ is suggested (Chai *et al*. 2013). Then, the weighted average value of s_u is calculated using the thicknesses of the soil layers in the PVD-improved zone.

3.6.5 Analyses of model tests

The soil parameters of the model ground of the six laboratory model tests and the drainage parameters of the Mini-PVDs adopted are listed in Tables 3.6 and 3.7, respectively. For the purpose of hand-calculation, the model ground was divided into three layers. For the surface and the bottom layers, both the vertical and horizontal drainages need to be considered, and their thickness was about 178 mm, the same as the diameter of the unit cell (a mini-PVD and its improvement area) (Xu and Chai 2014). And for the middle layer, only horizontal drainage needs to be considered, and it was about 294 mm thick.

Table 3.6 Parameters of model ground soil

Case	γ_t (kN/m^3)	e_0	C_c (C_s/ C_c)	k_v (m/day)	c_v (m^2/day)	p'_c (kPa) Sur	Mid	Bot
Cases 1 and 2	13.68	3.12	0.927 (0.1)	6.4×10^{-5}	1.7×10^{-3}	10	9.3	10
Cases 3 and 4	13.75	3.07	0.830 (0.1)	6.0×10^{-5}	1.65×10^{-3}	8	7.3	8
Cases 5 and 6	14.03	2.82	0.774 (0.1)	5.3×10^{-5}	1.6×10^{-3}	10	9.4	10

γ_t = total unit weight; e_0 = initial void ratio; C_c = compression index; C_s = swelling index; k_v = hydraulic conductivity in the vertical direction; c_v = coefficient of consolidation in the vertical direction; p'_c = pre-consolidation pressure. Sur = surface layer, thickness, 178 mm; Mid = middle layer, thickness, 294 mm; Bot = bottom layer, thickness, 178 mm.

Table 3.7 Parameters of Mini-PVD

D_e (m)	d_w (m)	d_s (m)	k_h/k_s	q_w (m^3/year)	l (m)
0.178	0.02	0.08	1.6	1.0	0.65

D_e = diameter of unit cell (a mini-PVD and its improvement area); d_w = diameter of mini-PVD; d_s = diameter of smear zone; k_h = horizontal hydraulic conductivity of undisturbed

zone; k_s = hydraulic conductivity of smear zone; q_w = discharge capacity of mini-PVD; l = drainage length.

For Cases 1 to 4, the values of s_u of the model ground after completion of tests were measured using laboratory mini-vane shear tests, and the results are shown in Fig. 3.28. Using these test results, a value of S_1 in Ladd (1992)'s equation of 0.33 was back-calculated. For Cases 5 and 6, after completion of the consolidation test under the total applied load of 60 kPa, further load was applied before the final termination of the tests. The further loaded part is not indicated in this study, and the measured values of s_u are not corresponding to the total applied load of 60 kPa and are also not shown in Fig. 3.28.
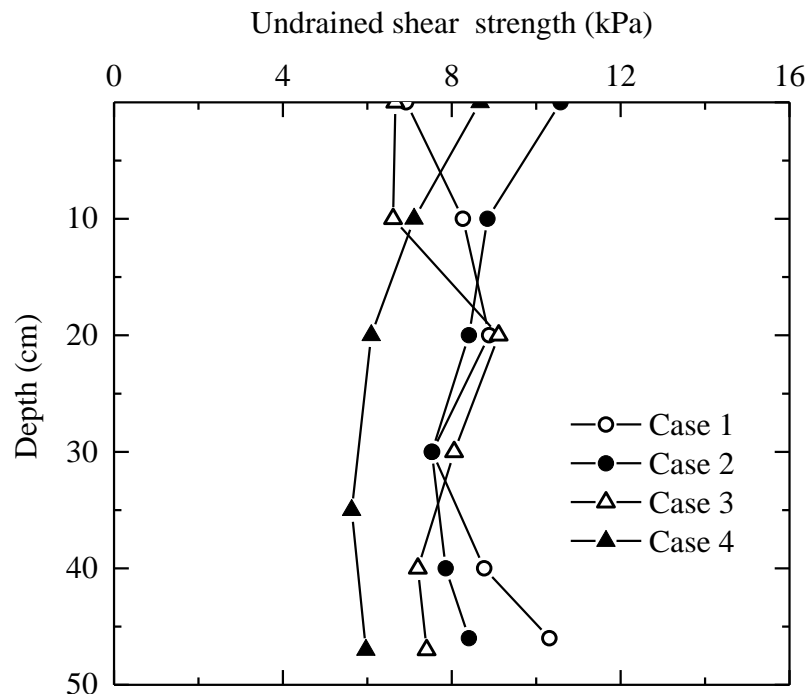
Fig. 3.28 Undrained shear strength profiles after test completion

In the analyses, the distribution of vertical stress in the model ground induced by the surcharge load were calculated based on Boussinesq (1883)'s solution. The analyzed settlement-time curves of the six model tests are compared with the measured data in Figs. 3.29-3.34 for Cases 1-6, respectively. It can be seen that the analyzed results agreed well with the measured data, which implies the correction of the calculated values of U. Then the calculated values of U, p_n, s_u, NLD and RLS and the final measured maximum lateral displacement (δ_m) and the ground surface settlement (S_f) on the central loading plate are listed in Table 3.8. It is observed that for the similar model ground (with the same initial

undrained shear strength) under the same total surcharge load, the value of *NLD* increases with the increase of loading rate.
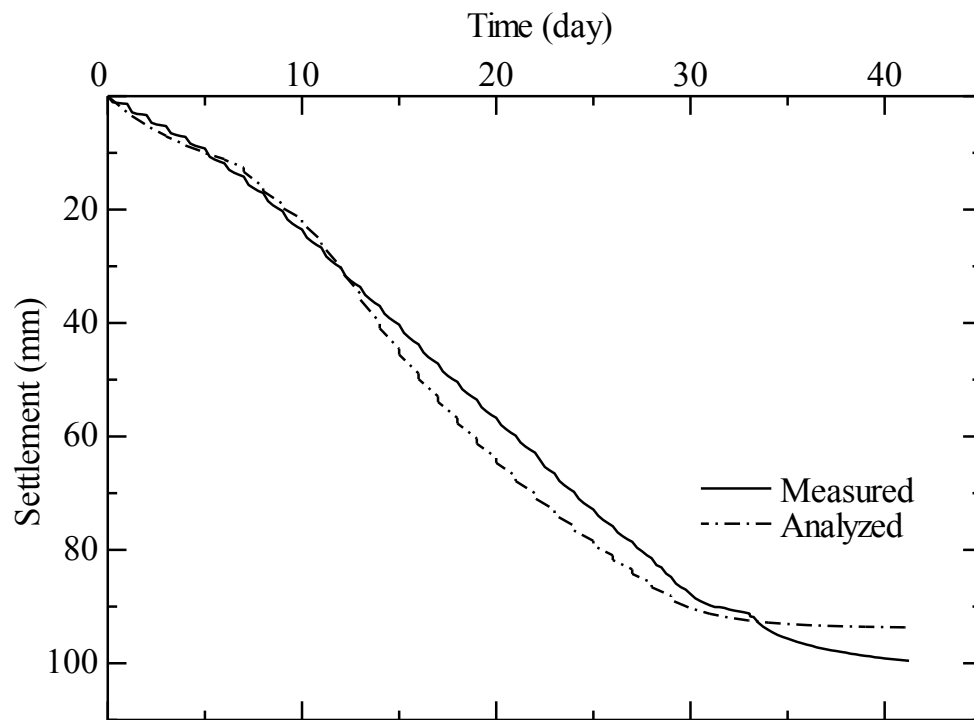
Fig. 3.29 Analyzed and measured ground settlements of Case 1
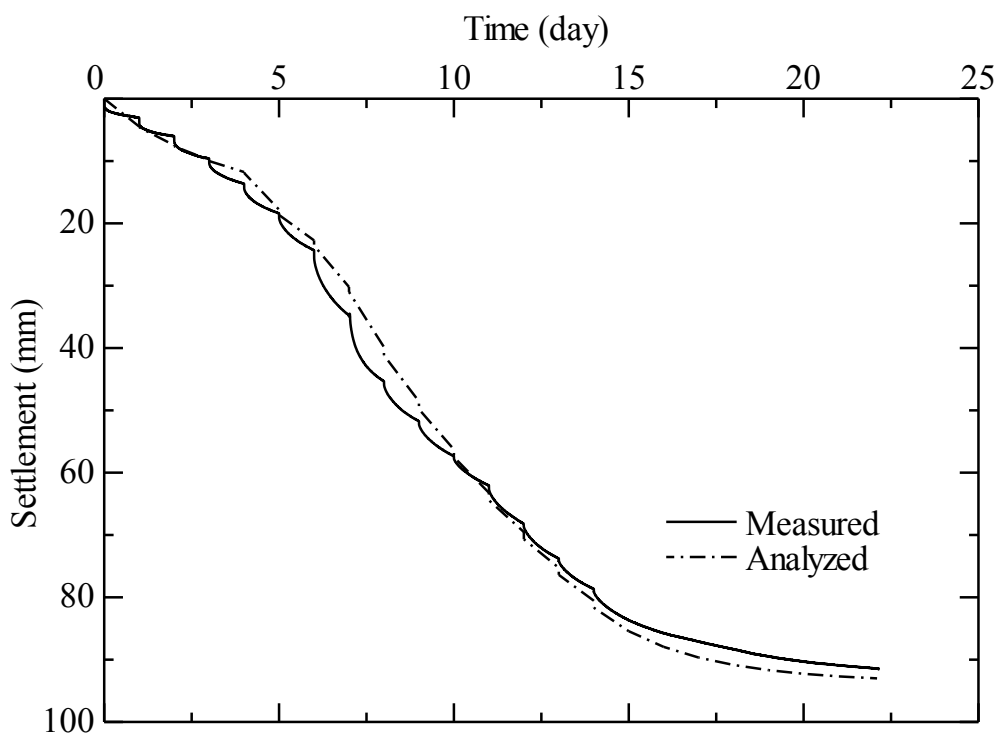
Fig. 3.30 Analyzed and measured ground settlements of Case 2
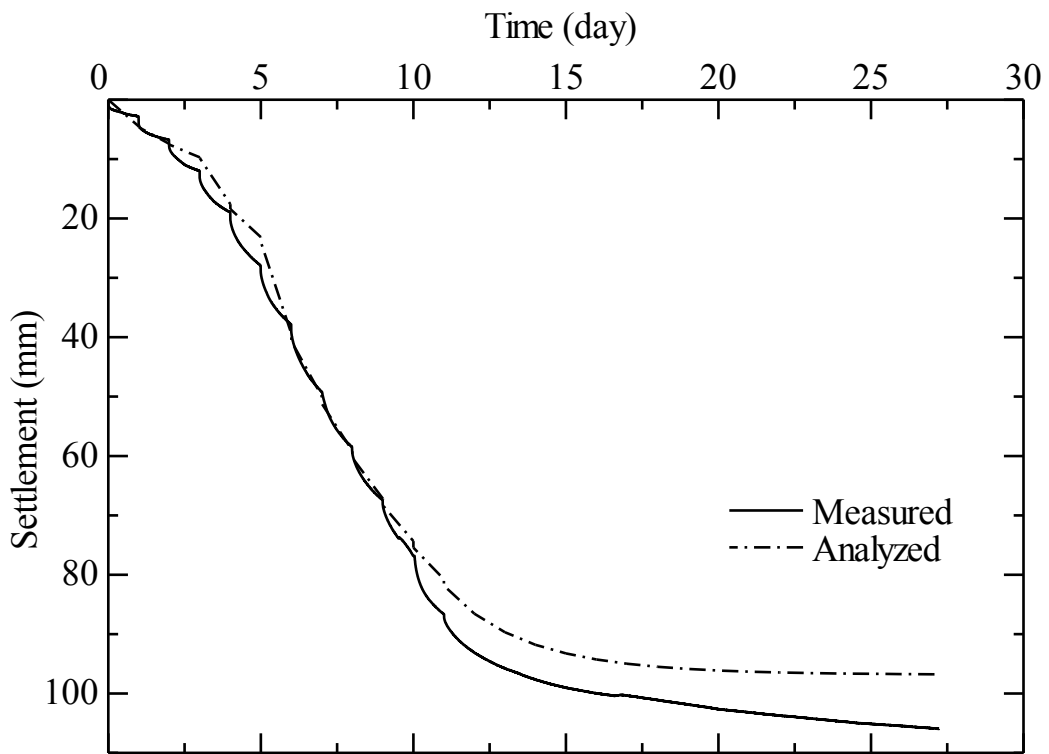
Fig. 3.31 Analyzed and measured ground settlements of Case 3
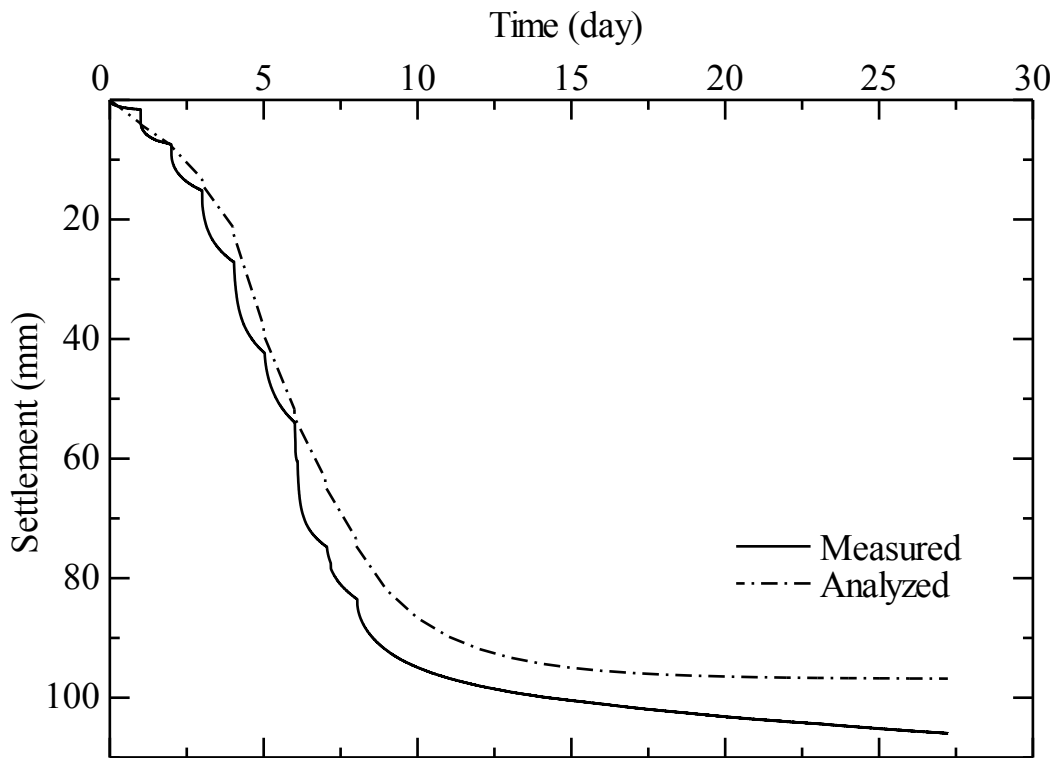
Fig. 3.32 Analyzed and measured ground settlements of Case 4
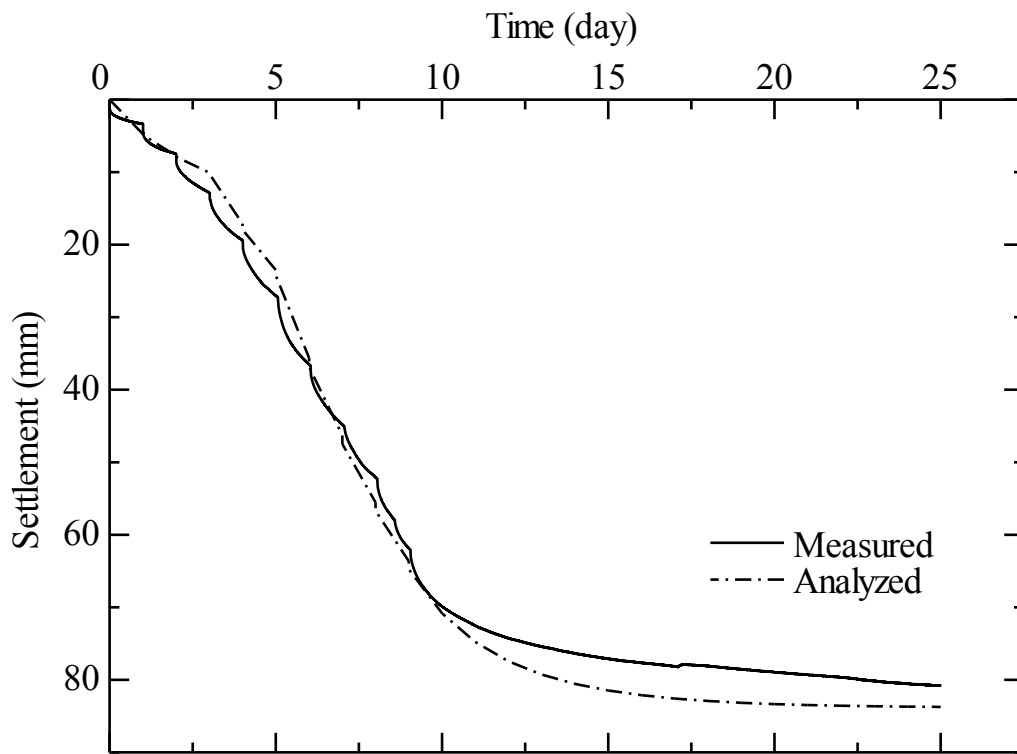
Fig. 3.33 Analyzed and measured ground settlements of Case 5
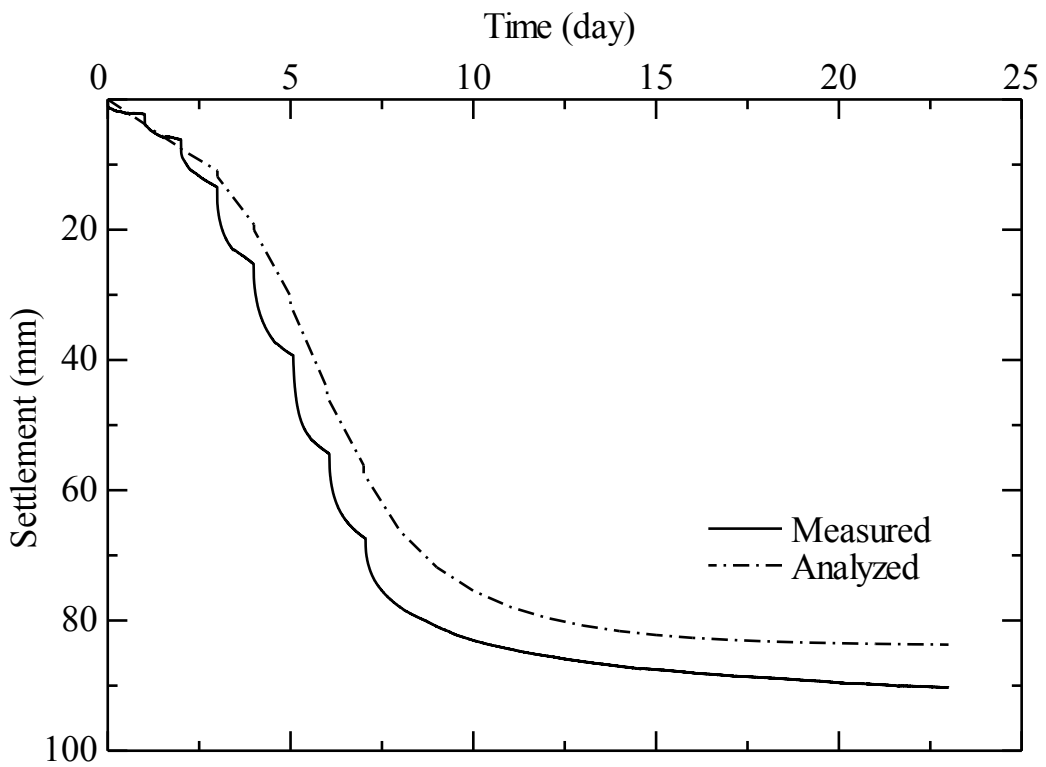
Fig. 3.34 Analyzed and measured ground settlements of Case 6

Table 3.8 Analyzed results of cases tested

Case	U (%)	p_n (kPa)	s_u (kPa)	RLS	S_f (mm)	δ_{mL} (mm)	δ_{mR} (mm)	NLD-L	NLD-R
Case 1	94.5	3.3	11.2	0.295	99.5	12.7	10.2	0.128	0.103
Case 2	87.4	7.6	10.4	0.727	91.5	15.7	13.0	0.172	0.142
Case 3	83.1	10.1	9.9	1.024	105.9	18.5	17.0	0.175	0.161
Case 4	76.6	14.0	9.2	1.526	106.0	27.0	21.5	0.255	0.203
Case 5	79.0	12.6	9.5	1.326	80.8	15.5	14.3	0.192	0.177
Case 6	72.7	16.4	8.8	1.861	90.3	17.5	16.2	0.194	0.179

The analyzed results of *NLD* and *RLS* are plotted in Fig. 3.36. It shows that *NLD* almost linearly increases with incresing *RLS*, which verifys that *RLS* is a controlling parameter of *NLD*.
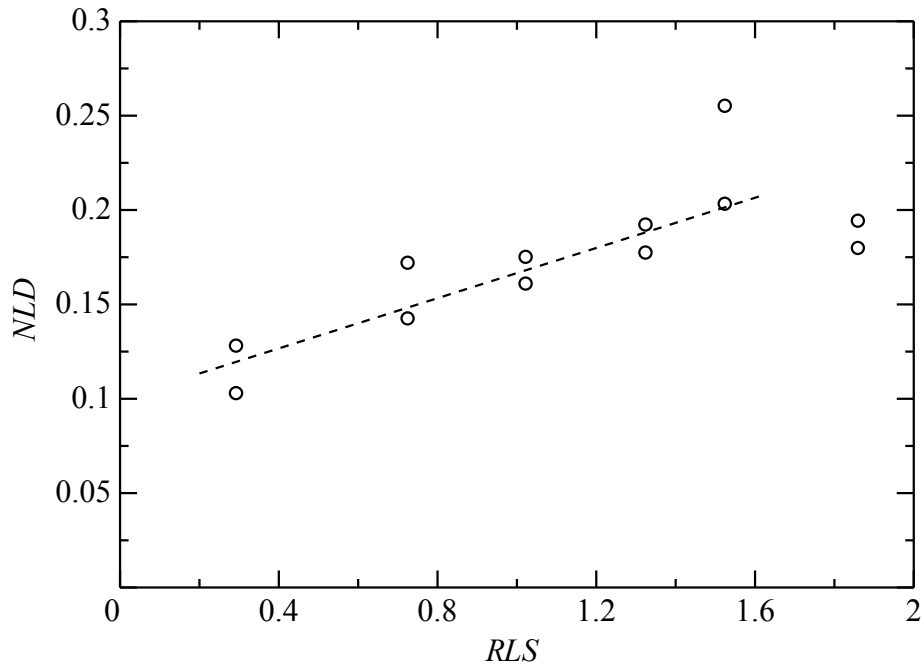
Fig. 3.36 Relationship of *NLD-RLS* from model tests

3.7 Summary and Comments

(1) The effect of surcharge loading rate and undrained shear strength of the ground on lateral displacement of PVD-improved deposits was investigated by a series of large-scale laboratory model tests. Based on the test results, the following points can be drawn:

(a) The maximum lateral displacement increased with the increase of surcharge loading rate (*LR*).

(b) For the cases tested, the normalized maximum lateral displacement (*NLD*) almost linearly increased with increasing *LR*.

(c) The undrained shear strength (s_u) of the ground is also an important factor affecting lateral displacement. And *NLD* reduces with increase of s_u.

(2) To consider the effects of the main factors affecting lateral displacement, a synthetic parameter termed as the ratio of an index load (p_n) to undrained shear strength of the model ground (*RLS*) has been used to analyze the model test results. The analyzed results showed that *NLD* almost linearly increased with increase of *RLS*. This verified that *RLS* can be a control factor to predict lateral displacement of PVD-improved deposits.

CHAPTER FOUR
INVESTIGATION OF CASE HISTORIES

4.1 Introduction

In Chapter 3, a series of laboratory model tests have been presented and analyzed. The results indicated that the normalized lateral displacement (*NLD*) almost linearly increased with the increase of a ratio of an index load to undrained shear strength (*RLS*) of the soft subsoil. In this chapter, field case histories were collected from different countries to further investigate the relationship between *NLD* and *RLS*.

4.2 Case Histories Collected

There are a lot of case histories about embankments constructed on PVD-improved deposits reported in literatures. To investigate the ground lateral displacement using *NLD* and *RLS*, a case history has to have following basic information:

(1) The maximum lateral displacement measured under the toe of the embankment (δ_m);

(2) The ground surface settlement measured on the embankment centerline (S_f);

(3) Basic soil properties, such as total unit weight (γ_t), initial void ratio (e_0), compression index (C_c) and if available, swelling index (C_s) and overconsolidation ratio (OCR). And it is preferable if the values of coefficient of consolidation (c_v and/or c_h), hydraulic conductivity (k_v and/or k_h) in the vertical and/or horizontal direction and undrained shear strength (s_u) are available.

(4) Embankment construction history and magnitude of embankment load.

After searching in literatures, totally thirteen case histories of embankments constructed on PVD-improved clayey deposits were collected from five different countries and then analyzed. As the behavior of clayey soil that has been improved by the installation of sand drains (SDs) is similar to that of PVD-improved soils, five case

histories with SD-improvement were also analyzed in order to increase the database. The total number of case histories analyzed was therefore 18.

4.2.1 Assumptions for determining necessary soil properties

For the 18 cases collected, some parameters of the soft subsoil were not directly reported in the source reference. To analyze these field cases, in this study the following assumptions were adopted to determine the necessary soil properties.

(1) Unless specified, the swelling index (C_s) is assumed as one tenth of the corresponding compression index (C_c) (Yoshioka $et\ al.$ 1994; Heo and Bae 2013). For some cases the values of C_c were back-calculated from reported values of the constrained compression modulus (E_s) of the soil layers and the corresponding effective stresses. In the case, where the stress condition corresponding to E_s was not reported, it was assumed that the reported E_s value corresponded to the stress increment from the initial effective stress state of the deposit to the effective stress state at the end of consolidation induced by the embankment loading.

(2) For the cases where the OCR values were not reported, values of OCR were back-calculated by fitting the measured compression of each soil layer or the ground surface settlement.

(3) In cases where there were no measured values of initial void ratio (e_0), but the water contents (w) and total unit weights (γ_t) of the soil were reported, values of e_0 were calculated using values of w and γ_t, assuming the specific gravity of the soil, $G_s = 2.7$ (Budhu 2000). In cases where only the value of w or γ_t is known, for calculating the value of e_0, it was assumed that the degree of saturation, $S_t = 1.0$.

(4) If the value of the coefficient of consolidation in the vertical direction (c_v) or in the horizontal derection (c_h) was not reported, it was back-calculated by fitting the measured settlement-time curve. In all calculations, if the value of the ratio c_h/c_v was not reported, $c_h = 2c_v$ was assumed for all clayey layers (except for filled surface layers, for which $c_h = c_v$ was adopted). The ratio of c_h/c_v or k_h/k_v may vary for different soil deposit, and it influences the calculated degree of consolidation (U). However, in this study by assuming $k_h/k_v = 2$, the value of c_h was back-calculated by fitting the measured settlement-time curve. Therefore, the calculated value of U at the end of embankment construction should be reasonably correct. If the hydraulic conductivity (k) and compression index (C_c) are known, the value of c_v was calculated using the known values of k, C_c and the initial yield stress.

4.2.2 Brief description of case histories

(1) Trial embankment on Muar Plain, Malasia (Case 1)

In 1986, the Malaysian Highway Authority constructed a series of trial embankments on the Muar Plain to assess the effectiveness of different ground improvement techniques for the soft marine clays (Indraratna *et al*. 1997). The embankment of Case 1 was constructed on the soft ground stabilized with geogrids and prefabricated vertical drains (PVDs). The cores of the PVDs were made of polyolefine and the diameter of the drainage holes was 0.2 mm with spacing of 2 mm. The equivalent diameter of the PVDs was 70 mm and they were installed in a squire grid of 2.0 m $\times$ 2.0 m to a depth of 20 m.

The soft marine deposit has a total thickness of about 18 m. A weathered surface layer of 2 m overllies a soft clay layer of 4 m. Below the soft clay layer, there are two soft silty clay layers with thicknesses of about 2 m and 10 m, respectively. Before construction of the embankment, a 0.5 m thick sand layer with horizontal drains in 50 mm diameter, spaced 2 m, was first paved on the ground surface. Then two layers of geogrids (Tensar SR 110) were placed and the embankment fill with average unit weight of 20.5 kN/m^3 was built to a maximum height of 8.7 m within 400 days. The embankment geometry, soil profiles and some soil parameters, PVD installation depth, location of inclinometer casing and the final measured lateral displacement profile are shown in Fig. 4.1.
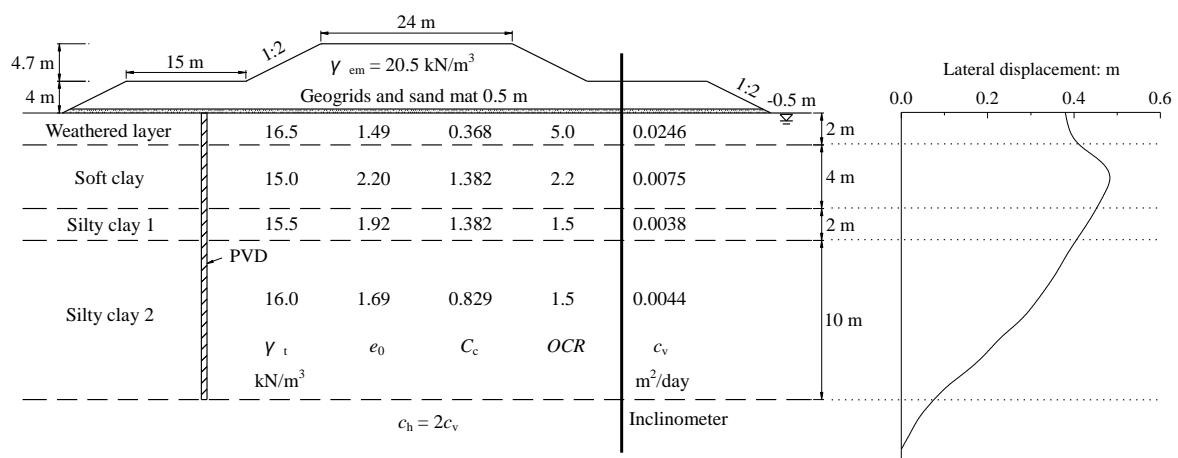
Fig. 4.1 Cross-section of embankment, soil profile and lateral displacement profile of Case 1

64

(2) Trial embankments at Second Bangkok International Airport (SBIA), Thailand (Cases 2 to 4)

Under the support of the Airport Authority of Thailand, the Asian Institute of Technology (AIT) constructed full-scale trial embankments at the Second Bangkok International Airport (SBIA) project (Bergado *et al.* 2002). Three test embankments (TS1 (Case 2), TS2 (Case 3) and TS3 (Case 4)) were analyzed in this study.

The SBIA is loacated at Nong Ngu Hao, about 30 km east of Bangkok. The soft deposit consits of a weathered crust of 2 m thick underlain by a very soft to soft clay layer of about 10 m. Below the soft clay layer, there is a 4 m thick medium stiff clay layer. The PVDs were installed in a square pattern to a depth of 12 m with spacings of 1.5 m, 1.2 m and 1.0 m for Cases 2 to 4, respectively. And the test embankments were built to a total hight of 4.2 m within about 240 days for Case 2 and Case 3 and within about 245 days for Case 4, respecitively.
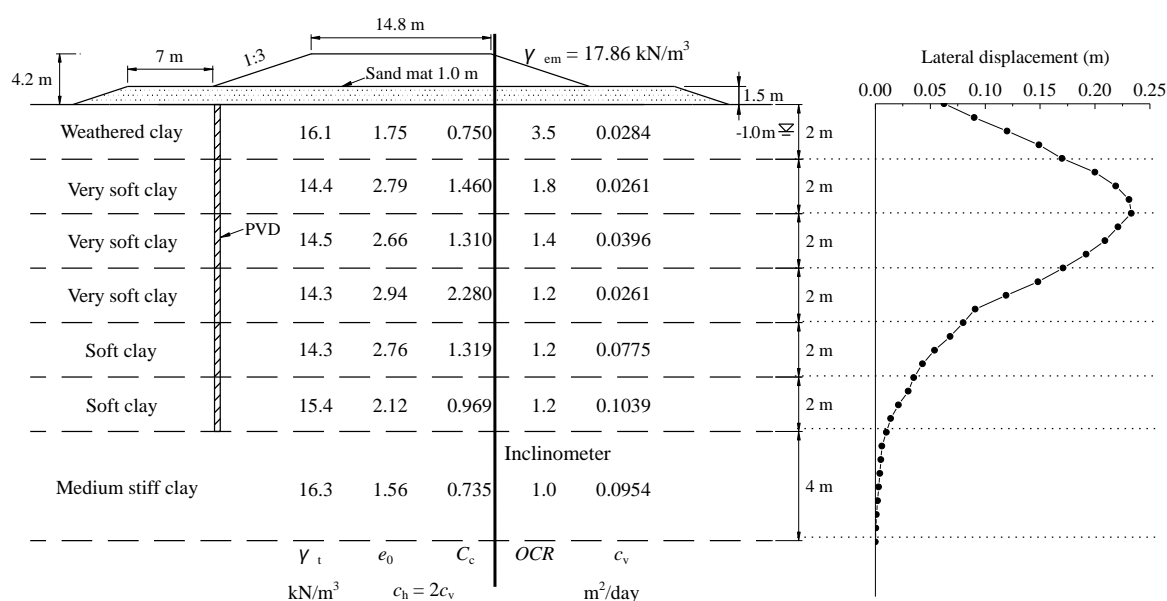
Fig. 4.2 Cross-section of embankment, soil profile and lateral displacement profile of Case 2

In analyzing Case 2, the soil parameters, final measured ground surface settlement and lateral displacement were sourced from Lin and Chang (2009). For Case 3, the final measured values of S_f and δ_m were obtained from Bergado *et al.* (1996), while the soil paramters were refered from Lin and Chang (2009). And for Case 4, the corss section of the embankent, the soil properties and the value of S_f were sourced from Indraratna and

65

Redana (2000), while the value of δ_m was obtained from Indraratna *et al.* (2007). The detailed embankment geometries, soil profiles and final measured lateral displacements are shown in Figs 4.2 to 4.4 for Cases 2 to 4, respectively.

Fig. 4.3 Cross-section of embankment, soil profile and lateral displacement profile of Case 3
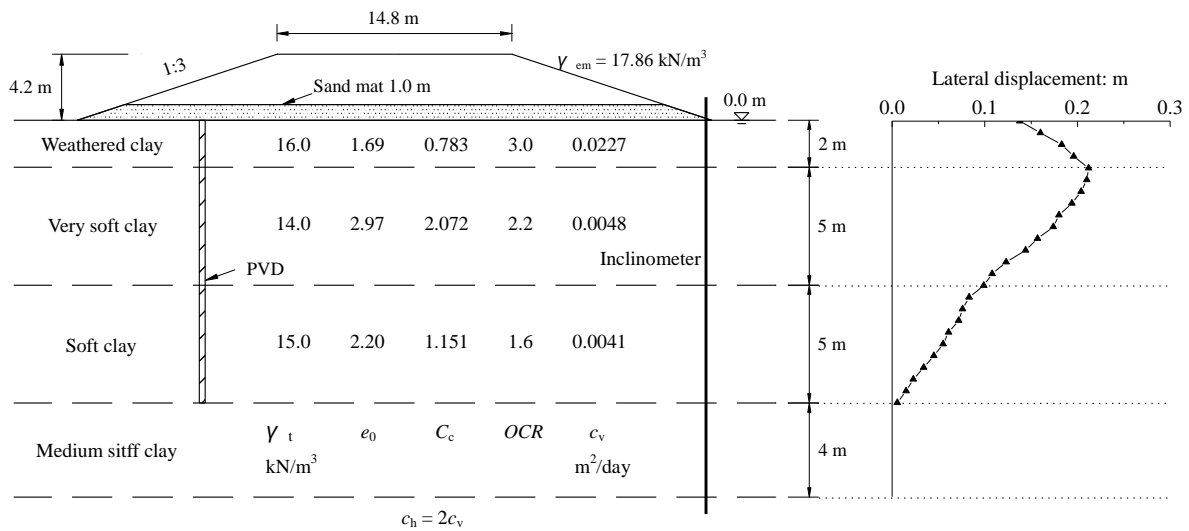
Fig. 4.4 Cross-section of embankment, soil profile and lateral displacement profile of Case 4

(3) Road emankment in Hong Kong, China (Case 5)

Cowland and Wong (1993) reported a road embankment constructed in the northwest of the New Territories of Hong Kong, China. The embankment was built on a soft clayey

deposit. At the ground surface, there is a 1 to 2.5 m thick lagoon deposits layer consists of a very soft, grey silty clay layer, underlain by a young alluvium layer with thickness of about 1 to 3.5 m. Then, a 2 to 3.5 m marine mud layer comprised by very soft, grey silty clay overlies an old alluvium layer with thickness of 2 to 6 m. The water level was at the ground surface.

A geocell mattresses raft foundation and PVDs had been used to improve the soft ground. The PVDs with coross section measuring 100 mm $\times$ 5 mm were installed fully penetrating the soft clayey layers in a triangular pattern with spacing of 1.5 m. Then, weathered granite with unit weight of 19 kN/m^3 was used as fill materail to built a 5 m high embankment. Fig. 4.5 shows the detailed information of this embankment. For this case, the lateral displacement profiles at two sides of the embankment were measured and the measurements are different.

							Lateral displacement (m)					
10 m												
1:1.5	γ_{em} = 19.0 kN/m^3											
5 m	Geogrid and sand mat 0.3 m			Geocell mattresses		0.0 m	0.16	0.08	0.0	0.1	0.2	0.3
Lagoon deposits	16.2	1.60	0.333	1.0	0.0012		2 m					
PVD												
Young alluvium	18.1	1.01	0.234	1.0	0.0067		2 m					
Marine mud	16.5	1.49	0.524	1.0	0.0032		2.5 m					
						Inclinometer						
	20.8	0.52	0.056	1.0	0.0423							
Old alluvium							4 m					
	γ_t	e_0	C_c	OCR	c_v							
	kN/m^3		$c_h = 2c_v$		m^2/day							
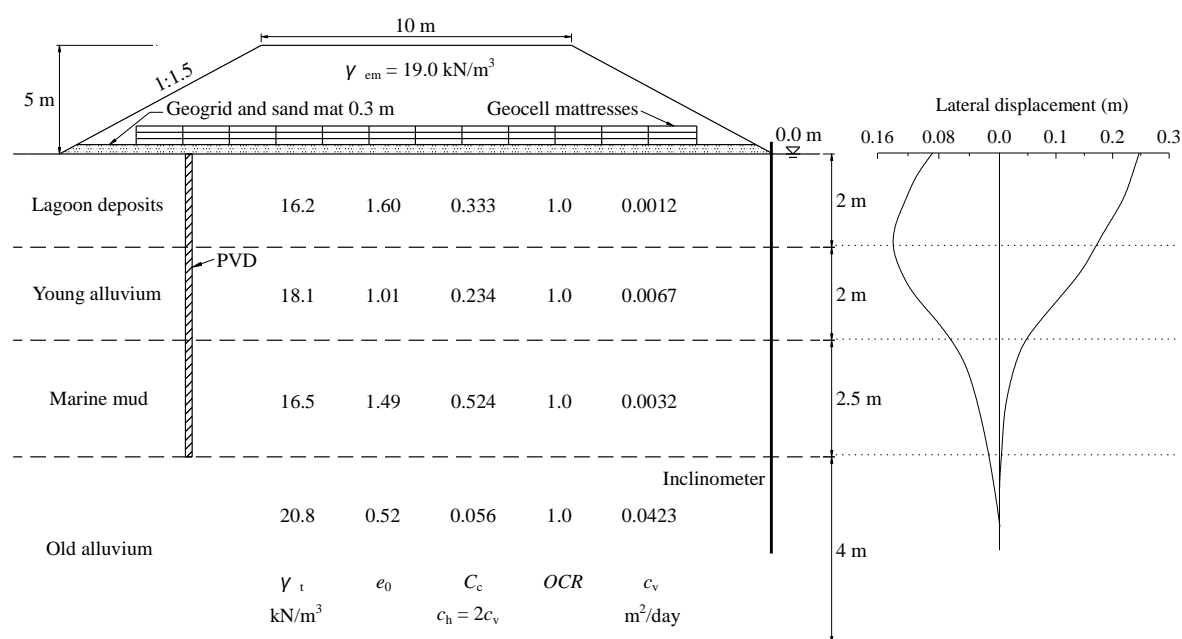
Fig. 4.5 Cross-section of embankment, soil profile and lateral displacement profile of Case 5

(4) Embankment on Hangzhou-Ningbo (HN) expressway, China (Case 6)

The HN expressway is one of the main trafic roads collecing the cities of Hangzhou and Ningbo, locating at Hangzhou Bay, Zhejiang Province, China. Twelve full-scale test embankments with different ground improment methods were constructed for collecting

data to guide the design and construction of the project (Chai *et al.* 2001). Here, one of the embankments with PVD improvement was analyzed.

The soft deposit has a total thickness of about 23 m. From the ground surface, a 1 to 1.5 m weathered crust layer overlies a silty clay layer of about 4 m. Then, a very soft mucky clay layer with thickness of about 10 m underlain by a soft mucky silty clay layer of about 4 m. The bottom layer is a silty clay layer of 3 to 5 m. The water lever is about 1.5 m below the ground surface. PVDs were installed in a triangular pattern, spaced 1.5 m, to a depth of 19 m. A sand mat of 0.5 m was first paved on the ground surdace functioned as a drainage layer. Then, compacted granite with unit weight of about 20 kN/m^3 was used to built a 5.88 m high embankment. The embankment corss section, soil profiles and measured lateral displacement are shown in Fig. 4.6.
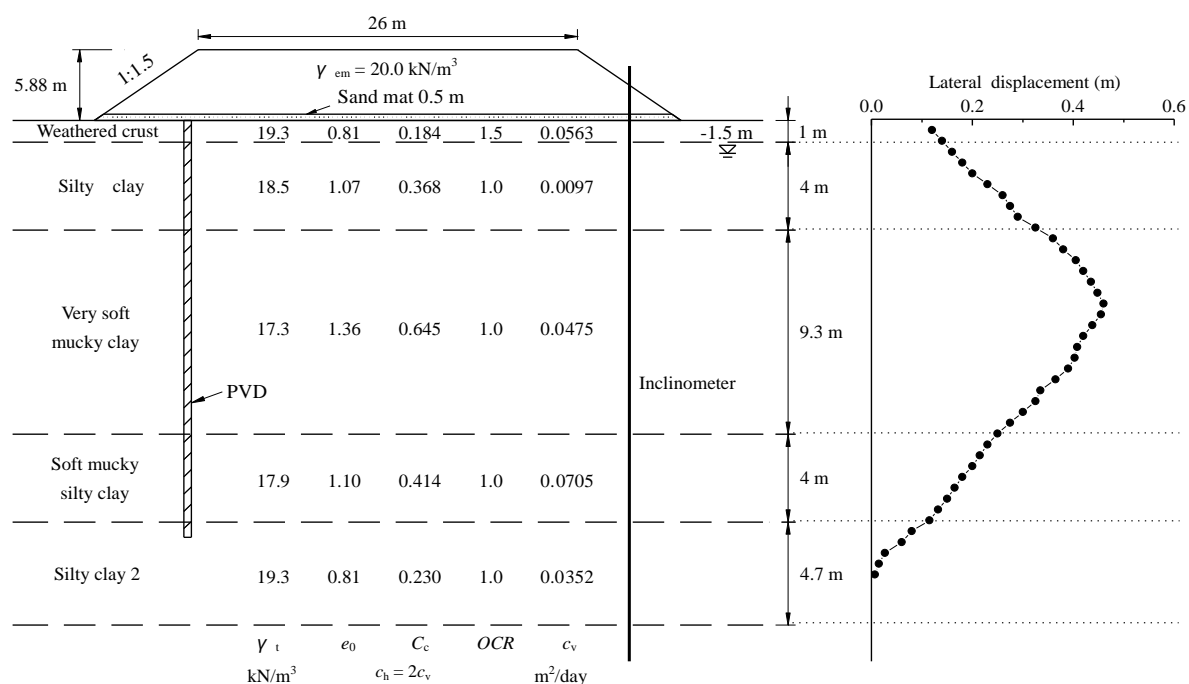
Fig. 4.6 Cross-section of embankment, soil profile and lateral displacement profile of Case 6

(5) Embankment at Nanjing, Jiangsu, China (Case 7)

The Nanjing Oil Refinery is loacated at the south shore of the Changjiang River. The soft deposit is a flood plain which mainly consists of a filled ground surface layer of about 4.5 m and a silty clay layer with thickness of about 18 m to 28 m. Due to the nonuniform thickness of the soft silty clay layer, unexpected tilt of the oil tank was observed when the

water filled into the tank reached a depth of 15 m. To reduce the large total settlement as well as the large differential settlement of the ground, preloading with installation of PVDs had been applied to improve the foundation of the newly constructed oil tank (He and Dai 2000). The PVDs were installed in a triangular pattern with spacing of 1.2 m and fully penetrited the silty clay layer. The preloading embankment was constucted to a maximum height of about 15.6 m, corresponding to a total preloading pressure of about 300 kPa. The embnkament geometry, soil profiles and measured lateral dispalcement are shown in Fig. 4.7.
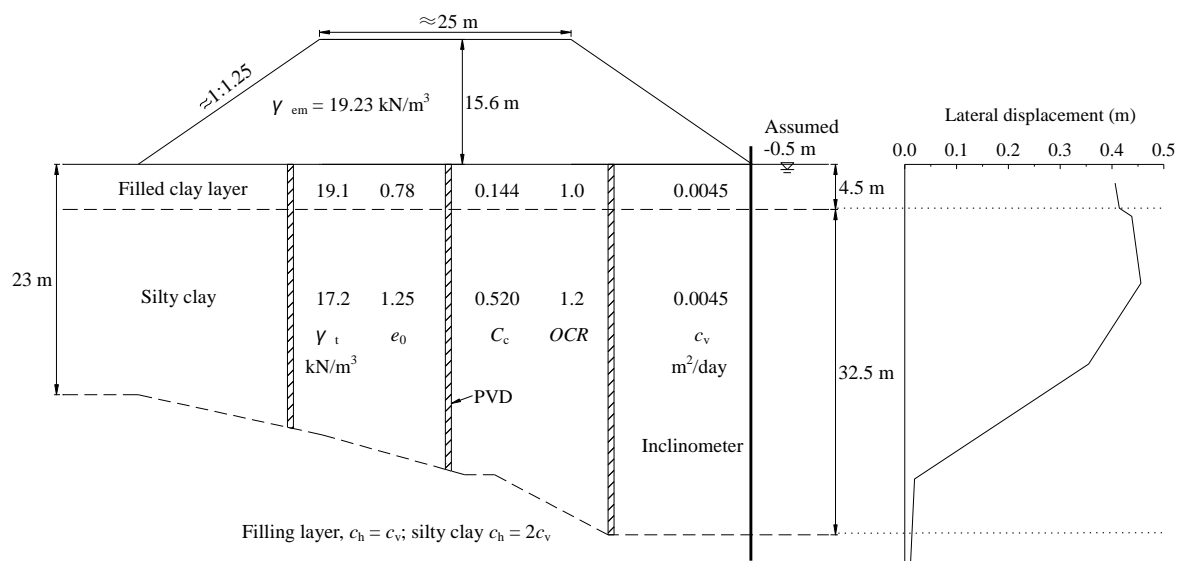
Fig. 4.7 Cross-section of embankment, soil profile and lateral displacement profile of Case 7

(6) Emankment in Zhejiang, China (Case 8)

The Zha-Jia-Su expressway is a main trafic line in Zhejiang Province, China, which connects the Hu-Ning expressway and the Hu-Hang expressway. It passes through the south area of the Hangzhou Bay, where the soft deposit is an alluvial formation. The analyzed embankment is the #7 investigated coross section of the expressway, locating at the mileage of K45 + 332. The soft deposit mainly consists of two soil layers, a surface mild clay layer of 0.7 to 4 m thick and a 1.2 to 31 m silty clay layer. PVDs was used to improve the soft deposit and they were installed to a depth of 25 m, spaced 1.2 m to form a triagular pattern. Then the embankment was built to a total height of about 6 m, corresponding to an embankment load of 122 kPa.

69
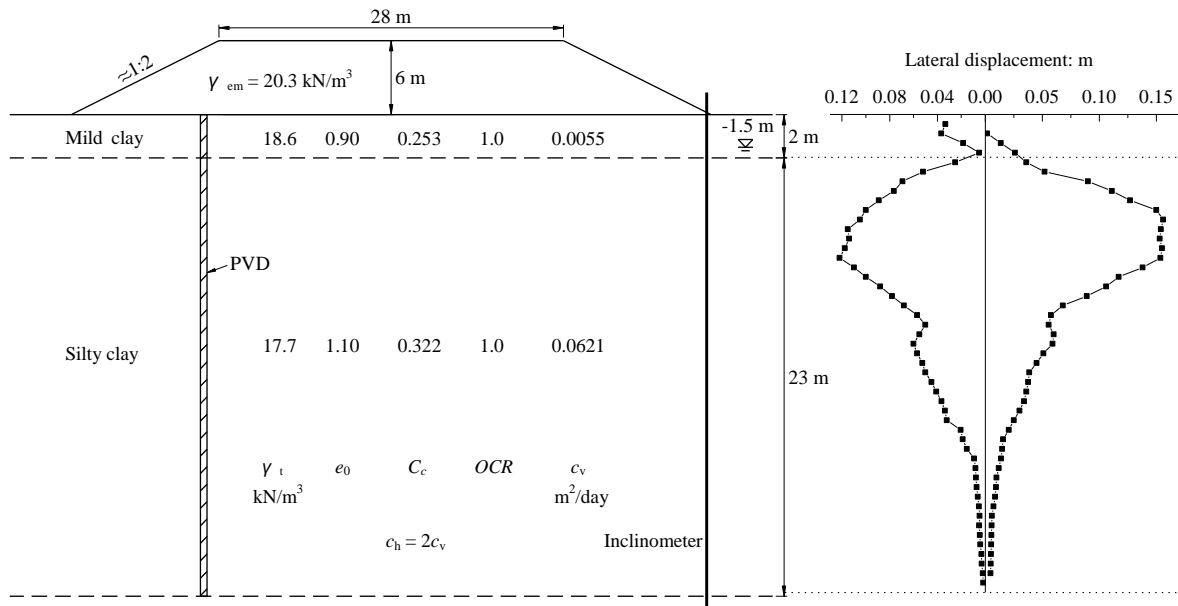
Fig. 4.8 Cross-section of embankment, soil profile and lateral displacement profile of Case 8

In the analysis, the soil parameters were sourced from Zheng (2006), while the measured values of S_f and δ_m were refered from Guo *et al.* (2006). The detailed information of this embnakment is shown in Fig. 4.8. It is observed that the ground latral displacement measured at the two sides of the embnakment are different.

(7) Embankment at a port in south of China (Case 9)

Shen (2012) reported a preloading project at a port in south of China. The analyzed preloading area with PVD-improvement measured 278 m $\times$ 95 m. The soft ground consists of a surface dredeged silty clay layer of 10 m underlain by a silty clay layer of 8 m.

A sand mat of 2 m was first placed on the ground surface as a drainage layer. The PVDs were installed to fully penetrate the the dredeged silty clay layer in a square pattern with spacing of 1 m. The top of the PVDs were kept 20 cm above the sand mat. Then, a fine to medium sand meterial with unit weight of 19 kN/m³ was filled on the sand mat by three steps (first step, 1.5 m; second step, 1 m; and third step, 1 m) to form a preloading embankment with total height of 5.5 m.

Only the parameters of the top 10 m dredeged silty clay layer with PVD improvement were reported (Shen 2012). In analyzing this case, the parameters of the silty clay layer below the depth of 10 m were assumed by fitting the measured amount of compression of

this soil layer. The detailed soil parameters, embankment cross section and measured lateral displacement are shown in Fig. 4.9
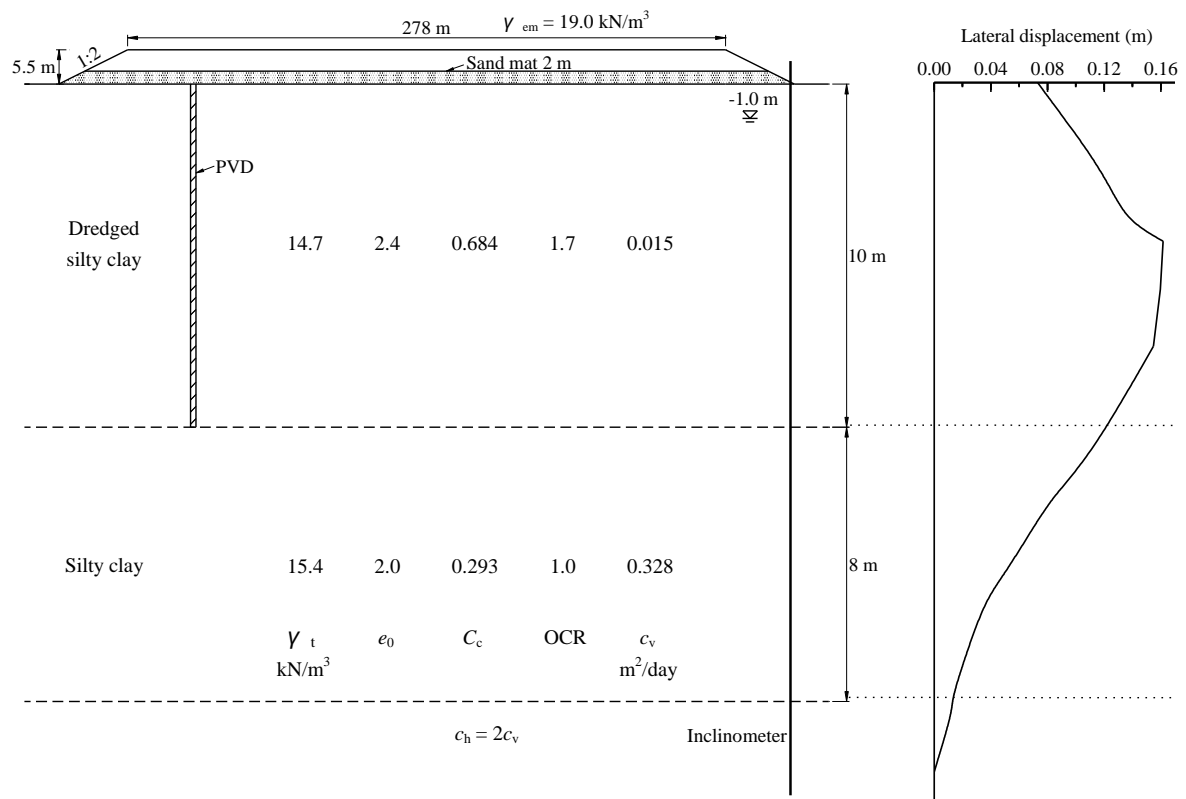
Fig. 4.9 Cross-section of embankment, soil profile and lateral displacement profile of Case 9

(8) Embankment in Sichuan, China (Cases 10 and 11)

The Suining-Ziyang expressway is an improtant component of the second trafic line from the east to the west of Sichuan Province, China. The expressway locates in the Sichuan Basin, and the soft ground mainly consists of fluvisols, diluvial soils and marsh sedimentary soils (Xiong 2012). The ground water lever is about 1 to 4 m below the ground surface. Prelaoding with installation of PVDs had been used to improve the soft ground.

The analyzed embankments are two sections (Case 10, K70 + 050; Case 11, K71 + 830) of this expressway. The soft ground can be mainly divided into a high liquid limit clay layer (locating at the ground surface) and a low liquid limit clay layer below it. For both of Cases 10 and 11, the former layer was about 2 m, while the later layer was 8 m for Case 10 and 9 m for Case 11. The PVDs used had a cross section measuring 100 mm $\times$ 4 mm and

they were installed in a square pattern with spacing of 1.5 m to fully penetrate the soft subsoil layers.
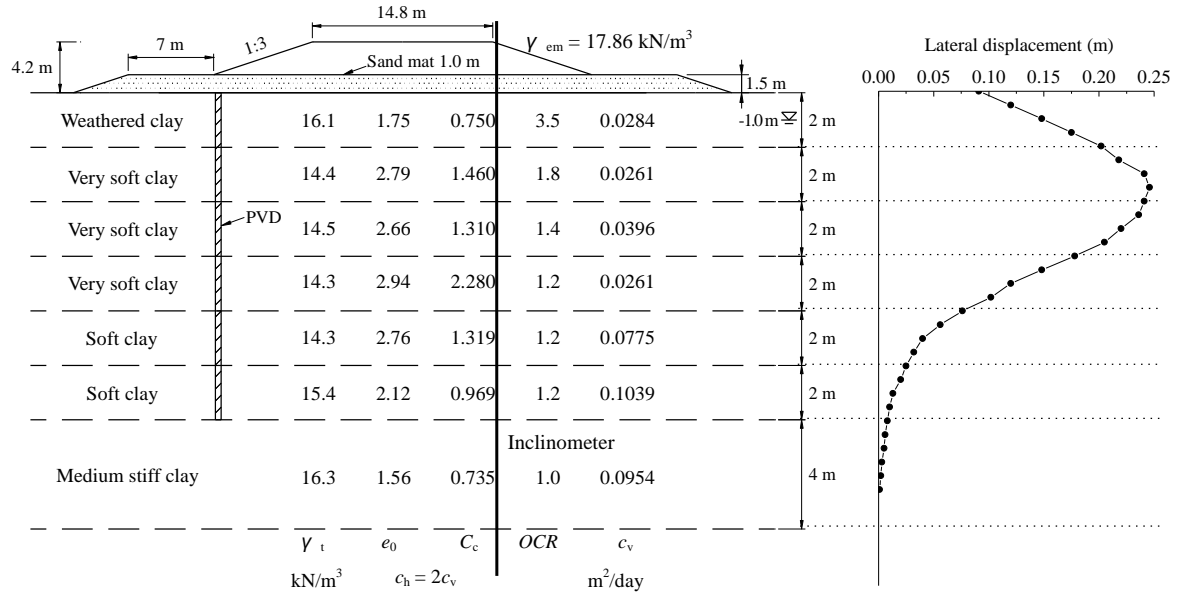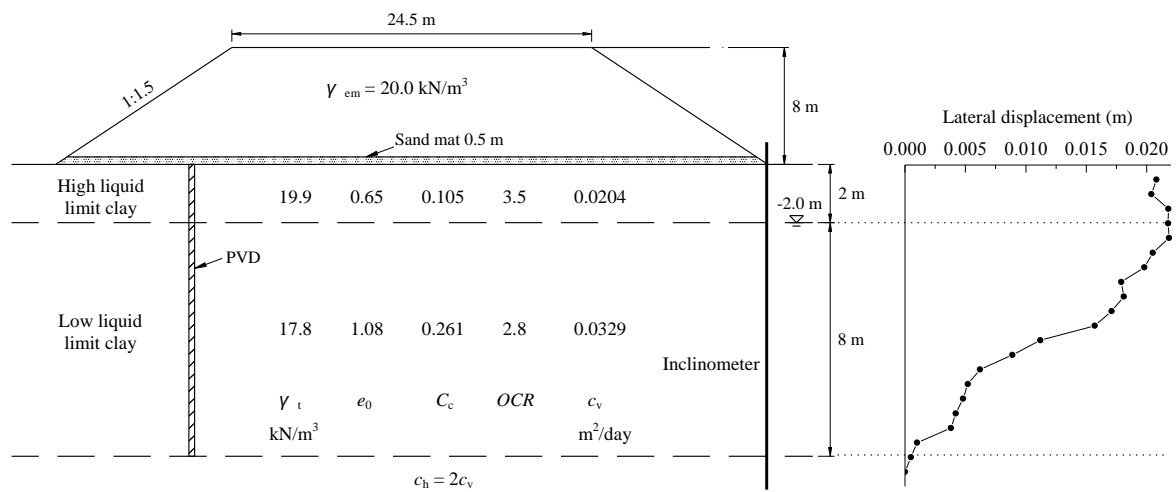

Fig. 4.10 Cross-section of embankment, soil profile and lateral displacement profile of Case 10
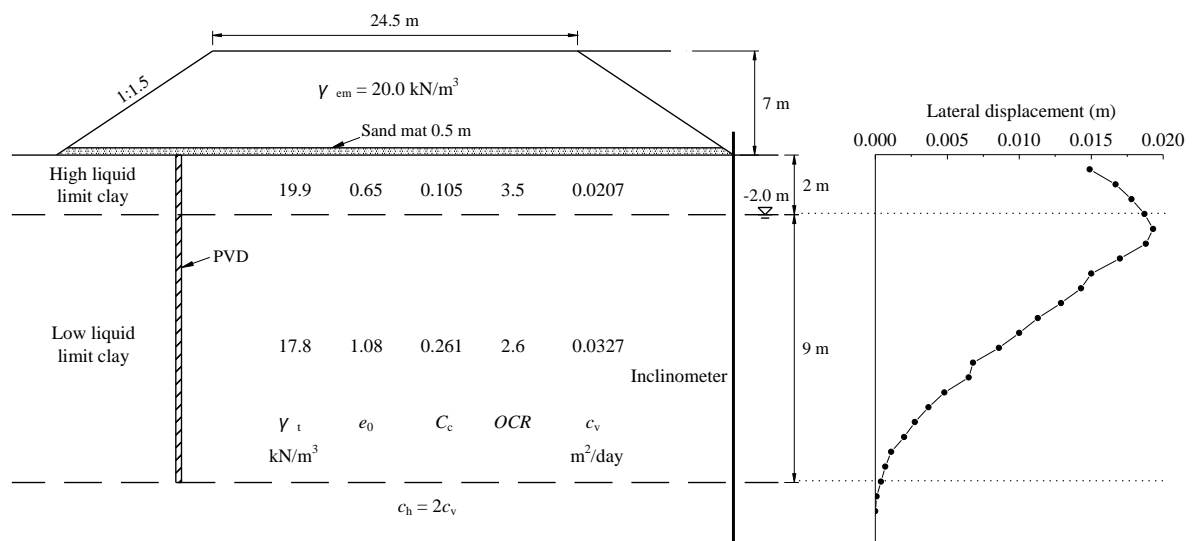
Fig. 4.11 Cross-section of embankment, soil profile and lateral displacement profile of Case 11

A 0.5 m thick gravel sand layer was first placed on the ground surface, then the embankment fill with unit weight of about 20 kN/m^3 was used to built an embankment with a total height of 8 m for Case 10 and 7 m for Case 11. The detailed soil parameters, embankment geometry as well as the measured lateral displacement are shown in Figs 4.10 and 4.11 for Cases 10 and 11, respectively.

(9) Embankment in Belfast, UK (Case 12)

Kelln *et al*. (2007) reported a highway embankment stabalized by geotextiles on a soft estuarine deposit in Belfast, Northern Ireland. To reduce the consolidation time as well as to increase the rate of strenght gain of the soft subsoil, PVDs were used to improve the soft deposit.

The highway embankment was constructed in a preglacial valley. The water lever is approximately 0.5 m below the ground surface. The surface soil layer of about 1.5 m thick is a recent alluvial deposit which consists of clayey sandy silt with trace gravel, soft sandy silty clay with occasional roots and soft slightly organic silty clay with occasional thin seams of peat. The second layer is a estuarine deposit with thickness of about 8.5 m and it mainly consists of very soft organic silt clay with decayed lenses and stems, occasional thin layers of silty fine to medim sand, and very soft grey organic silty clay with occasional thin seams of brown silty peat and grey brown fine sand. Below the soft estuarine deposit, there is a gravle layer underlain by a outwash sand layer with interbedded gravel and silts and clays. In the analysis, the surface soil layer was termed as a weathered layer and the second soil layer was termed as a silty clay layer and their properties are listed in Fig. 4. 12.
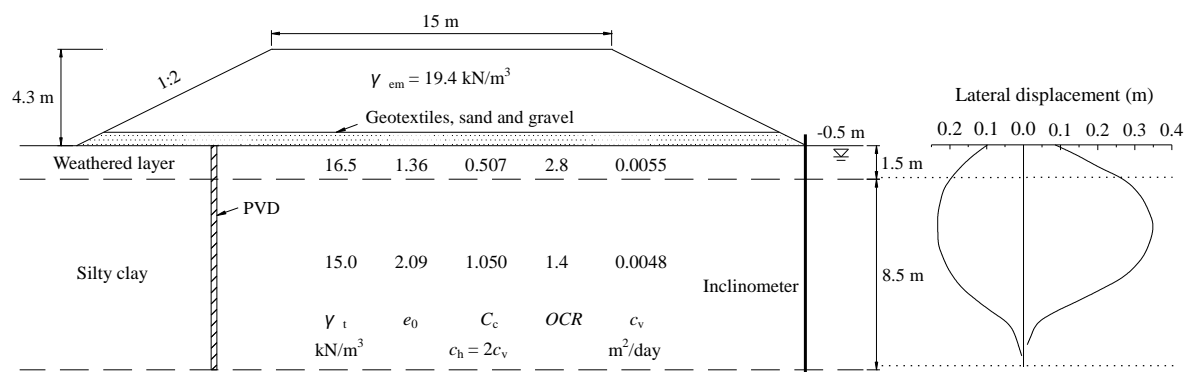
Fig. 4.12 Cross-section of embankment, soil profile and lateral displacement profile of Case 12

After placing the first reinforcement layer of geotextiles with sand and gravel, the PVDs were instlled fully penetrating the estuarine deposit in a triangular pattern with spacing of 1.5 m. The width of the PVD-improved area was wider than the base of the embankent. The tops of the PVDs were cut off more than 0.5 m above the existing ground surface within the base area of the embankment and 0.3 m above the ground beyond the toes of the embankment. Then, the upper geotextile reinforcement layer was placed. The

73

cohesive fill with average unit weight of 19.4 kN/m^3 was applied to construct an embankment with maximum height of about 4.3 m.

(10) Test embankment in Queensland, Australia (Case 13)

The development of economic and increase of population in the region of Sunshine Coast, Queensland, Australia, had brought high pressure to the main trafic line of Sunshine Motorway in this area. In order to collect data and experience for the design of future trafic lines, a well instrumented full-scale test embankment was constructed and investigated in 1992 (Sathananthan 2005).
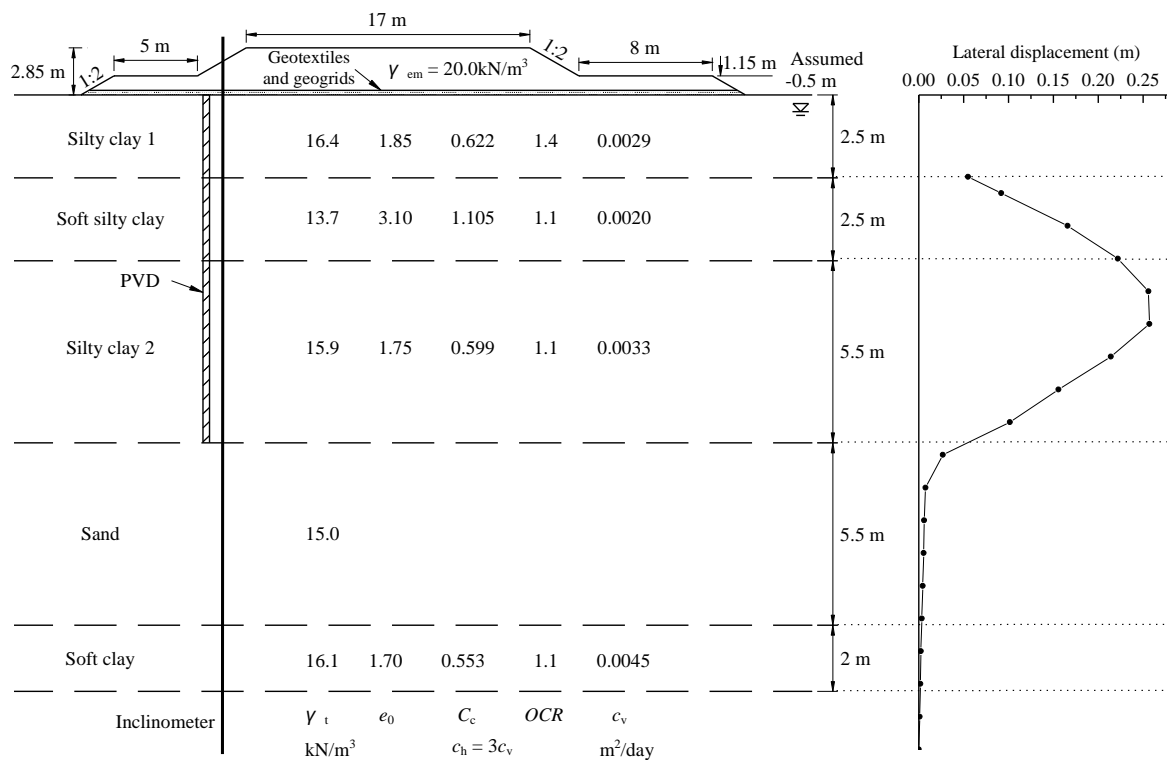
Fig.4.13 Cross-section of embankment, soil profile and lateral displacement profile of Case 13

The soft subsoil is comprised by very soft saturated marine clays with high compressibility and high sensitivity. A 10.5 m thick silty clay layer locats at the ground surface. This layer can be further subdivided into a 2.5 m silty clay layer, a 2.5 m soft silty clay layer and another silty clay layer with thickness of 5.5 m. Below the silty clay layer, there is a 5.5 m thick sand layer overlies a soft clay layer of 2 m thick. The swelling index for the soil layers were found to be about one tenth of the corresponding compression

74

index. And all the soil layers were lightly overconsolidated with overcosolidation ratio varying between 1.0 to 1.6. The soil parameters of the soil layers are shown in Fig. 4.13.

The trial embankment covered an area measuring 90 m $\times$ 40 m and it was devided into three sections: Section A (35 m long with PVD spacing of 1 m), Section B (35 m long without PVD improvement), and Section C (20 m long with PVD spacing of 2 m). Here, the embankment of Section A was analyzed. A reforcement layer consisted of geotextiles and geogrids were first placed on the ground surface. Then a working platform formed by a 0.5 m thick screenings drainage material and a 1.5 m thick selected fill was constructed. PVDs were then installed to a depth of 11 m, spaced 1 m with a triagular pattern. Then a 2.85 m high embankment was built by stage construction using a compacted granular material with average unit weight of 20 kN/m^3. The embankment geometry and measured lateral displacement are also presented in Fig. 4.13.

(11) Embankment in China (Cases 14 and 15)

A 5.85 km long two-way road was constructed in a costal regin in China (Hu 2004). The soft deposit is a shoal (madflat) and ground water level was about 2 m below the ground surface. A sludge layer with thickness varying from 0.5 m to 19 m widely destributs at the ground surface and underlain by two silty clay layers.

To accelerate the consolidation process as well as to increase the rate of strengh gain of the soft subsoils, sandwick drains were installed to improve the soft ground. The vertical drains used had a diameter of 0.07 m and they were install in a triangular pattern with spacing of 1 m. For Case 14, the length of the vertical darins was 7 m. While for Case 15, the exact length of the PVDs is not clear, and by referring the reported range of PVDs lengths (Hu 2004), a value of 7.0 m was assumed.

The detailed soil profiles and soil properties as well as the embankment cross section and the measured lateral displacement are shown in Figs 4.14 and 4.15 for Cases 14 and 15, respectively. For these two cases, the measured ground settlement cannot be fitted with values of C_c back-calculated from the reported compression moduli (E_s) by using average effective vertical stress during consolidation process. As a result the values of C_c listed in Figs 4.14 and 4.15 were back-calculated assuming that the reported values E_s are corresponding to stress increement from 100 kPa to 200 kPa (a value generally given in site investigation report in China).

Fig. 4.14

52 m

$\gamma_{em} = 19.0$ kN/m³   3.73 m

1:2

Lateral displacement (m)
0.00   0.02   0.04   0.06

Sludge layer	15.9	1.73	0.496	1.5	0.0056	-2.0 m	3.2 m
SD						Inclinometer	
Silty clay 1	18.9	0.83	0.101	1.2	0.0330		3.8 m
Silty clay 2	18.9	0.83	0.101	1.0	0.0773		18 m
	γ_t	e_0	C_c	OCR	c_v		
	kN/m³		$c_h = 2c_v$		m²/day		
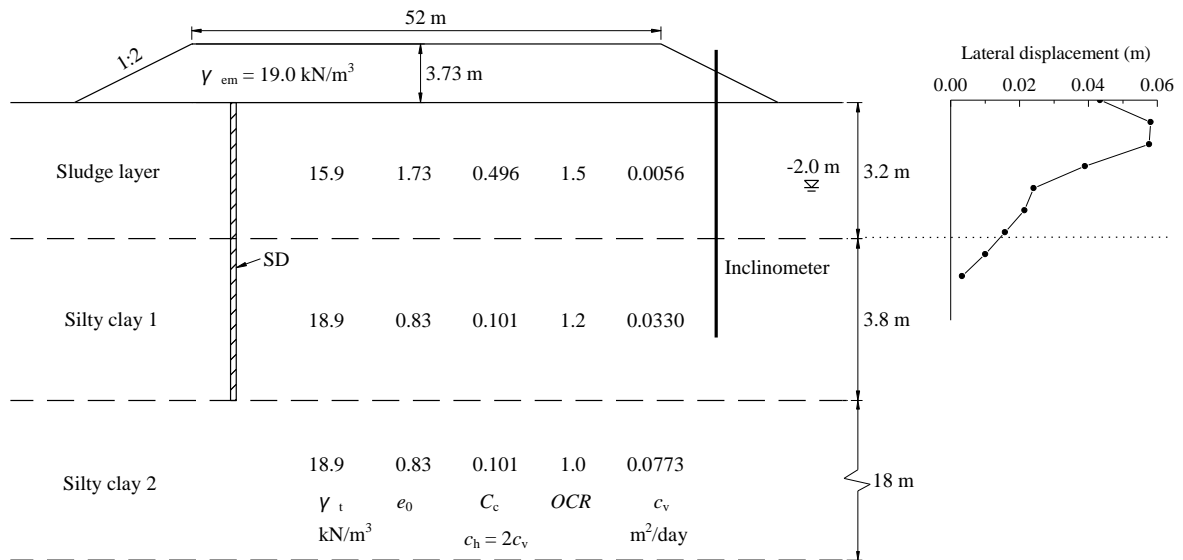
Fig. 4.14 Cross-section of embankment, soil profile and lateral displacement profile of Case 14

Fig. 4.15

52 m

$\gamma_{em} = 19.0$ kN/m³   5.37 m

1:2

Lateral displacement (m)
0.00   0.05   0.10   0.15   0.20

Sludge layer	15.9	1.73	0.496	1.0	0.0090	-2.0 m	5.6 m
SD						Inclinometer	
Silty clay 1	18.9	0.83	0.101	1.0	0.0524		1.4 m
Silty clay 2	18.9	0.83	0.101	1.0	0.1298		18 m
	γ_t	e_0	C_c	OCR	c_v		
	kN/m³		$c_h = 2c_v$		m²/day		
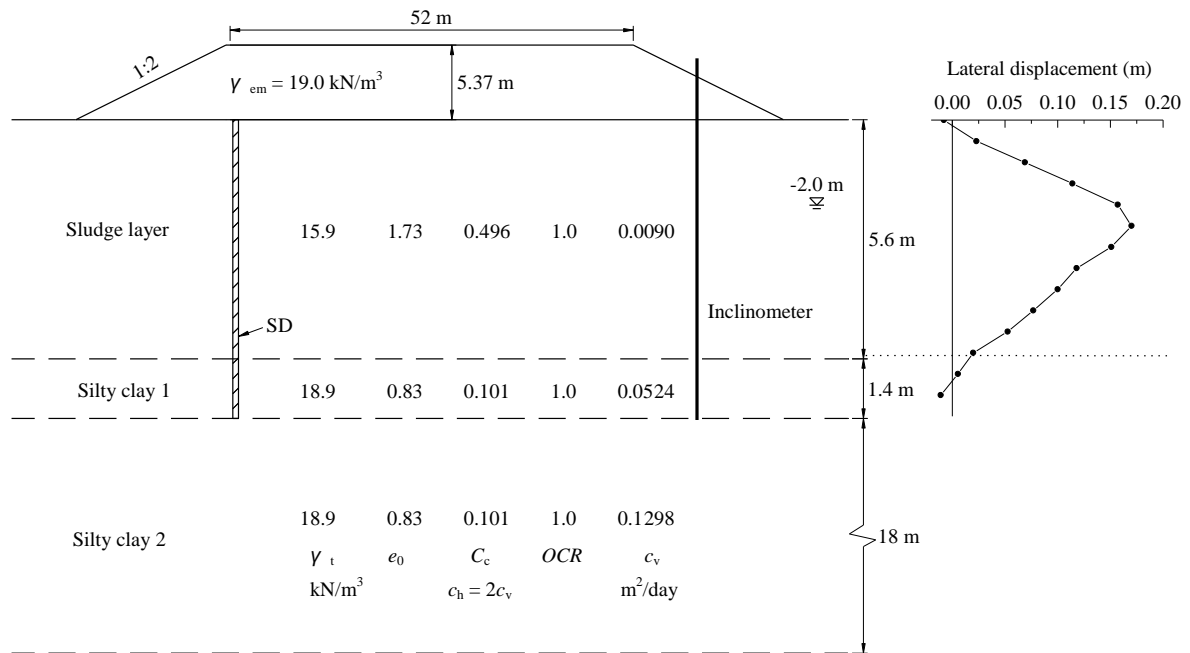
Fig. 4.15 Cross-section of embankment, soil profile and lateral displacement profile of Case 15

(12) Embankment on the Muar Plain, Malaysia (Case 16)

Redana (1999) reported an embankment stabalized by sand compaction piles (SCPs) on Muar clayey deposit, Malaysia. The thickness of the soft deposit is about 20 m. A weathered surface layer of 2 m followed by four soft silty clay layers with thickness of 3.5 m, 2.5 m, 2 m and 10 m, respectively. The soil parameters using in analysis are presented in Fig. 4.16.

Sand compaction piles were installed in a suqare pattern with a spacing of 2.2 m. The diameters of the SCPs were 1.4 m for the first 10 m thick soil layers and 1 m for the silty clay layer from 10 m to 20 m. The diameter of the smear zones were estimated as 2 times of the diameters of the SCPs. The discharge capacity were 500 m^3/year and 300 m^3/year for the SCPs with diameter of 1.4 m and 1 m, respectively. A compacted fill with unit weight of 20.5 kN/m^3 was used to construct an embankment with maximum height of 9.3 m.
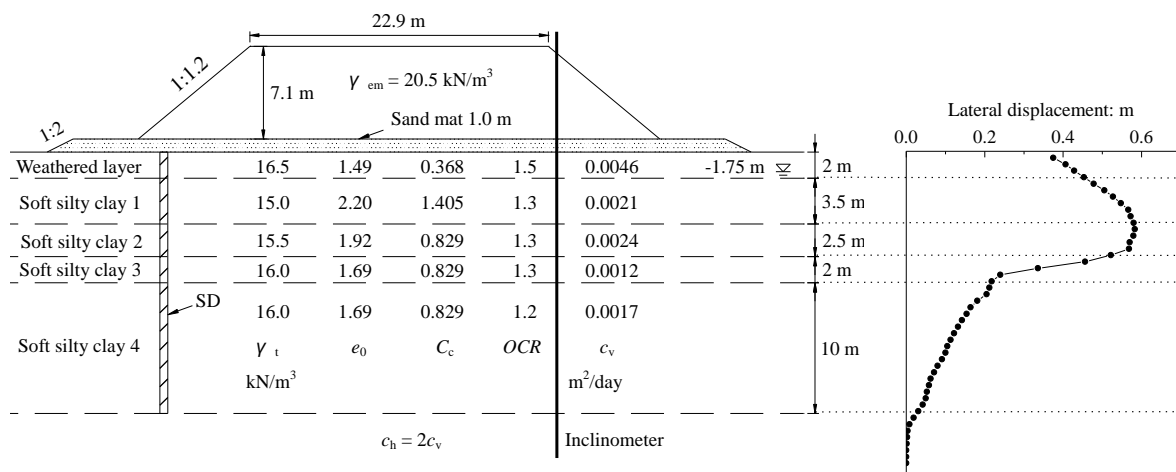
Fig. 4.16 Cross-section of embankment, soil profile and lateral displacement profile of Case 16

Generally, the behavior of the soft ground improved by SCPs is different from that has been improved by sand drains or PVDs due to the relative higher stiffness of the SCPs. However, in this field case, the final measured settement at the ground surface on the embankment centerline reached about 2.8 m, i.e., a relatively large value, and so it is considered that the so-called SCPs might actually have functioned more like sand drains (SDs), and hence it is included into this study as a SD case. Furthermore, for this case the final embankment fill thickness was 9.3 m. However, when the embankment reached about 8.1 m fill thickness at about 201 days of elasped time from the start of the embankment construction, this fill thickness was maintained untill about 415 days of total elapsed time, i.e., a consolidation period under constant load of about 214 days. Then the additional 1.2 m thickness of fill was applied (Redana 1999). The available measured lateral displacemnt profile is at the elapsed time of 201 days from the beginning of embankment construction. Considering these factors, the embankment was analyzed assuming a fill thickness of 8.1 m, and the measured settlement just before applying the final 1.2 m of fill (at the elapsed time of 415 days) was used in the analysis.

(13) Embankments in Samutprakarn Province, Thailand (Cases 17 and 18)

Three test embankments, T1 and T2 on sandwick drains improved ground and T3 on natural deposit, were constructed to investigate the performance of the soft ground in Samutprakarn Province, Thailand. Here the sandwick drains imrpoved cases T1 and T2 were analyzed regarded as Cases 17 and 18, respectively.

The soft subsoil has a total thickness of 17 m and can be divided into five layers. A weathered clay layer of 3 m overlies a very soft clay layer of 5 m, followed by three soft clay layers with thicknesses of 3.5 m, 2.5 m and 3 m, respectively. The water content of the subsoils varies between 40% to 75%, and the unit weight varies within 15 to 18 kN/m^3. The soil profiles and the necessary soil properties are shown in Figs 4.17 and 4.18 for Cases 17 and 18, respectivley.
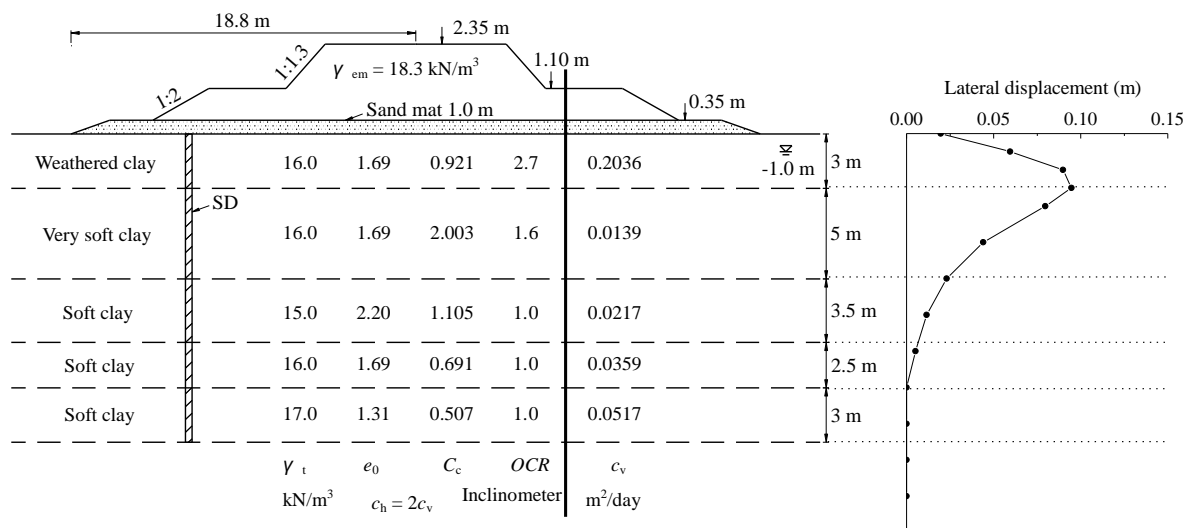
Fig. 4.17 Cross-section of embankment, soil profile and lateral displacement profile of Case 17

The sandwick drains used were comprised by a fibrous materail with high permeability filled with dry sand and had a diameter of 5 cm. The drains were installed in the ground to a depth of 17 m and formed a square pattern with spacings of 1.5 m and 2.5 m for Cases 17 and 18, respectivley. The embankments were constructed to a maximum height of 2.35 m. A Sand mat of 0.35 m was first placed on the ground surface, then the embankment fill was built to a height of 1.1 m and finally raised to 2.35 m. The embankment geometry, soil parameters and measured lateral displacement for Cases 17 and 18 were shown in Figs 4.17 and 4.18, respectively.

78

18.8 m   2.35 m

1.10 m

$\gamma_{em} = 18.3$ kN/m³

Sand mat 1.0 m

1:2   1:1.3   0.35 m

Lateral displacement (m)
0.00   0.05   0.10   0.15   0.20

-1.0 m

Soil layer	γ_t kN/m³	e_0	C_c	OCR	c_v m²/day	Thickness
Weathered clay	16.0	1.69	0.921	2.7	0.2036	3 m
Very soft clay	16.0	1.69	2.003	1.6	0.0139	5 m
Soft clay	15.0	2.20	1.105	1.0	0.0217	3.5 m
Soft clay	16.0	1.69	0.691	1.0	0.0359	2.5 m
Soft clay	17.0	1.31	0.507	1.0	0.0517	3 m

SD

$c_h = 2c_v$ Inclinometer
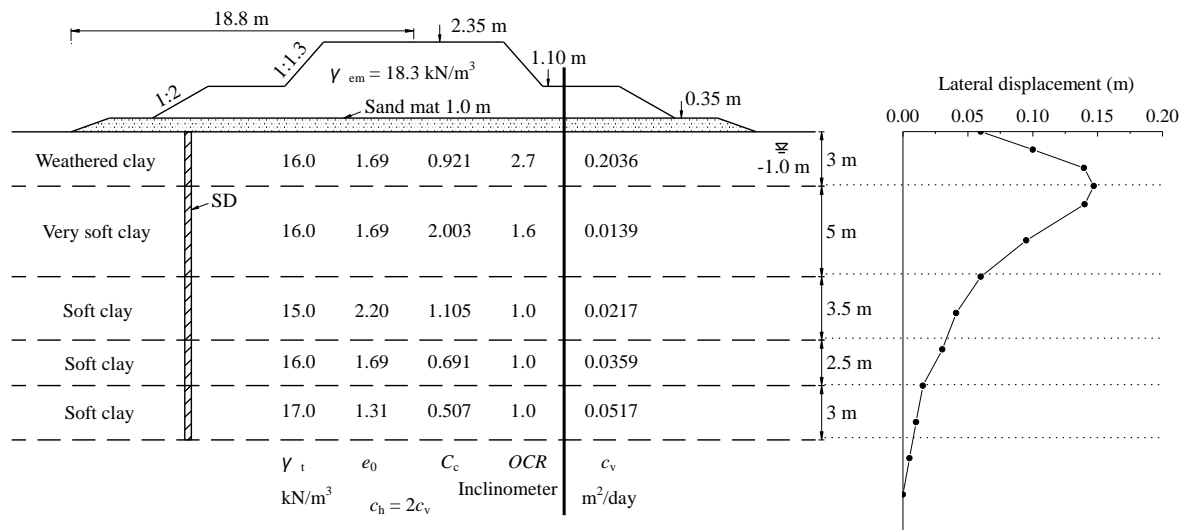
Fig. 4.18 Cross-section of embankment, soil profile and lateral displacement profile of Case 18

4.2.3 Summary of case histories

The location, loading history, parameter determination methods and sources of the 18 case histories are summarized in Table 4.1. The embankment geometry, soil profile, PVD/SD installation depth, location of inclinometer casing and the final measured maximum lateral displacement profiles are shown in Figs 4.1-4.18 for Case 1 to Case 18, respectively. Values of initial total unit weight (γ_t), initial void ratio (e_0), compression index (C_c), OCR and c_v, as well as the location of groundwater level are included in the figures. Embankment loading history and parameters for analyzing the PVD/SD-induced consolidation are summarized in Table 4.2.

For most cases, the lateral displacments were measured under the toe of the embankment. However, in some cases they were measured under the berm or under the slope of the embankment. While, in the analyses, the available measurements were directly used in the analysis.

There are four (4) cases for which basal reinforcement, e. g., geotextile, was placed under the embankments. However, at working load conditions the reinforcement does not have a significant effect on reducing the maximum lateral displacement (e.g., Chai *et al.* 2002). The effect of embankment geometry is only considered when calculating the total vertical stress increment in the ground (Osterberg, 1957), and for simplicity its effect on the shear stresses induced in the ground is not considered.

Table 4.1 Summary of case histories and parameter determination methods

Case	Project and section	Construction history (days)	M	C	A	R	Source
			Parameter determination method				
1	Embankments on the Muar Plain, Malaysia	400	γ_t, C_c	e_0, OCR, c_v, c_h	d_s, k_h/k_s, q_w		Indraratna $et\ al.$ (1997)
2		240	γ_t, C_c^a	e_0, OCR, c_v, c_h		d_s, k_h/k_s, q_w	Lin and Chang (2009)
3	Embankments at Second Bangkok International Airport (SBIA), Thailand	240	γ_t, C_c^a	e_0, OCR, c_v, c_h		d_s, k_h/k_s, q_w	Bergado $et\ al.$ (1996); Lin and Chang (2009)
4		245	γ_t, e_0	OCR, c_v, c_h		d_s, k_h/k_s, q_w	Indraratna and Redana (2000); Indraratna $et\ al.$ (2007);
5	Embankments at Hong Kong, China	320	γ_t	e_0, C_c, OCR, c_v, c_h		d_s, k_h/k_s, q_w	Cowland & Wong (1993)
6	Embankments at Hangzhou-Ningbo (HN) Expressway, China	257	γ_t, e_0, C_c	OCR, c_v, c_h		d_s, k_h/k_s, q_w	Chai $et\ al.$ (2001);
7	Embankments at Jiangsu, China	622	γ_t, e_0	C_c, OCR, c_v^b, c_h	d_s, k_h/k_s, q_w		He & Dai (2000)
8	Embankment at Zhejiang, China	250	γ_t, e_0, C_c	OCR, c_v, c_h	d_s, q_w	k_h/k_s	Guo $et\ al.$ (2006); Zheng (2006)
9	Embankment at a port in south of China	102	γ_t, C_c	e_0, OCR, c_v, c_h	d_s, q_w	k_h/k_s	Shen (2012)
10	Embankment at Sichuan province, China	165	γ_t,	e_0, C_c, OCR, c_v, c_h	d_s, k_h/k_s, q_w		Xiong (2012)
11		217	γ_t,	e_0, C_c, OCR, c_v, c_h	d_s, k_h/k_s, q_w		
12	Embankment at Belfast, Britain	218	γ_t, C_c	e_0, OCR, c_v, c_h	d_s, k_h/k_s, q_w		Kelln $et\ al.$ (2007)
13	Embankment at Queensland, Australia	56	γ_t, e_0, C_c	OCR, c_v, c_h	d_s, q_w	k_h/k_s	Sathananthan (2005)
14	Embankment in China	189	γ_t	e_0, C_c, OCR, c_v, c_h	k_h/k_s, q_w	d_s	Hu (2004)
15		284	γ_t	e_0, C_c, OCR, c_v, c_h	k_h/k_s, q_w	d_s	
16	Embankments on the Muar Plain, Malaysia	201	γ_t, C_c	e_0, OCR, c_v, c_h	k_h/k_s	d_s, q_w	Redana (1999)
17	Embankments at Samutprakarn Province, Thailand	121	γ_t, C_c	e_0, OCR, c_v, c_h	k_h/k_s	d_s, q_w	
18		121	γ_t, C_c	e_0, OCR, c_v, c_h	k_h/k_s	d_s, q_w	

Notes: d_s = diameter of smear zone; q_w = discharge capacity of PVD/SD; and k_h/k_s = hydraulic conductivity ratio where k_h and k_s are the hydraulic conductivities of natural soil in the horizontal direction and smear zone respectively; and OCR = overconsolidation ratio.

M: measured value; C: back-calculated or calculated from other known values of the related parameters; A: assumed; R: obtained from the source reference;

[a]The value of C_c of the surface layer is assumed. [b]The value of c_v of the filled surface layer is assumed.

Table 4.2 Loading conditions and parameters for PVD/SD consolidation

Case	H_{em} (m)	γ_{em} (kN/m^3)	p_{em} (kPa)	PVD/SD parameters						Remark
				D_e (m)	d_w (m)	d_s (m)	k_h/k_s	q_w (m^3/year)	H_L (m)	
1	8.7	20.5	178.4	2.26	0.07	0.3	2	100	18	Muar Plain, Malaysia
2	4.2	17.86*	75	1.695	0.052	0.168	8	65	12	Bangkok, Thailand
3	4.2	17.86*	75	1.356	0.052	0.168	8	65	12	
4	4.2	17.86*	75	1.13	0.06	0.3	1.8	60	12	
5	5.0	19	95	1.575	0.053	0.26	2	100	6.5	Hong Kong, China
6	5.88	20	117.6	1.575	0.053	0.355	13.8	100	19	HN Expressway, China
7	15.6	19.23	300	1.26	0.052	0.25	2	50	30	Jiangsu, China
8	6.0	20.3	122	1.26	0.052	0.25	10	50	25	Zhejiang, China
9	5.5	19	104.5	1.13	0.052	0.25	3	100	10	South of China
10	8.0	20	160	1.695	0.052	0.25	2	100	10	Sichuan, China
11	7.0	20	140	1.695	0.052	0.25	2	100	11	
12	4.3	19.4	83.4	1.575	0.052	0.21	2	100	10	Belfast, Northern Ireland
13	2.85	20.0	57.0	1.05	0.07	0.2	2.65	100	10.5	Queensland, Australia
14	3.73	19	71	1.05	0.07	0.3	8	100	7	China
15	5.37	19	102	1.05	0.07	0.3	8	100	7	
16	8.1	20.5	166.1	2.48	1.4, 1	2.8, 2	2	500, 300	10, 20	Muar Plain, Malaysia
17	2.35	18.3	43	1.695	0.1	0.6	2.0	50	17	Samutprakarn, Thailand
18	2.35	18.3	43	2.825	0.1	0.6	2.0	50	17	

*Average value.

4.3 *NLD-RLS* Relationship of Case Histories Collected

4.3.1 Basic equations

The main equations for determining the values of *NLD* and *RLS* are as follows:

$$NLD = \frac{\delta_m}{S_f} \tag{4.1}$$

$$RLS = \frac{p_n}{s_u} \tag{4.2}$$

$$p_n = p_{em}(1-U) \tag{4.3}$$

$$s_u = S_l \sigma'_v (OCR)^m \tag{4.4}$$

where δ_m is the maximum lateral displacement in the ground under the toe of an embankment; and S_f is the settlement of the ground surface on the centerline of an embankment. p_{em} is the maximum value of the embankment load; and U and s_u are the

average degree of consolidation and representative undrained shear strength of the PVD-improved zone corresponding to the end of embankment construction, respectively. OCR is overconsolidation ratio; and S_1 and m are costants. Detailed discussions of Eqs. (4.1) to (4.4) can be found in Chapter 3.

In analyzing the field cases, to verify the correctness of the parameters adopted, the simulated settlement-time curve may need to be compared with the measured one. For this purpose and for a clayey deposit improved by the installation of PVDs that only partially penetrate the deposit, the degree of consolidation of the clayey sub-layer without the PVDs also needs to be evaluated. In this study, the method proposed by Ong *et al*. (2012) for evaluating the degree of consolidation was used due to its simplicity, accuracy and ease of use in comparison with other approximate methods (e.g. Zeng and Xie 1989) or semi-analytical solutions (Tang and Onitsuka 1998; Zhang *et al*. 2005).

4.3.2 Analzed results

The measured maximum lateral displacements (δ_m) and the settlments (S_f) of the ground surface on the centerline of the embankments and the calculated values of U, p_n, s_u, *NLD* and *RLS* are listed in Table 4.3.

Table 4.3 Calculated values of *NLD* and *RLS*

Case	U (%)	p_n (kPa)	s_u (kPa)	*NLD*	S_f (m)	δ_m (m)	*RLS*	Remark
1	59.9	71.5	40.0	0.180	2.72	0.49	1.788	Muar Plain, Malaysia
2	50.6	37.1	19.1	0.182	1.28	0.233	1.940	
3	60.2	29.9	20.8	0.167	1.47	0.246	1.435	Bangkok, Thailand
4	76.8	17.4	22.3	0.156	1.40	0.218	0.780	
5	60.7	37.3	19.6	0.288[*]	0.66	0.19[*]	1.905	Hong Kong, China
6	67.2	38.6	40.9	0.236	1.95	0.46	0.943	HN Expressway, China
7	81.6	55.2	84.8	0.156	2.909	0.453	0.651	Jiangsu, China
8	76.5	28.7	49.6	0.101[*]	1.38	0.139[*]	0.578	Zhejiang, China
9	79.0	21.9	29.1	0.138	1.169	0.1617	0.754	South of China
10	96.6	5.4	54.7	0.116	0.189	0.02184	0.099	Sichuan, China
11	96.8	4.5	51.8	0.112	0.172	0.0193	0.086	
12	60.9	32.6	19.5	0.228[*]	1.28	0.292[*]	1.672	Belfast, Northern Ireland
13	33.2	38.1	13.1	0.329	0.78	0.257	2.915	Queensland, Australia
14	72.7	19.4	22.7	0.193	0.3	0.058	0.855	China
15	76.9	23.6	28.8	0.230	0.74	0.17	0.818	
16	51.6	80.4	39.1	0.232	2.51	0.583	2.055	Muar Plain, Malaysia
17	56.0	18.9	20.3	0.128	0.74	0.095	0.930	Samutprakarn, Thailand
18	39.5	26.0	18.9	0.253	0.59	0.149	1.374	

[*]Average of the values from both sides of the corresponding embankment.

The calculated data points of (*RLS*, *NLD*) are plotted in Fig. 4.19. For Cases 5, 8 and 12, the lateral displacements at both sides of the embankments were measured, so ranges of value of *NLD* are also indicated in Fig. 4.19.
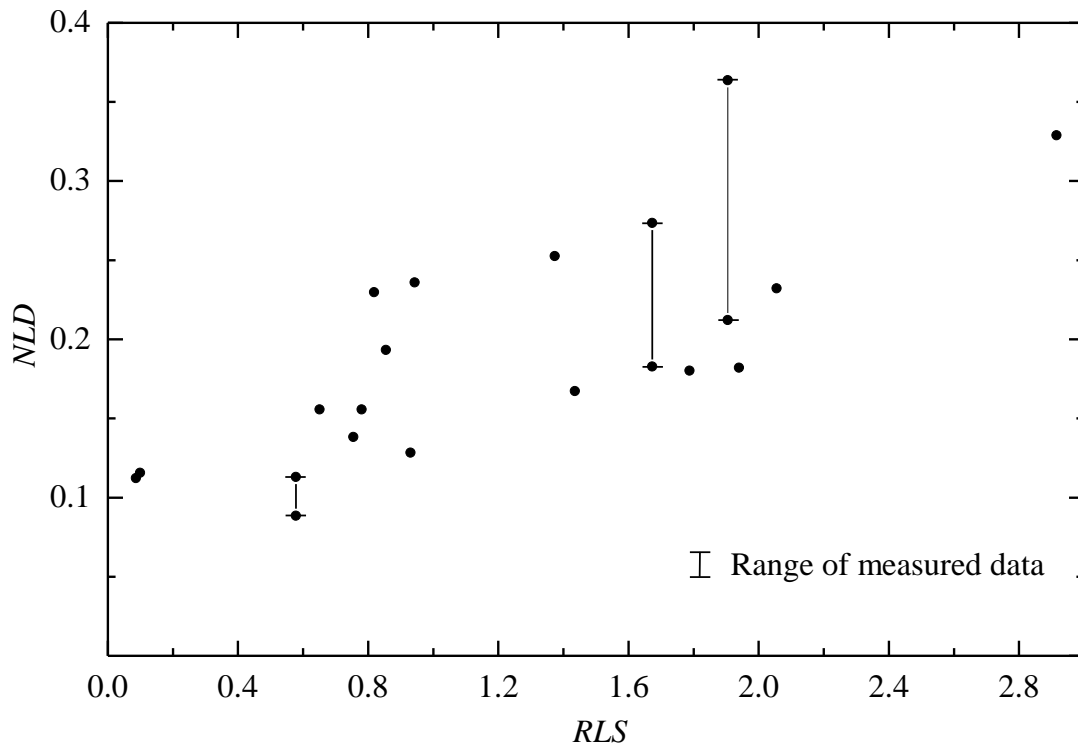
Fig. 4.19 Analyzed *NLD* and *RLS* from field case histories

In Fig. 4.19, it shows considerable scatter of the data points. However, there is a general overall trend of *NLD* increases with increase of *RLS*, as revealed by the laboratory model tests reported in Chapter 3. The possible reasons for the scatter of the data points are:

(1) The 18 field cases analyzed had different embankment geometeries, different subsoil profiles and different construction processes;

(2) For some cases the lateral displacements were not measured under the toe of the embankment, which might have caused some scatter of the data points;

(3) The method used involves the main factors infuencing lateral displacment. However, there are other factors that may also have effects on the lateral displacement (e.g. the slope of the embnakment, embankment stiffness and foundation roughness) and they are not involved in calculating *RLS*.

4.4 Summary and Comments

For investigating the ground lateral displacement, 18 field case histories of embankments constructed on PVD or SD improved deposits were collected from five different countries and then analyzed. For each of them, the basic information required to investigate the lateral displacement, i.e. measured maximum lateral displacement (δ_m) and ground surface settlement (S_f), and total unit weight (γ_t), initial void ratio (e_0), compression index (C_c), swelling index (C_s), coefficient of consolidation and overconsolidation ratio (OCR) of the soft subsoil were directly obtained or indirectly back-calculated from the source references. Then, each case has been analyzed using normalized lateral displacement (*NLD*, designated as the ratio of δ_m/S_f) and a ratio of load to undrained shear strength (s_u) of the soft subsoil (*RLS*).

NLD can be directly calculated from the measured data. While *RLS* is a parameter approximately inversely proportional to the factor of safety of the system (FS), and to get its value the degree of consolidation (*U*) and the undrained shear strength of the subsoil layers are calculated first and then *RLS* is calculated using Eq. (4.2). The analyzed results of *NLD* and *RLS* for the 18 cases are presented in a *NLD-RLS* plot (Fig. 4.19). It shows a general trend of *NLD* increases with increase of *RLS*.

CHAPTER FIVE
PROPOSED PREDICTION METHOD

5.1 Introduction

Construction of embankments on soft clayey deposits improved by installation of prefabricated vertical drains (PVDs) as one of the most efficient and cost-effective methods has been widely used. Embankment load not only induces consolidation pressures but also shear stresses in the soft clayey deposit. The shear stresses will cause outward lateral displacement of the ground. Normally, the maximum lateral displacement occurs on the vertical line around the toe of an embankment. If an embankment is going to be constructed in urban area or near existing buildings or structures, predicting the lateral displacement of the ground will often be an essential requirement. However, due to the complexities of natural deposit, predicting the lateral displacement remains as a difficult task in geotechnical engineering.

The main factors affecting lateral displacement are the magnitude of the preloading load, loading rate, and the compression, consolidation and strength properties of the soft subsoil. In this chapter, considering the effects of these main affecting factors, a method has been proposed for predicting the maximum lateral displacement of PVD-improved deposit under embankment loading with and without the application of vacuum pressure. The method is based on the investigations of a series of large-scale laboratory model tests and more than 30 field case histories.

5.2 Methodology

The proposed method is an empirical relationship between the normalized maximum lateral displacement (*NLD*) and a ratio of load to undrained shear strength of the soft

subsoil (*RLS*). The main equations for determining the values of *NLD* and *RLS* are as follows:

$$NLD = \frac{\delta_m}{S_f} \qquad (5.1)$$

$$RLS = \frac{p_n}{s_u} \qquad (5.2)$$

$$p_n = p_{em}(1-U) \qquad (5.3)$$

$$s_u = S_1 \sigma_v' (\mathrm{OCR})^m \qquad (5.4)$$

where δ_m is the maximum lateral displacement in the ground under the toe of an embankment; and S_f is the settlement of the ground surface on the embankment centerline. p_{em} is the maximum value of the embankment load; and U and s_u are the average degree of consolidation and representative undrained shear strength of the PVD-improved zone corresponding to the end of embankment construction, respectively. OCR is overconsolidation ratio; and S_1 and m are costants. Detailed discussions of Eqs. (5.1)-(5.4) can be found in Chapter 3.

Based on the analyzed results of the laboratory model tests and field case histories, a relationship between *NLD* and *RLS* has been proposed. The value of *RLS* and S_f can be calculated prior an embankment construction. And then from the *NLD-RLS* relationship, a value of *NLD* is obtained, and therefore δ_m can be predicted.

5.3 Proposed Method for Predicting Lateral Displacement

The analyzed values of *NLD* and *RLS* from laboratory model tests reported in Chapter 3 and the field case histories under embankment loading collected in Chapter 4 are presented in a *NLD-RLS* plot, as Fig. 5.1. There is a general trend of *NLD* increases with increase of *RLS*.

A regression analysis for the *NLD-RLS* relationship has been made based on the data plotted in Fig. 5.1, and the regression line established is as:

$$NLD = 0.066 \cdot RLS + 0.11 \ (0.05 \leqslant RLS \leqslant 3.0) \qquad (5.5)$$

For the laboratory model tests and some field cases the lateral displacement at two sides of the embankment (or loading area) were measured. In the regression analysis, the average values of *NLD* calculated from the measurements at two sides were used.
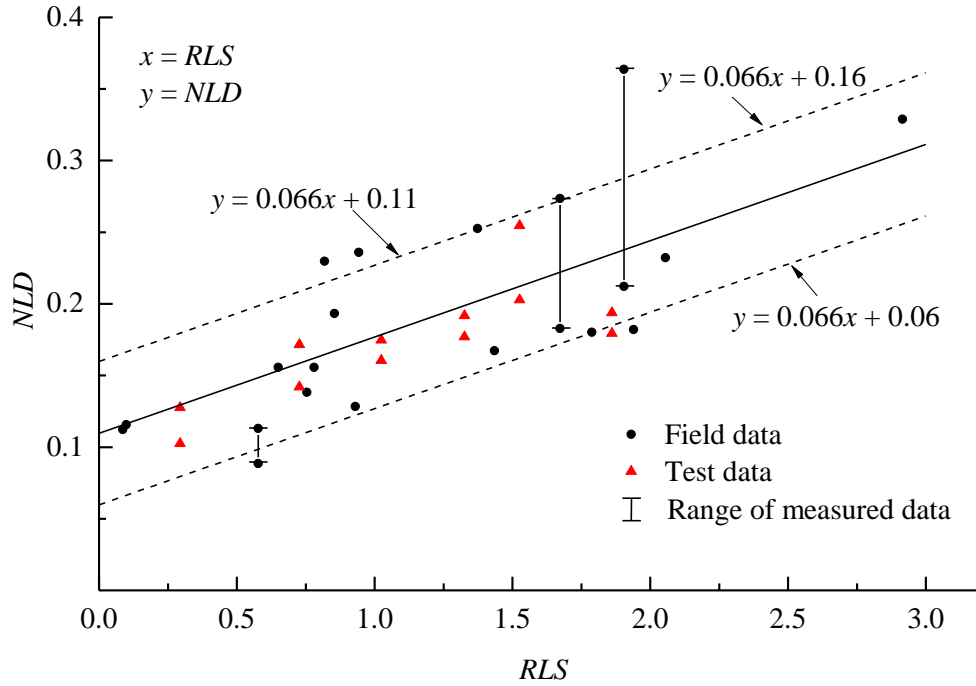
Fig. 5.1 *NLD-RLS* relationship for the case of only embankment loading

The *NLD-RLS* correlation given by Eq. (5.5) provides a general trend for the field-measured data and the results of laboratory model tests, but considerable scatter about this average trend is still noted. The case histories collected from different countries had different embankment geometeries, different subsoil profiles and different construction processes, and there are other factors that may also have effects on the lateral displacement (e.g. the slope of the embnakment and embankment stiffness, which are not considered in the prediction method). It is considered that estimating a likely range for the values of *NLD* instead of a unique line may be more practical. Therefore, it is proposed that the likely ranges of values of *NLD* are predicted by Eq. (5.5) $\pm$ 0.05, and expressed as:

$$NLD = 0.066 \cdot RLS + 0.11 \pm 0.05 \ (0.05 \leqslant RLS \leqslant 3.0) \tag{5.6}$$

The proposed range for predicting values of *NLD* are also indicated in Fig. 5.1 with dashed lines. In the figure, it is observed that all of the data points used in the regression analysis are within the proposed range or very close to the bounds of the range. The fact that even for the same embankment or the same model test, the measured lateral displacements at two sides are different supports the idea of proposing a range for predicting the values of *NLD* instead of a unique line.

With the range of the values of *NLD* and the predicted ground surface settlment on the embankment centerline (S_f), the likely ranges of values of maximum lateral displacemnt (δ_m) can be calculated using Eq. (5.1).

5.4 Discussions

Chai *et al*. (2013) made a similar analysis for the field cases of PVD-improved deposits under embankment loading but with the application of vacuum pressure and proposed a *NLD-RLS* relationship for the combined loading condition. However, due to the application of vacuum pressure and the fact that there might be inward lateral displacement near the ground surface and outward lateral displacement below a certain depth, a maximum net lateral displacement (δ_{nm}, the maximum outward value subtracting the maximum inward value) was used to calculate the value of *NLD*:

$$NLD = \frac{\delta_{nm}}{S_f} \tag{5.7}$$

Also, the vacuum pressure (p_{vac}) was included in calculating the index load (p_n):

$$p_n = p_{em} - \left(\left|p_{vac}\right| + p_{em}\right)U \tag{5.8}$$

For comparison, the regression line generated by Chai *et al*. (2013) is plotted together with the regression line proposed in present study, as shown in Fig. 5.2. The *NLD-RLS* relationship for the case with vacuum pressure is as:

$$NLD = 0.168 \cdot RLS + 0.05 \pm 0.05 \ \ (\text{-}1.5 \leq RLS \leq 0.75) \ \text{(with vacuum pressure)} \tag{5.9}$$
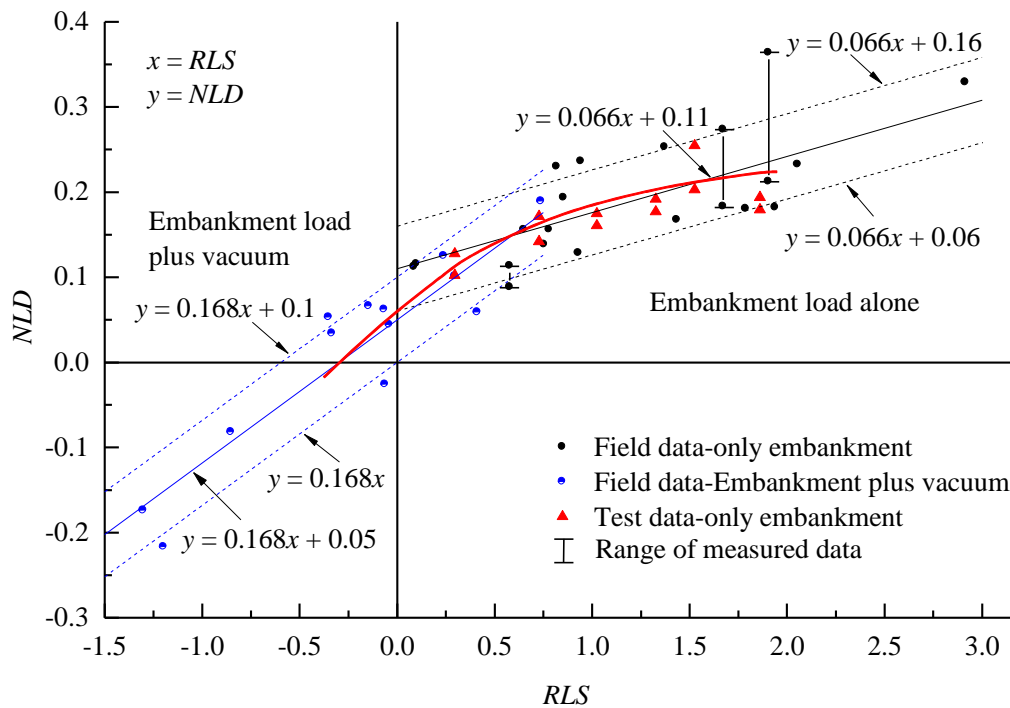
Fig. 5.2 Combined *NLD-RLS* relationships (with and without vacuum pressure)

In Fig. 5.2, it can be seen that the relationship proposed in present study for the case of only embankment loading intercepts the line proposed by Chai *et al*. at a *RLS* value of about 0.6. *RLS* = 0.6 is close to the upper limit of *RLS* value of 0.75 to using Eq. (5.9) for the case with vacuum pressure. In addition, the gradient of the lines for the case with and without vacuum pressure are different. The line for the case without vacuum is less steep. Generally, the cases with embankment load alone have larger maximum outward lateral displacement than the cases of combined vacuum pressure and embankment load. The larger maximum lateral displacement implies larger shear straining in the zones above and below the location where the maximum lateral displacement occurs, resulting a greater constraining effect for further development of the maximum lateral displacement. This kind of mechanism is illustrated in Fig. 5.3. As a result, the rate of increase of *NLD* with *RLS* is seen to reduce with increasing *NLD* (Fig. 5.2), namely for cases without application of vacuum pressure.

$$\tau_{a1} < \tau_{a2}; \ \tau_{b1} < \tau_{b2}$$
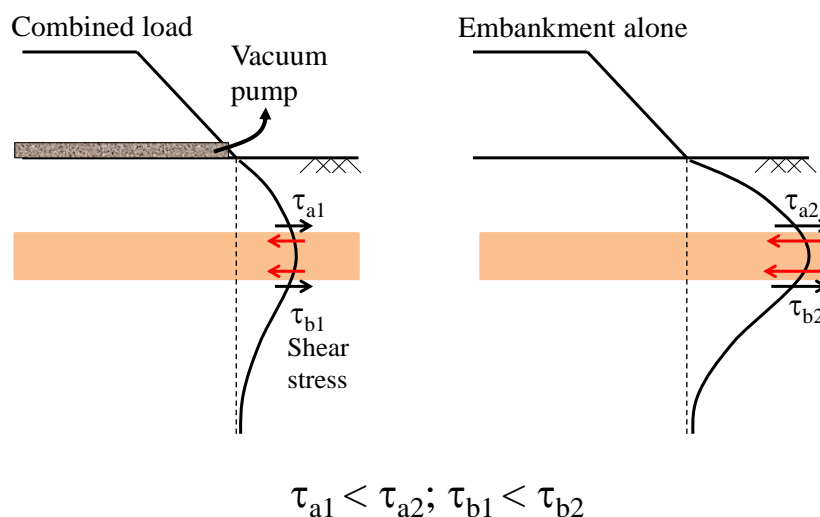
Fig. 5.3 Illustration of shear stresses induced by lateral displacement in the ground

In Fig. 5.2, viewing only the data points (excluding the regression lines), it can be observed that the overall *NLD-RLS* relationship for both the cases with and without vacuum pressure may not be two segmented straight lines, but entirely curved, i.e. *NLD* does not linearly increase with the increase of *RLS*. A general nonlinear relationship between *NLD* and *RLS* is also indicated in Fig. 5.2, as the red curve line. While the differences between the curved line and the straight lines are small, and for simplicity, it is still proposed to use the straight lines in design.

Another point is that for the case of embankment loading alone, there is only one data point for $RLS > 2.1$. A model test was conducted with a higher loading rate, intending to result in a larger value of RLS, but the model ground was collapsed before the planed total surcharge load of 60 kPa was applied. Based on the model test results and considering the factor of only one (1) data point for $RLS > 2.1$, it is suggested to limit the upper bound of RLS to 2.1. Then, the proposed prediction equations from this study are as follows:

$$NLD = 0.168 \cdot RLS + 0.05 \pm 0.05 \ (\text{-}1.5 \leqslant RLS \leqslant 0.6) \ (\text{with vacuum pressure}) \quad (5.10a)$$

$$NLD = 0.066 \cdot RLS + 0.11 \pm 0.05 \ (0.6 \leqslant RLS \leqslant 2.1) \ (\text{without vacuum pressure}) \quad (5.10b)$$

And the predicted ranges of *NLD-RLS* relationship are shown in Fig. 5.4.
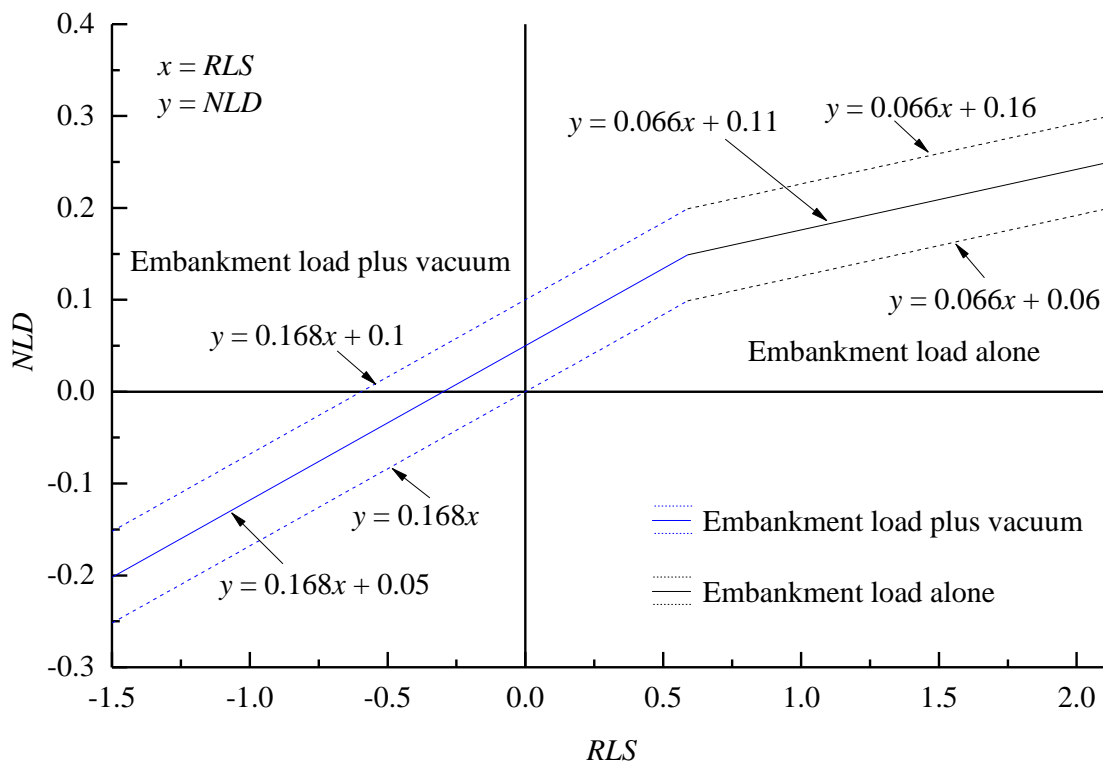
Fig. 5.4 Relationship of *NLD-RLS* use in design

5.5 Verification of the Proposed Method

The proposed *NLD-RLS* relationship is based on investigations of field case histories and laboratory model tests. Here, the proposed method is applied to analyze some new field cases and new laboratory model tests under only embankment load or under combined embankment load and vacuum pressure, which were not included in developing

the prediction method, to verify the usefulness of the proposed method and also to demonstrate on how to use this method.

5.5.1 New field cases under only embankment loading

(1) Brief description

Feng (2013) reported two highway embankments constructed on PVD-improved deposits in Sichuan Province, China. The embankments are parts of the expressway connecting the cities of Suining and Ziyang (SZ expressway).

The expressway passes through some alluvial soft clayey deposits. The soft deposits can be mainly divided into a very soft clay layer with high liquid limit locating at the ground surface and a soft clay layer with low liquid limit below it. In this region, PVDs were installed for accelerating the highway embankment induced consolidation of the soft deposits.

The two embankments reported are at the mileages of K85 + 330 and K89 + 100, respectively. The groundwater level is about 0.5 m below the ground surface. For the embankment at K85 + 330, the soft ground consits of a 6 m thick very soft clay layer overlying a 3.5 m thick soft clay layer. While for the embankment at K89 + 100, the soft ground mainly comprises a 7.5 m thick soft clay layer.

The PVDs used to improve the soft deposit had a cross section measuring 100 mm $\times$ 4 mm and they were installed to fully penetrate the soft clayey layers in a triangular patern, with spacings of 1.3 m and 1.5 m for the embankments at K85 + 330 and K89 + 100, respectively. The parameters related to PVD consolidation are listed in Table 5.1, which are referred from the commonly used PVDs in the market.

Table 5.1 Parameters for PVD consolidation of embankments at SZ expressway

Mileage	D_e (m)	d_w (m)	d_s (m)	q_w (m3/year)	k_h/k_s	l
K85 + 300	1.365	0.052	0.26	100	4.44, 3.75	9.5
K89 + 100	1.575	0.052	0.26	100	4.44	7.5

D_e = diameter of unit cell (a mini-PVD and its improvement area); d_w = diameter of mini-PVD; d_s = diameter of smear zone; k_h = horizontal hydraulic conductivity of undisturbed zone; k_s = hydraulic conductivity of smear zone; q_w = discharge capacity of mini-PVD; l = drainage length of PVD.
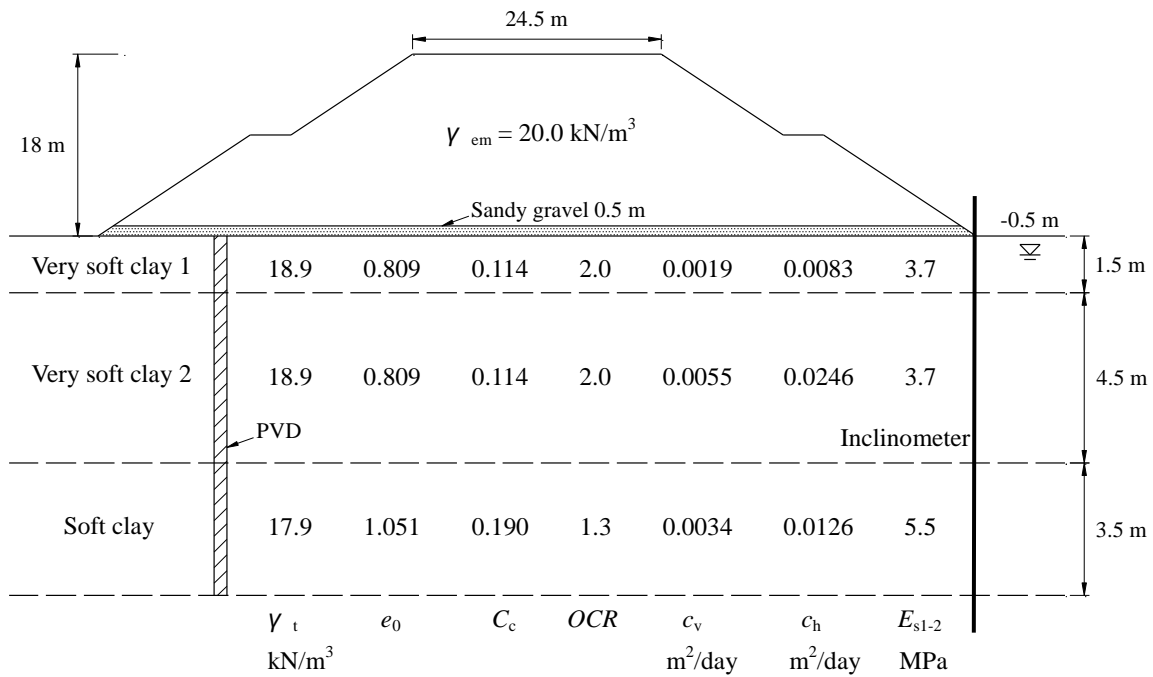
Fig. 5.5 Cross-section and soil profile of embankment at K85 + 330

	γ_t kN/m³	e_0	C_c	OCR	c_v m²/day	c_h m²/day	$E_{s1\text{-}2}$ MPa	
Very soft clay 1	18.9	0.809	0.114	2.0	0.0019	0.0083	3.7	1.5 m
Very soft clay 2	18.9	0.809	0.114	2.0	0.0055	0.0246	3.7	4.5 m
Soft clay	17.9	1.051	0.190	1.3	0.0034	0.0126	5.5	3.5 m

(Embankment: 18 m high, top width 24.5 m, γ_{em} = 20.0 kN/m³, Sandy gravel 0.5 m, PVD, Inclinometer, water table -0.5 m)
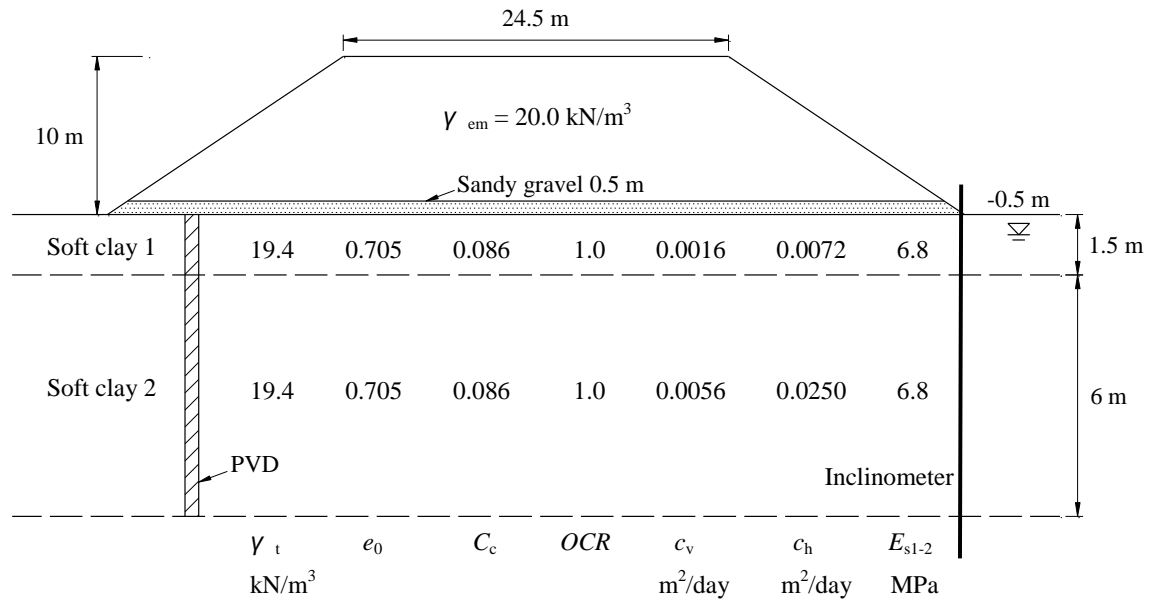
Fig. 5.6 Cross-section and soil profile of embankment at K89 + 110

	γ_t kN/m³	e_0	C_c	OCR	c_v m²/day	c_h m²/day	$E_{s1\text{-}2}$ MPa	
Soft clay 1	19.4	0.705	0.086	1.0	0.0016	0.0072	6.8	1.5 m
Soft clay 2	19.4	0.705	0.086	1.0	0.0056	0.0250	6.8	6 m

(Embankment: 10 m high, top width 24.5 m, γ_{em} = 20.0 kN/m³, Sandy gravel 0.5 m, PVD, Inclinometer, water table -0.5 m)

During the construction of the embankments, a 0.5 m thick sandy gravel layer was first placed on the ground surface to act as a surface drainage layer. Then the embankment fill with unit weight of about 20 kN/m³ was used to built an embankment with a total height of 18 m at K85 + 330 and 10 m at K89 + 100, corresponding to total embankment loads of 360 kPa and 200 kPa, respectively. The top width of the constructed embankment is 24.5

m. The detailed embankment geometries, soil profiles and some basic soil parameters are presented in Figs. 5.5 and 5.6 for the embankments at K85 + 330 and K89 + 100, respectively and the embankment construction histories are presented in Fig. 5.7. In Figs. 5.5 and 5.6, E_{s1-2} means compression modulus corresponding to effective stress increment of 100 to 200 kPa and the values of c_v, c_h and OCR were back-calculated by fitting the measured ground surface settlement-time curves. In the analyses, the surface soil layer had been subdivided into two layers with the first sub-layer had a thickness of 1.5 m, which is about the diameter of the unit cell of the PVD-improvement.
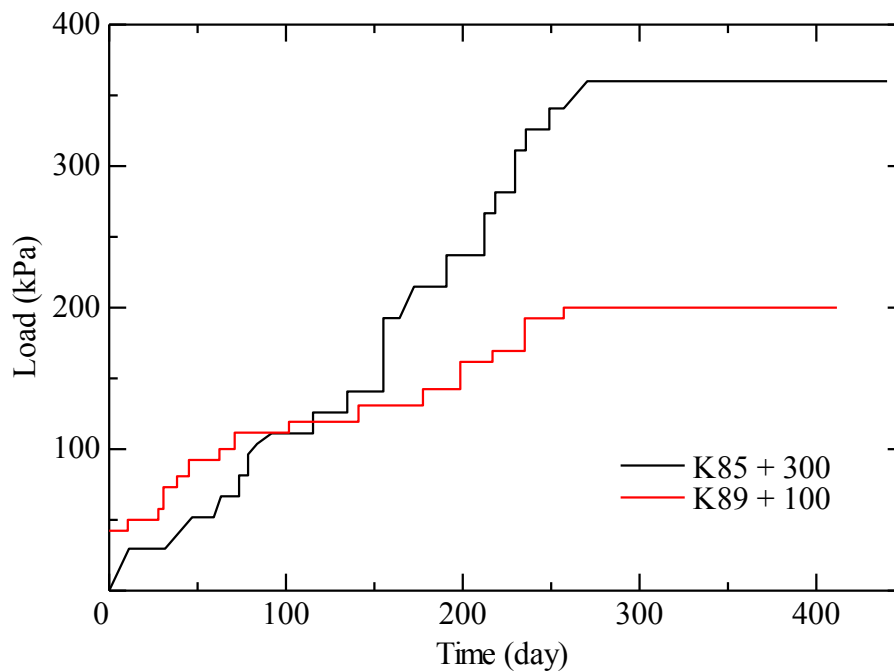
Fig. 5.7 Embankment loading histories of K85 + 300 and K89 + 100

(2) Predicting maximum lateral displacement

(a) Calculations of S_f, U and s_u

With the soil parameters given in Figs. 5.5 and 5.6 and the loading histories presented in Fig. 5.7, the ground surface settlement-time curves, the degree of consolidation (U) and undrained shear strength (s_u) of the PVD-improved zone corresponding to the end of embankment construction are calculated first.

In calculating the degree of consolidation as well as the settlement-time curves, the whole embankment loading process was simulated by 4 steps of stepwise loading for both

of the embankments. The ground surface settlements at the embankment centerline (S_f) is calculated under one-dimensional compression assumption but considering the spreading of vertical stress in the ground due to the embankment load by Osterberg (1957)'s chart. The value of U is calculated using Terzaghi (1925)'s 1D consolidation theory and Hansbo (1981)'s solution, and considering stepwise loading by the method of Chai and Miura (2002). The value of s_u is calculated using Ladd (1991)'s equation. The calculated values of S_f, U and s_u are listed in Table 5.2.

Table 5.2 Predicted results of embankments at SZ expressway

Mileage	U (%)	p_n (kPa)	s_u (kPa)	S_f (m)	RLS	Predicted NLD	Predicted δ_m (m)	Measured δ_m (m)
K85 + 300	65.4	124.56	70.3	0.531	1.772	0.177 to 0.277	0.096 to 0.150	0.125
K89 + 100	71.9	56.2	45.9	0.313	1.224	0.141 to 0.241	0.044 to 0.075	0.056

The analyzed final surface settlements on the embankment centerline are 0.531 m and 0.313 m, which are quite close to the measured values of 0.541 m and 0.311 m for the embankments at K85 + 300 and K89 + 100, respectively. The measured and analyzed ground settlement-time curves are presented in Figs. 5.8 and 5.9. It clearly shows that the analyzed curves agree reasonably well with the measured ones, which implies the correctness of the calculated degree of consolidation.
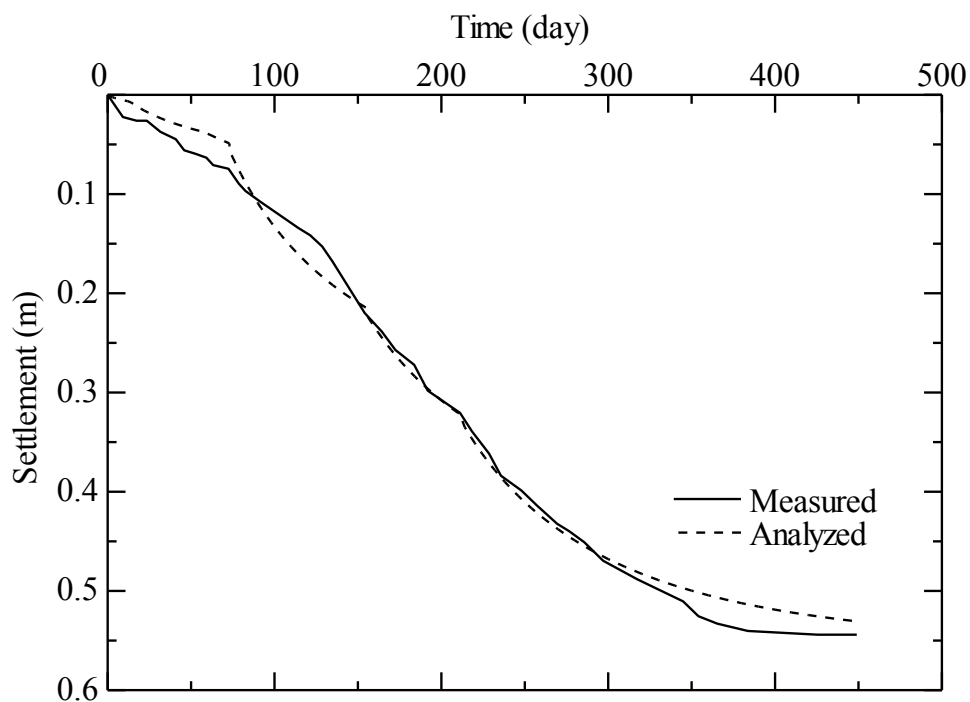
Fig. 5.8 Measured and calculated settlement-time curves at K85 + 300
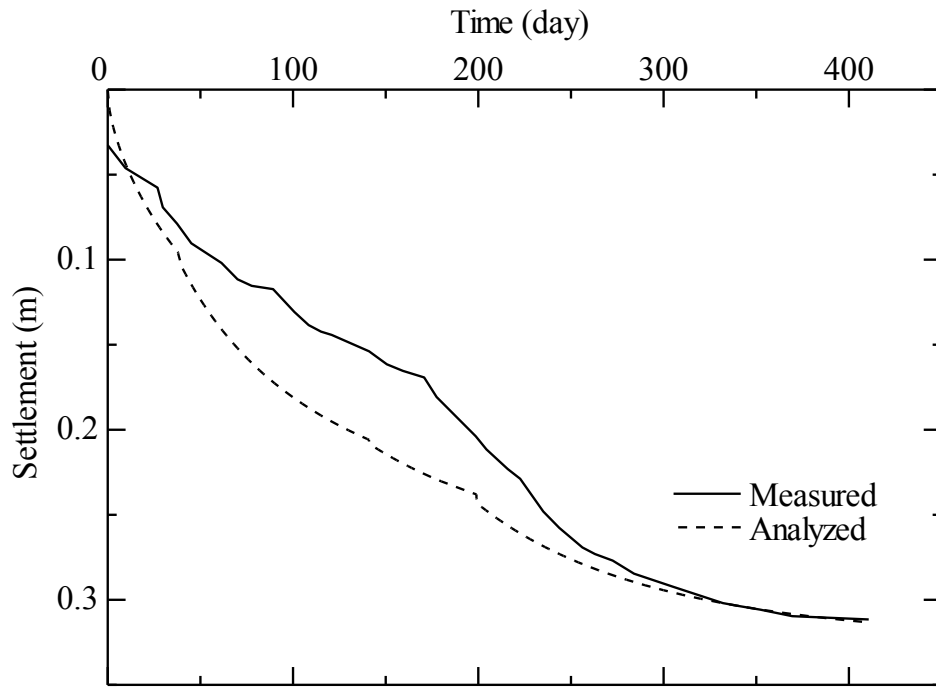
Fig. 5.9 Measured and calculated settlement-time curves at K89 + 100

(b) Calculation of *RLS*

With the known values of U, s_u and embankment load (p_{em}), the values of *RLS* are calculated as follows (using Eqs. (5.2) and (5.3)):

For embankment at K85 + 300;

$$p_n = p_{em}(1-U) = 360 \times (1-0.654) = 124.56 \text{ kPa}$$

$$RLS = \frac{p_n}{s_u} = \frac{124.56}{70.3} = 1.772$$

For embankment at K89 + 100;

$$p_n = p_{em}(1-U) = 200 \times (1-0.719) = 56.2 \text{ kPa}$$

$$RLS = \frac{p_n}{s_u} = \frac{56.2}{45.9} = 1.224$$

The calculated values of p_n and *RLS* are also listed in Table 5.2.

(c) Prediction of *NLD*

With *RLS* known, the value of *NLD* can be predicted using the proposed prediction method. The analyzed two embankments are cases under only embankment load, therefore Eq. (5.10b) is used. The calculated values of *NLD* are as follows:

For embankment at K85 + 300;

$$NLD = 0.066 \cdot RLS + 0.11 \pm 0.05 = 0.066 \times (1.772) + 0.11 \pm 0.05 = 0.227 \pm 0.05$$

For embankment at K85 + 300;

$$NLD = 0.066 \cdot RLS + 0.11 \pm 0.05 = 0.066 \times (1.224) + 0.11 \pm 0.05 = 0.191 \pm 0.05$$

As a result, the predicted ranges of *NLD* are 0.177 to 0.277 and 0.141 to 0.241 for embankments at K85 + 300 and K89 + 100, respectively, as listed in Table 5.2.

(d) Prediction of lateral displacement

Using the values of S_f and *NLD*, the maximum lateral displacement (δ_m) is predicted as (using Eq. (5.1)):

For embankment at K85 + 300;

$$\delta_m = S_f \times NLD = 0.541 \times NLD$$

For embankment at K89 + 100;

$$\delta_m = S_f \times NLD = 0.311 \times NLD$$

For both of these two embankments, the final measured values of S_f were available. Here the measured values of S_f were used instead of the calculated values to predict δ_m. The predicted ranges of δ_m are 0.096 m to 0.150 m and 0.044 m to 0.075 m for embankments at K85 + 300 and K89 + 100, respectively, as listed in Table 5.2.

(3) Comparison of the predicted and measured lateral displacements.

The measured maximum lateral displacement profiles under the toe of the embankment at mileages of K85 + 300 and K89 + 100 are shown in Figs. 5.10 and 5.11, respectively. It is observed that the maximum value of lateral displacement appeared at a depth of about 1.5 m to 2.5 m. And the values of δ_m were about 0.125 m and 0.056 m which are close to the average values of the predicted ranges of 0.096 m to 0.150 m and 0.044 m to 0.075 m, as listed in Table 5.2. The values of *NLD* calculated from the measurements of S_f and δ_m are 0.231 and 0.180, and the data points of (*RLS*, *NLD*) are plotted in Fig. 5.12 together with the predicted range from the proposed *NLD-RLS* relationship.
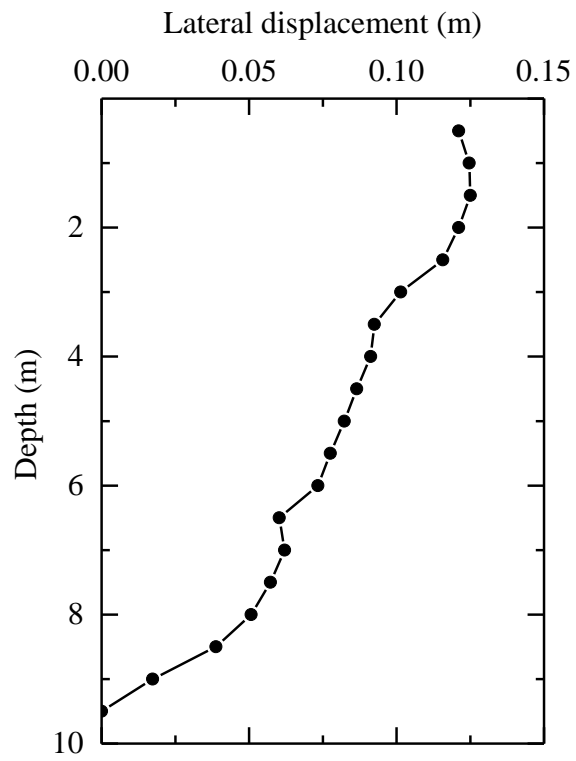
Fig. 5.10 Measured lateral displacement at K85 + 300 (after Feng 2013)
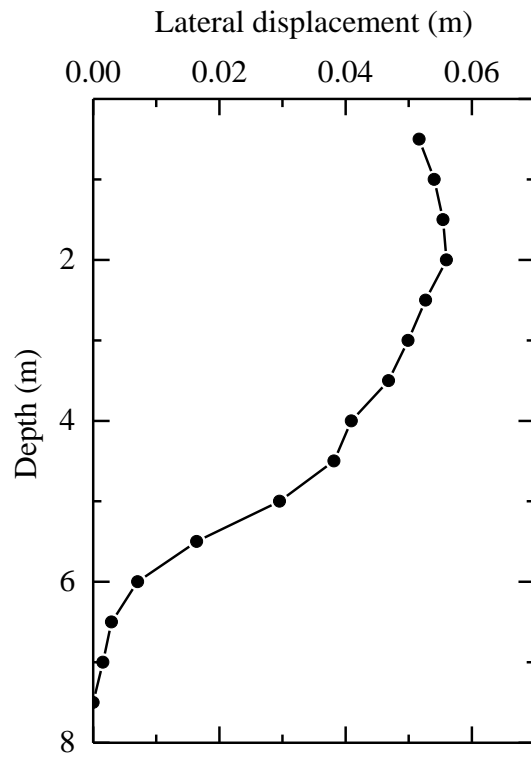
Fig. 5.11 Measured lateral displacement at K89 + 100 (after Feng 2013)
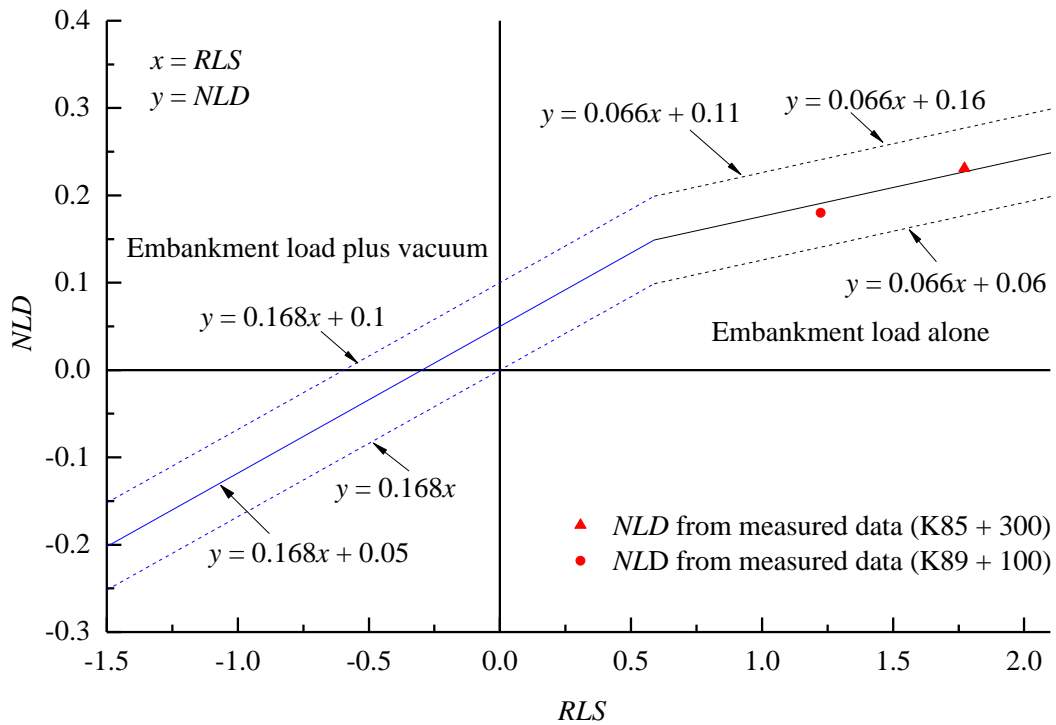
Fig. 5.12 Comparison of measured and predicted *NLD* of embankments at SZ expressway

In Fig. 5.12, it clearly shows that the measured data is quite close to the centerline of the predicted range of *NLD*, which supports the usefulness of the proposed method.

5.5.2 A new field case under combined embankment loading and vacuum pressure

(1) Brief description

The analyzed case was a trial embankment of Beijing-Shanghai high-speed railway, located in Kunshan, Jiangsu, China, and it was reported by Deng (2009) and Wang (2010). The trial site is from the mileage of K0 + 000 to K0 + 850, and the analyzed embankment is at mileage of K0 + 448. The ground consists of several soft soil layers, with total thickness of about 17.9 m. A surface clay layer has a thickness of 2.8 m overlying a mucky clay layer of about 11. 8 m thick. The third and fourth layers are two silty clay layers with thickness of 1.3 m and 2.2 m, respectively. Below the silty clay layer, there is a silty sand layer. The ground water level varies with seasons and is about 0.5-2.0 m under the ground surface. The soil properties reported by Deng (2009) as well as the cross section of the embankment are presented in Fig. 5.13. For the value of OCR, it was back-calculated by

fitting the measured ground surface settlement. In the analysis, the surface soil layer was subdivided into two soil layers with the first sub-layer had a thickness of 1.3 m.
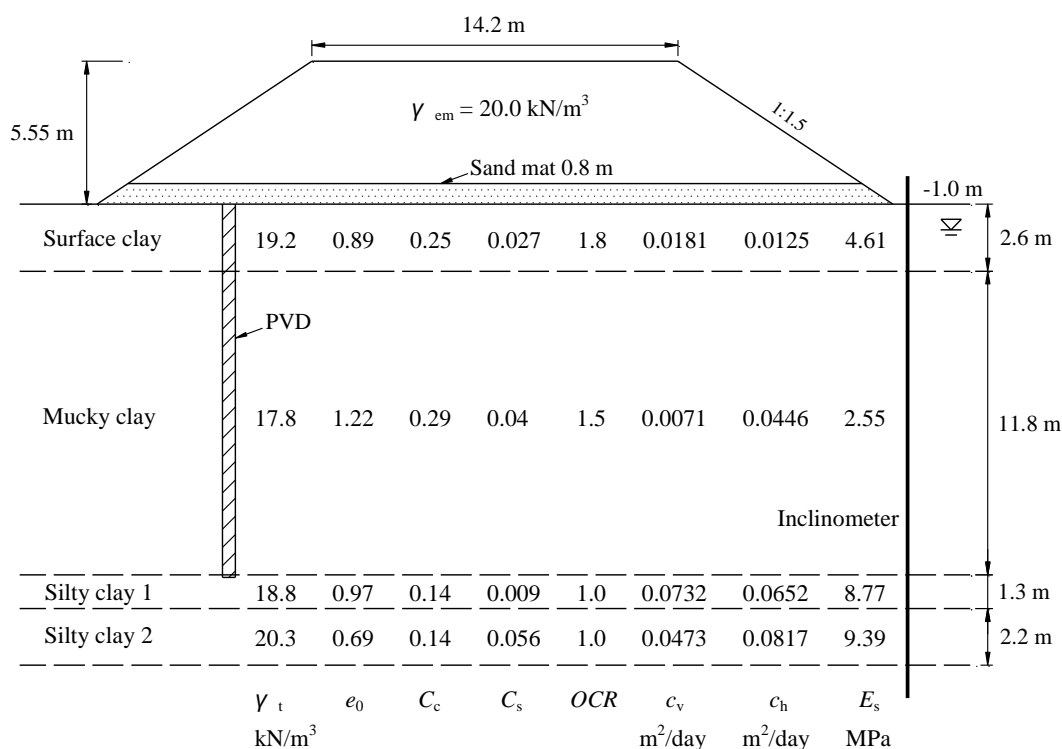
Fig. 5.13 Cross-section and soil profile of embankment at Kunshan

Combination of vacuum pressure and embankment load was used to improve the soft deposit as well as to reduce the post-construction settlement of the railway foundation. The PVDs were installed to a depth of 14.5 m in a triangular pattern with spacing of 1.2 m. The parameters related to PVD consolidation are listed in Table 5.3, referring from the commonly used PVDs.

Table 5.3 Parameters for PVD consolidation of embankment at Kunshan

D_e (m)	d_w (m)	d_s (m)	q_w (m3/year)	k_h/k_s [*]	l
1.26	0.052	0.26	100	2	14.5

*The value of k_h/k_s is assumed.

A sand mat of about 0.8 m was first placed at the ground surface functioned as a drainage layer and sealed by geomembranes. Then, the vacuum pressure was applied and an embankment was constructed to 5.55 m height within about 150 days. The vacuum pressure reached 80 kPa within a short time and varied around 77 kPa in a total application

period of about 190 days. The width of the top of the embankment is 14.2 m, and the slope is 1:1.5. The unit weight of the embankment fill was about 20 kN/m^3, as a result, the total embankment load was 111 kPa. The detailed embankment loading history and the variation of vacuum pressure are shown in Fig. 5.14.
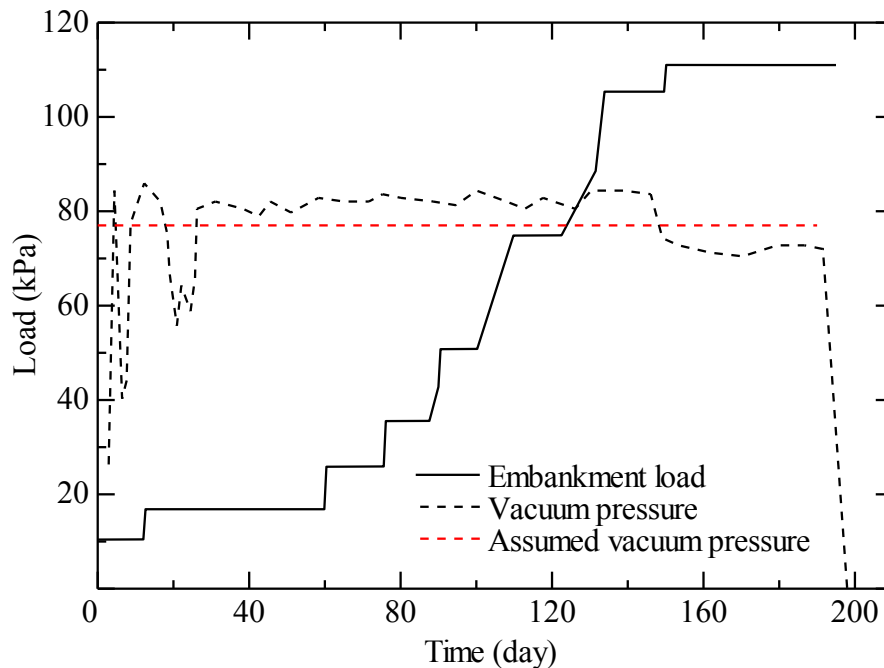
Fig. 5.14 Embankment and vacuum loading histories of embankment at Kunshan

(2) Predicting maximum net lateral displacement

(1) Calculations of S_f, U and s_u

With the soil parameters, embankment geometry, embankment loading history and variations of vacuum pressure, the values of S_f, U and s_u are calculated first. In the analysis, the whole embankment loading process was simulated by 4 steps of stepwise loading and the vacuum pressure at the ground surface was simplified as a constant load of 77 kPa (as represented by the red dash line in Fig. 5.14). Generally, in engineering practice, the vacuum pressure gradually reduces with increase of ground depth, and for this case the measured vacuum pressure in the PVD at buried depth of 12 m during the period of 115 days to 135 days after applying vacuum pressure was about 46 kPa (Deng 2009). There was no measured data reported at the end of vacuum preloading. For simplicity, in the

100

analysis, it is assumed that the final vacuum pressure at the bottom of the PVD (depth of 14.5 m) was 46 kPa and it linearly increased to 77 kPa at the ground surface.

The analyzed results of S_f, U and s_u are listed in Table 5.4. The calculated value of S_f at the end of vacuum preloading is 0.94 m, which is quite close to the measured value of 0.95 m. The measured and analyzed ground settlement-time curves are presented in Fig. 5.15. It clearly shows that the analyzed curve agrees well with the measured one.

Table 5.4 Predicted results of embankment at Kunshan

U (%)	p_n (kPa)	s_u (kPa)	S_f (m)	RLS	Predicted NLD	Predicted δ_{nm} (m)	Measured δ_{nm} (m)
92.3	-62.524	57.0	0.94	-1.097	-0.184 to -0.084	-0.175 to -0.080	-0.153 to -0.089
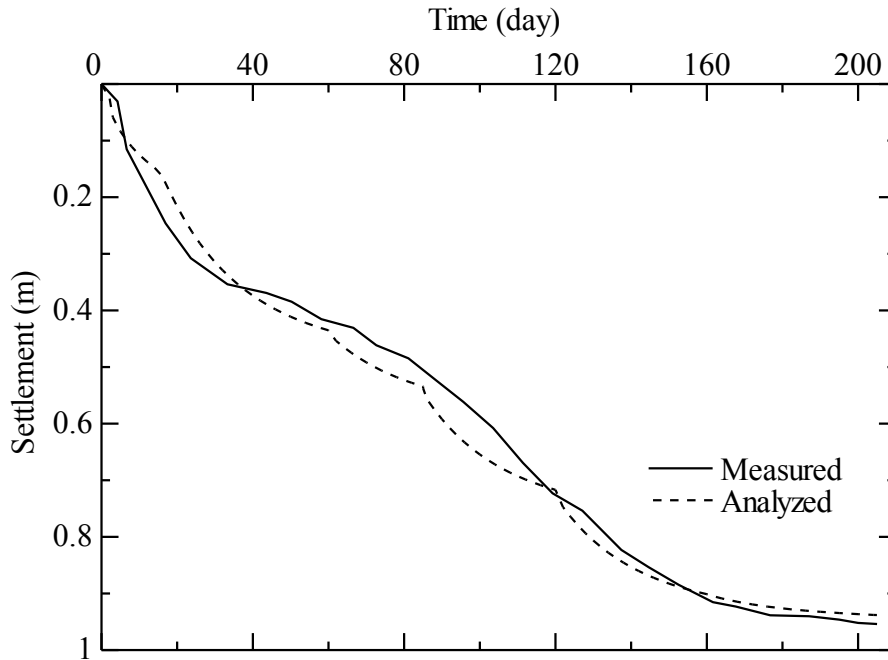
Fig. 5.15 Measured and calculated settlement-time curves of embankment at Kunshan

(2) Calculation of RLS

With the known values of U, s_u, embankment load (p_{em}) and vacuum pressure (p_{vac}), the value of RLS is calculated as follows (using Eqs. (5.2) and (5.8)):

$$p_n = p_{em} - \left(\left| p_{vac} \right| + p_{em} \right) U = 111 - (77 + 111) \times 0.923 = -62.524 \text{ kPa}$$

$$RLS = \frac{p_n}{s_u} = \frac{-62.524}{57.0} = -1.097$$

The calculated values of p_n and RLS are also listed in Table 5.4.

(3) Prediction of *NLD*

With *RLS* known, the value of *NLD* can be predicted. This field example is a case with embankment load and vacuum pressure, therefore Eq. (5.10a) is used. The calculated value of *NLD* is as:

$$NLD = 0.168 \cdot RLS + 0.05 \pm 0.05 = 0.168 \times (-1.097) + 0.05 \pm 0.05 = -0.134 \pm 0.05$$

As a result, the predicted range of *NLD* is -0.184 to -0.084, which is also presented in Table 5.4.

(4) Prediction of lateral displacement

With S_f and *NLD* known, the maximum net lateral displacement (δ_{nm}) is predicted as (using Eq. (5.7)):

$$\delta_{nm} = S_f \times NLD = 0.95 \times NLD$$

The predicted range of δ_{nm} is -0.175 to -0.080 as listed in Table 5.4.

(3) Comparison of the predicted and measured lateral displacements.

For this field case, the final measured lateral displacements near the toe of the embankment are shown in Fig. 5.16, in which the negative value means the lateral displacement is inward (toward the center of the embankment). The measured lateral displacements at two sides of the embankment are different. However, similar deformation behavior is noted, i.e. the lateral displacement adjacent to the ground surface is inward and it becomes outward below the depth of about 4.0 m.

For the measurement at the left side of the embankment, the maximum outward lateral displacement (δ_{mo}) was about 0.039 m and the maximum inward lateral displacement (δ_{mi}) was about -0.192 m, yielding a value of δ_{nm} about -0.153 m. For the measurement at the right side, the values of δ_{mo} and δ_{mi} were about 0.027 m and -0.116 m, respectively, yielding a value of δ_{nm} about -0.089 m. As a result, the measured range of δ_{nm} is about -0.153 m to -0.089 m, which is close to the predicted range of -0.175 to -0.080. The measured values of *NLD* are compared with the predicted range in Fig. 5.17. It is observed that the predicted *NLD* agrees reasonably well with the measured data.
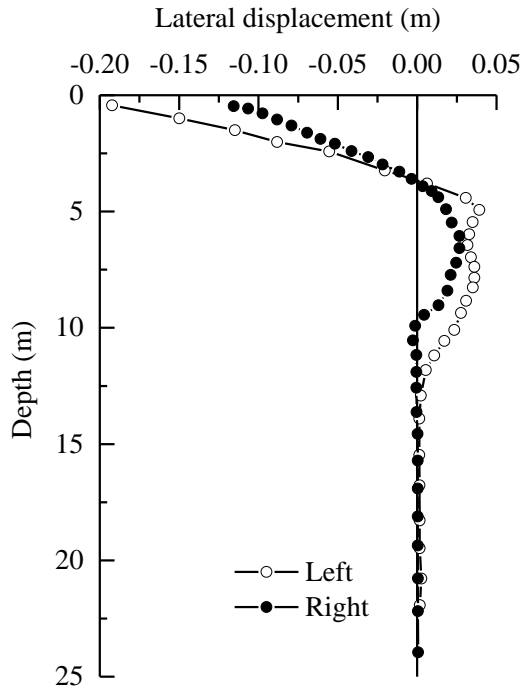
Fig. 5.16 Measured lateral displacements of embankment at Kunshan (after Wang 2010)
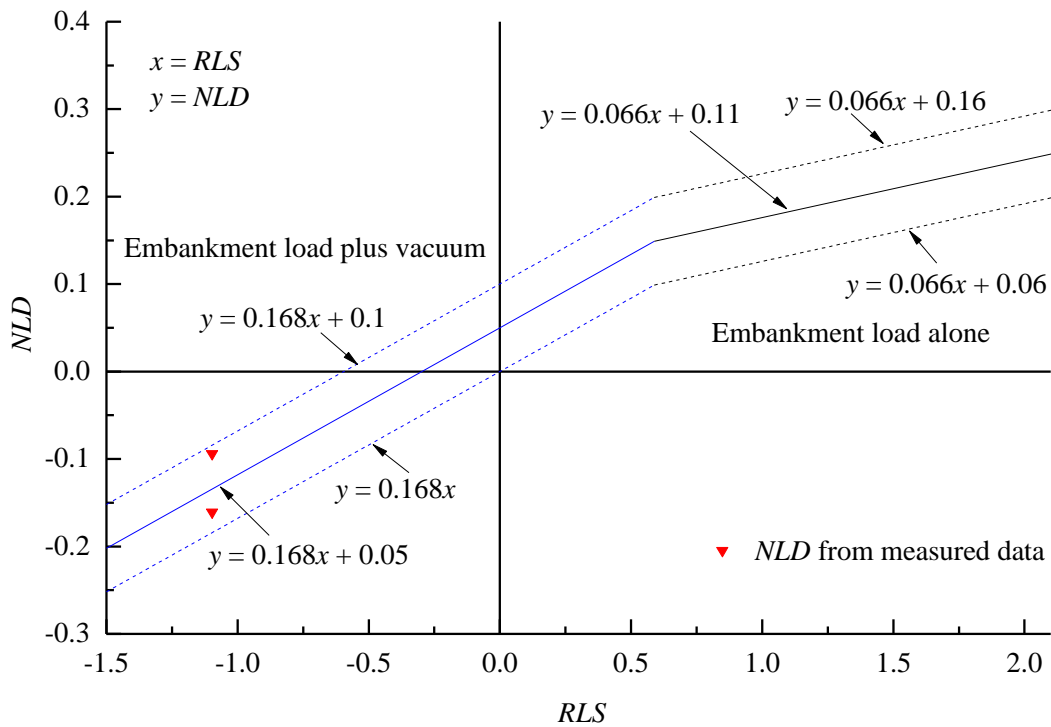
Fig. 5.17 Comparison of measured and predicted *NLD* of embankment at Kunshan

5.5.3 A new laboratory model test under only embankment loading

A new model test was conducted under total surcharge load of 60 kPa and with loading rate of 8 kPa/day. The model ground parameters and the consolidation properties of mini-PVDs used are listed in Tables 5.5 and Table 5.6, respectively.

Table 5.5 Parameters of model ground soil of new laboratory model test

γ_t (kN/m^3)	s_u (kPa)	e_0	C_c (C_s/ C_c)	k_v (m/day)	c_v (m^2/day)	p'_c (kPa)		
						Sur	Mid	Bot
13.85	4.7	2.95	0.913 (0.1)	5.7×10^{-5}	1.63×10^{-3}	10	9.3	10

p'_c = pre-consolidation pressure; Sur = surface layer, thickness, 178 mm; Mid = middle layer, thickness, 294 mm; Bot = bottom layer, thickness, 178 mm.

Table 5.6 Parameters for Mini-PVD of new model test

D_e (m)	d_w (m)	d_s (m)	k_h/k_s	q_w (m^3/year)	l (m)
0.178	0.02	0.08	1.6	1.0	0.65
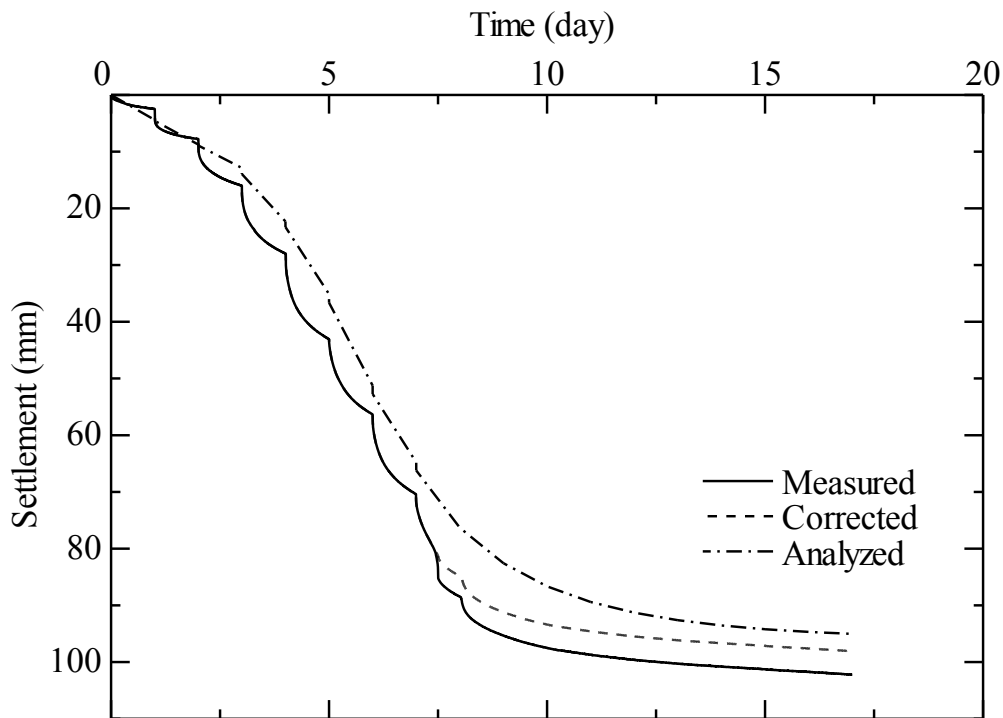
Fig. 5.18 Measured and calculated settlement-time curves of new model test

The measured settlement-time curve on the central loading plate and the final measured lateral displacement profiles at two sides of the surcharge loading area are shown in Figs. 5.18 and 5.19, respectively. For this test, it can be seen from Fig. 5.18 that the settlement rate had a sudden increase during the total elapsed time of about 7.4 days to 8 days. The reason is that at the time point of about 7.4 days the loading plates at two sides tilted too

much so that the loading Bellofram cylinders departed from them, i.e. the load applied on the loading plates at two sides was removed. Because of no confinement at two sides, the central loading plate punched into the model ground and increased the rate of settlement. This issue was noticed at the time point of 8 days and then fixed.
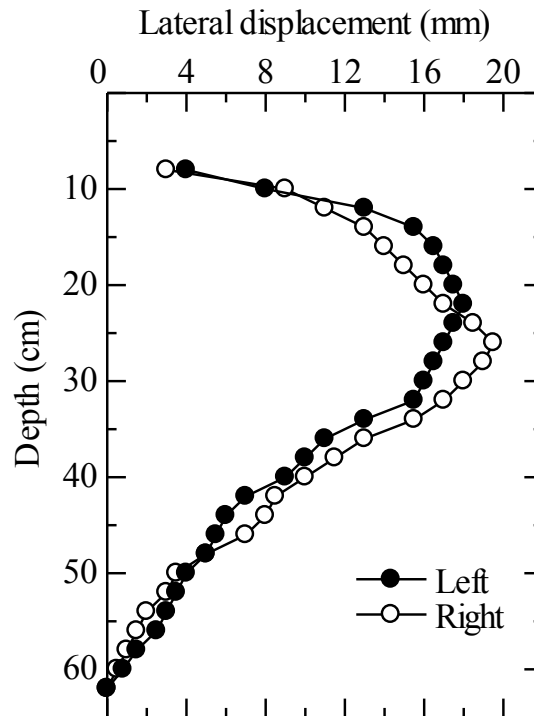
Fig. 19 Measured lateral displacements of new model test

It is considered that the sudden punching increase of settlement of the central loading plate might not cause considerable increase of the maximum lateral displacement measured at the outer edges of the loading plates at two sides. As a result, it can cause a reduction of the measured *NLD*. Considering this possibility, the measured settlement curve has been corrected by cutting the punching induced settlement increment and given in Fig. 5.18 as the dashed line. The calculated settlement-time curve is also shown in Fig. 5.18. It can be seen that the corrected settlement-time curve agrees better with the calculated one. For this new model test, the measured value of *NLD* has been calculated using the corrected settlement curve.

In Chapter 3, a model test was conducted under the same loading condition as this new model test. However, the undrained shear strengths of the two model grounds are different. The relationship between *NLD* and s_u for these two tests is presented in Fig. 5. 20. It verifies that *NLD* reduces with increase of s_u.
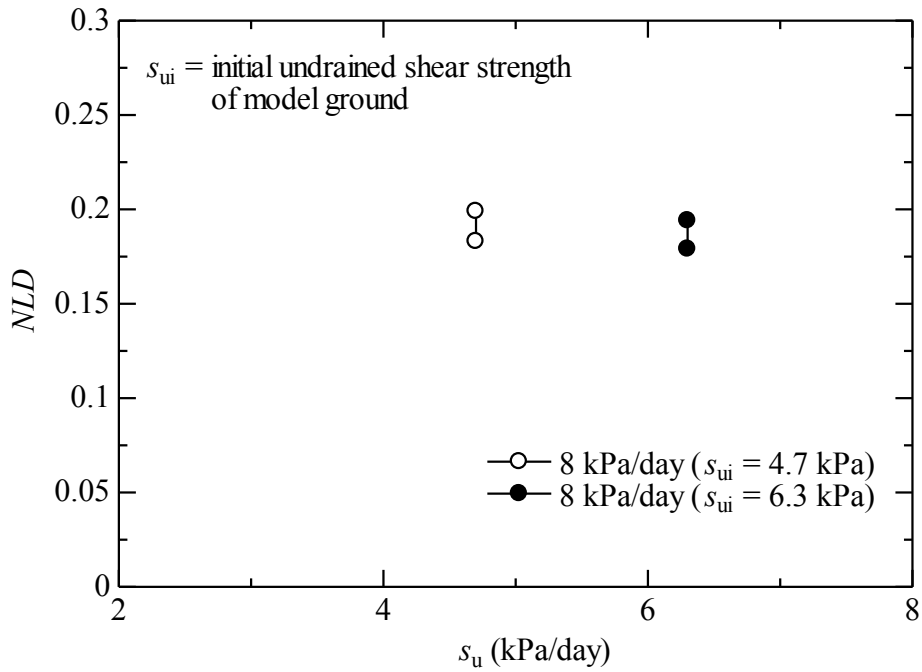
Fig. 5.20 Effect of undrained shear strength on *NLD*

The predicted and measured results are listed in Table 5.7 and are compared with each other in Fig. 5.21. It can be seen that the values of *NLD* calculated from the measurements are within the predicted range.
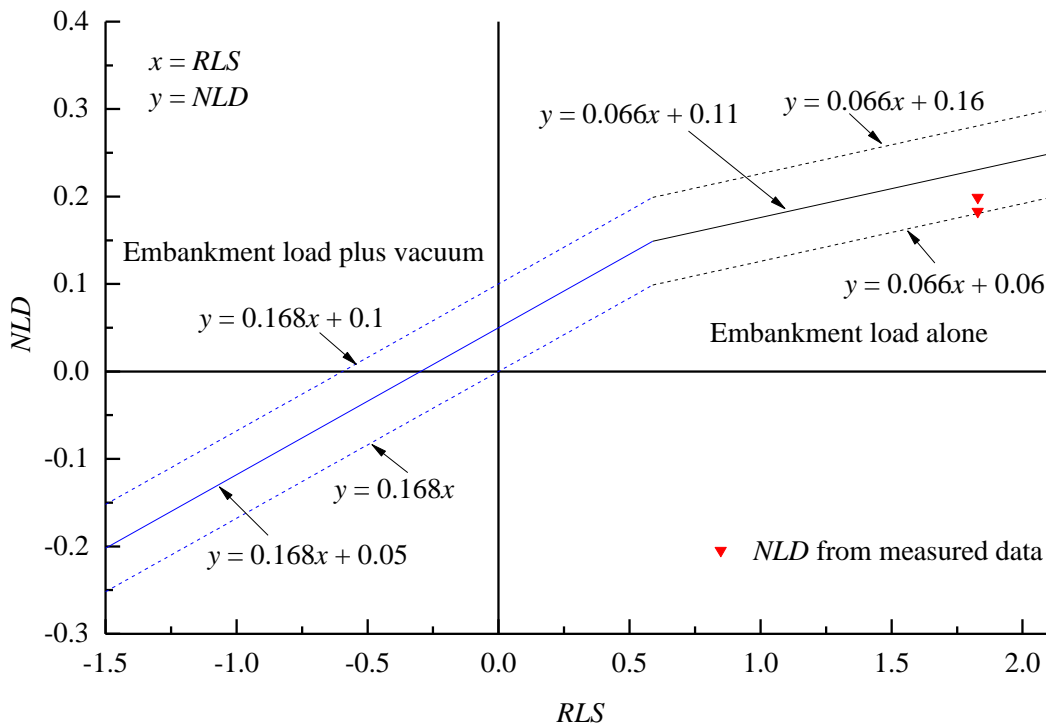
Fig. 5.21 Comparison of measured and predicted *NLD* of new model test

Table 5.7 Predicted and measured results of new model test

U (%)	p_n (kPa)	s_u (kPa)	S_f (mm)	RLS	Predicted NLD	Measured NLD	Predicted δ_m (mm)	Measured δ_m (mm)
73.1	16.1	8.8	98.1	1.829	0.183 to 0.283	0.183 to 0.199	17.9 to 27.7	18.0 to 19.5

5.5.4 Model tests under combined embankment loading and vacuum pressure

Ong (2011) reported some model tests using the same equipment as used in this study but under the combination of surcharge load and vacuum pressure. The lateral displacements of two tested cases from Ong (2011) were predicted using the proposed method. The consolidation properties of mini-PVDs used and the model ground soil parameters are given in Table 5.6 (Ong-1 and Ong-2) and Table 5.8, respectively. In Table 5.8, the values of c_v were back-calculated fitting the settlement-time curves measured at the model ground surface.

Table 5.8 Parameters of model ground soil of Ong (2011)'s tests

Case	γ_t (kN/m^3)	e_0	C_c (C_s/ C_c)	k_v (m/day)	c_v (m^2/day)	p'_c (kPa)
Ong-1	13.5	3.39	0.691 (0.1)	4.85×10^{-5}	8.1×10^{-4}	10
Ong-2	13.5	3.39	0.691 (0.1)	4.85×10^{-5}	7.1×10^{-4}	10

The case of Ong-1 was conducted under total applied surcharge load of 60 kPa and vacuum pressure of 40 kPa, while for the case of Ong-2 the total applied surcharge load and vacuum pressure were 40 kPa and 60 kPa, respectively. For both of the cases, the surcharge loading rate was 6 kPa/day. The predicted and measured results are listed in Table 5.9.

Table 5.9 Predicted and measured results of Ong (2011)'s tests

Case	RLS	Predicted		Measured	
		δ_{nm} (mm)	NLD	δ_{nm} (mm)	NLD
Ong-1	0.532	6.85 to 14.55	0.089 to 0.189	12.0	0.156
Ong-2	-0.327	-5.39 to 4.41	-0.055 to 0.045	-2.0 to 1.0	-0.020 to 0.010

The values of NLD calculated from the measurements are compared with the predicted range in Fig. 5.22. Again it shows that the measured data locate close to the centerline of the predicted range.
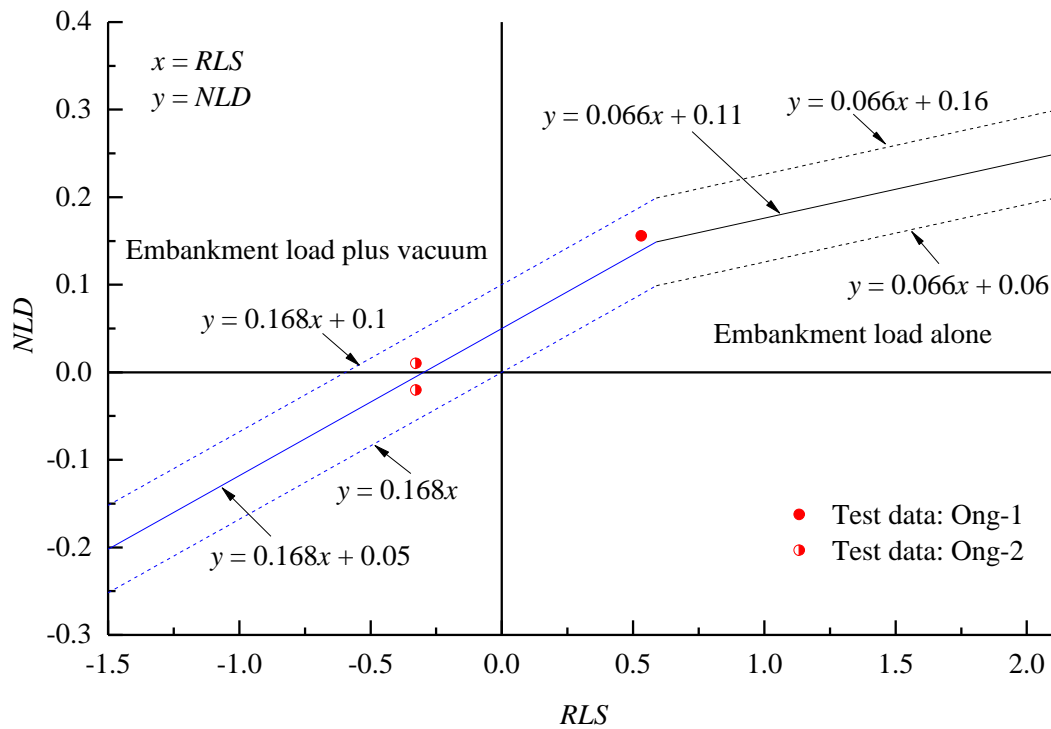
Fig. 5.22 Comparison of measured and predicted *NLD* of Ong (2011)'s tests

5.6 Summary

Based on the results of laboratory model tests as well as more than 30 field case histories, an empirical method has been proposed for predicting the maximum net lateral displacement (δ_{nm}, the maximum outward lateral displacement subtracting the maximum inward lateral displacement) of prefabricated vertical drains (PVDs) improved deposit under embankment loading with and without the application of vacuum pressure.

In this prediction method, the ratio of the maximum net lateral displacement to the final ground surface settlement on the embankment centerline (S_f) has been defined as the normalized maximum net lateral displacement ($NLD = \delta_{nm}/ S_f$). With consideration of the effects of the main factors affecting lateral displacement, i.e. the magnitudes of vacuum pressure and embankment load, loading rate, and the compression, consolidation and strength properties of the soft subsoil, another parameter termed as a ratio of load to undrained shear strength of the soft subsoil (*RLS*) was introduced as a key parameter for predicting *NLD*. Then, two segmented linear ranges for the relationship between *NLD* and *RLS* have been proposed to predict the maximum net lateral displacement of the PVD-improved deposits.

The proposed method had been verified by using it to predict the maximum net lateral displacements of three new field case histories and three laboratory model tests.

The main steps for using this method in design are as follows:

(1) With the designed total embankment load (p_{em}), vacuum pressure (p_{vac}, for the case with vacuum pressure) and construction process, and the basic soil properties, calculate the final ground surface settlement on the embankment centerline (S_f), degree of consolidation (U) and undrained shear strength (s_u) of the PVD-improved zone corresponding to the end of embankment construction.

(2) With known values of U, s_u, p_{em} and p_{vac} (for the case with vacuum pressure), calculate the value of RLS (refer Eqs. (5.2) and (5.8)).

$$RLS = \frac{p_n}{s_u} \tag{5.2bis}$$

$$p_n = p_{em} - \left(\left| p_{vac} \right| + p_{em} \right) U \tag{5.8bis}$$

(3) With RLS known, estimate the value of NLD using Eqs. (5.10a)-(5.10b) or Fig. 5.4.

$NLD = 0.168 \cdot RLS + 0.05 \pm 0.05$ ($-1.5 \leqslant RLS \leqslant 0.6$) (with vacuum pressure) (5.10a bis)

$NLD = 0.066 \cdot RLS + 0.11 \pm 0.05$ ($0.6 \leqslant RLS \leqslant 2.1$) (without vacuum pressure) (5.10b bis)

(4) With known values of S_f and NLD, predict the maximum net or maximum lateral displacement (δ_{nm} or δ_m) using Eq. (5.11):

$\delta_{nm} = S_f \cdot NLD$ (with vacuum) or $\delta_m = S_f \cdot NLD$ (without vacuum) (5.11)

CHAPTER SIX
CONCLUSIONS AND RECOMMENDATIONS

6.1 Conclusions

In this study, both laboratory model tests and analyses of field case histories were carried out to investigate the behavior of lateral displacement of prefabricated vertical drains (PVDs) improved deposits under embankment loading with and without vacuum pressure. Based on the analyzed results, an empirical method has been proposed to predict the maximum lateral displacement of the PVD-improved ground.

6.1.1 Investigation of main influencing factors on lateral displacement

(1) Laboratory model tests

A series of larger scale laboratory model tests were conducted under the same total applied surcharge (embankment) load but with different loading rate to investigate the effect of surcharge loading rate (LR) on the lateral displacement of the model ground. Meanwhile, the effect of the undrained shear strength (s_u) on the lateral displacement of the model ground was also investigated.

(a) For the cases tested, the normalized lateral displacement (NLD), i.e. the ratio of maximum lateral displacement (δ_m) to the ground surface settlement (S_f) at the centerline of the surcharge loading area ($NLD = \delta_m/S_f$), almost linearly increased with the increase of LR.

(b) Value of s_u of the model ground also had a considerable effect on lateral displacement. Under the same loading condition, NLD reduced with the increase of s_u.

(2) Analyses of model test results

Except the embankment loading rate and undrained shear strength of the ground, other main parameters affecting the magnitude of lateral displacement are magnitudes of embankment load and vacuum pressure, and deformation and consolidation properties of the soft subsoil. To consider the effects of all these factors on *NLD*, a synthetic parameter termed as the ratio of an index pressure (p_n) to undrained shear strength of the PVD-improved zone ($RLS = p_n/s_u$) has been used to analyze the model test results. p_n is calculated as:

$$p_n = p_{em} - \left(\left| p_{vac} \right| + p_{em} \right) U \qquad (5.8\text{bis})$$

where p_{em} = embankment load; p_{vac} = vacuum pressure (for the case of embankment load alone, p_{vac} is 0); and U = average degree of consolidation of the PVD-improved zone corresponding to the end of embankment construction.

For each case tested, the values of *NLD* and *RLS* have been calculated. The analyzed results showed that *NLD* almost linearly increased with increasing *RLS*, which verified that *RLS* can be a control parameter to predict lateral displacement of PVD-improved deposits.

(3) Field case histories and *NLD-RLS* relationship

More than 30 field case histories were collected from different countries. For each case, the values of *NLD* and *RLS* were calculated.

The analyzed results of the laboratory model tests and the field case histories show that there is a general trend of *NLD* increases with increasing *RLS* for PVD-improved deposits under embankment load with and without vacuum preloading.

6.1.2 Proposed method for predicting maximum lateral displacement

The proposed prediction method is a bilinear empirical relationship between *NLD* and *RLS*, expressing as:

$$NLD = 0.168 \cdot RLS + 0.05 \pm 0.05 \ (-1.5 \leqslant RLS \leqslant 0.6) \ \text{(with vacuum pressure)} \quad (5.10\text{a bis})$$

$$NLD = 0.066 \cdot RLS + 0.11 \pm 0.05 \ (0.6 \leqslant RLS \leqslant 2.1) \ \text{(without vacuum pressure)} \ (5.10\text{b bis})$$

The main steps for using this method in design are as follows:

(1) With the designed total embankment load (p_{em}), vacuum pressure (p_{vac}, for the case with vacuum preloading), construction process and the basic soil properties, calculate the ground surface settlement on the embankment centerline (S_f), degree of consolidation (U)

and undrained shear strength (s_u) of the PVD-improved zone corresponding to the end of embankment construction.

(2) With known values of U, s_u, p_{em} and p_{vac}, calculate the value of *RLS* using Eq. (5.2) and Eq. (5.8).

$$RLS = \frac{p_n}{s_u} \qquad (5.2\text{bis})$$

(3) With *RLS* known, estimate the value of *NLD* using Eqs. (5.10a)-(5.10b) or Fig. 5.4.
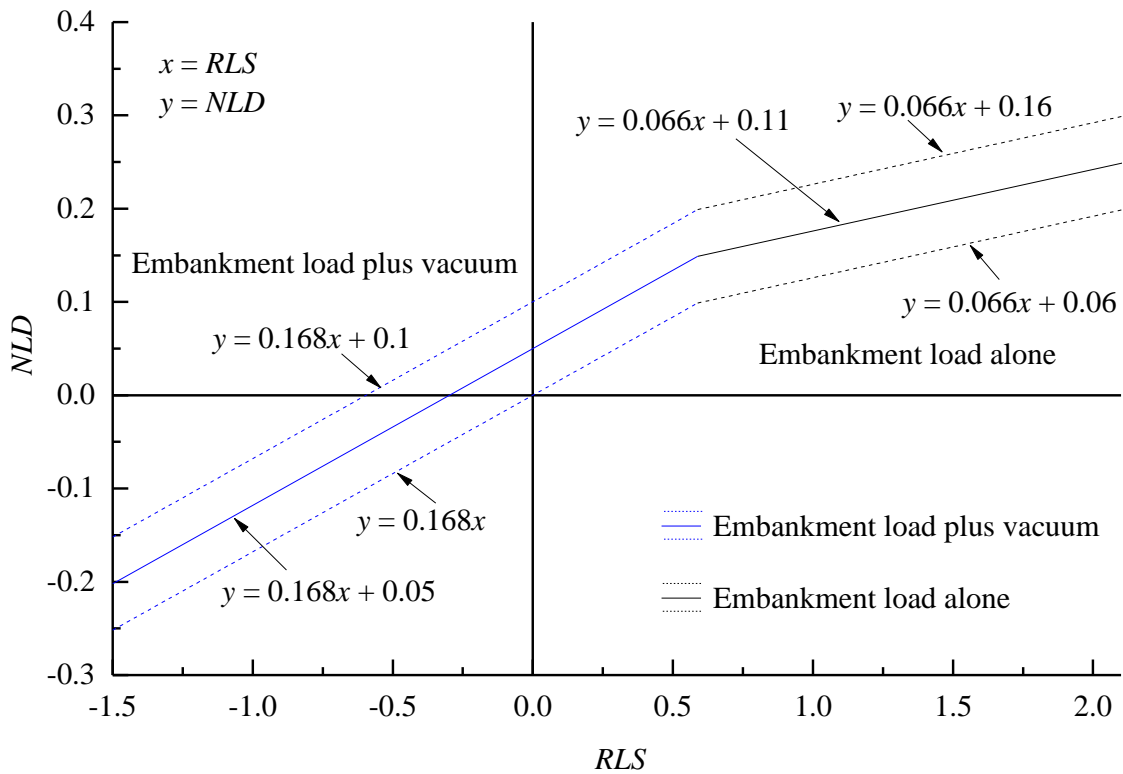
Fig. 6.1 Relationship of *NLD-RLS* use in design (Fig. 5.4bis)

(4) With known values of S_f and *NLD*, predict the value of maximum net lateral displacement (δ_{nm}, the maximum outward value subtracting the maximum inward (if any) value) using Eq. (5.7).

$$NLD = \frac{\delta_{nm}}{S_f} \qquad (5.7\text{bis})$$

The proposed method was verified by applying it to predict the maximum net lateral displacements of newly collected case histories and newly conducted laboratory model tests under embankment load with or without the application of vacuum pressure. The proposed method predicted the measured results reasonably well.

6. 2 Recommendations for Future Study

The present study has proposed a method for predicting the maximum lateral displacement of PVD-improved deposit under embankment loading with and without the application of vacuum pressure. Some recommendations and suggestions for future study related to this area are as follows:

(1) For the case of PVD-improved deposit under combined embankment loading and vacuum pressure, the ground may have inward lateral displacement adjacent to the ground surface and outward lateral displacement below a certain depth. The present study is just applicable for predicting the maximum net lateral displacement (the maximum outward lateral displacement reduced by the maximum inward lateral displacement) under this kind of loading condition. There is a requirement to predict both the maximum values of the inward and the outward lateral displacements.

(2) Method for predicting the location where the maximum lateral displacement occurs is required. Although some statistic studies had been made on this issue in literatures, further numerical investigation on this issue may be needed.

(3) Combination of preloading with installation of PVD and other ground improvement techniques, such as deep cement mixing and dry jet cement mixing, has been used in engineering practice. Studying on the lateral displacement under this kind of combined ground improvement condition is also desirable.

(4) In some regions, the maximum lateral displacement at the property boundary of the highway and railway is restricted to a small value, for example it is required to be less than $\pm$ 50 mm in Japan. Therefore, developing a technique for controlling or reducing the embankment load induced lateral displacement of soft deposits is required.

REFERENCES

Akagi, T. (1977). Effect of mandrel-driven sand drains on strength. *Proceedings 10th International Conference on Soil Mechanics and Foundation Engineering*, Tokyo, Vol. 1 pp. 3-6.

Akai, K., Shibata, T., Tominaga, M. and Tamura, T. 1974. Analysis of lateral displacement to be caused by embankment loading in ore-yard. *Proceeding 9th Japan National Conference on Soil Mechanics and Foundation Engineering*, E-2. 117:461-461.

Asaoka, A. (1978). Observational procedure of settlement prediction. *Soils and Foundations*, **18**(4): 87-101.

Barron, R. A. (1948). Consolidation of fine-grained soils by drain wells. *Transactions of the ASCE*, **113**(2346): 718-754.

Basu, D., Basu, P. and Prezzi, M. (2006). Analytical solutions for consolidation aided by vertical drains. *Geomechanics and Geoengineering: An International Journal*, **1**(1): 63-71.

Bergado, D. T., Asakami, H., Alfaro, M. C. and Balasubramaniam, A. S. (1991). Smear effects of vertical drains on soft Bangkok clay. *Journal of Geotechnical Engineering*, **117**(10): 1509-1530.

Bergado, D. T., Alfaro, M. C. and Balasubramaniam, A. S. (1993). Improvement of soft Bangkok clay using vertical drains. *Geotextiles and Geomembranes*, **12**(7): 615-663.

Bergado, D. T., Chai, J. C., Miura, N. and Balasubramaniam, A. S. (1998). PVD improvement of soft Bangkok clay with combined vacuum and reduced sand embankment preloading. *Geotechnical Engineering, Southeast Asian Geotechnical Society*, **29**(1), pp. 95-121.

Bergado, D. T., Long, P. V. and Balasubramaniam, A. S. (1996). Compressibility and flow parameters from PVD improved soft Bangkok clay. *Geotechnical Engineering Journal*, **27**, No. 1, 1-20.

Biot, M. A. (1941). General theory of three-dimensional consolidation. *Journal of applied physics*, **12**(2): 155-164.

Bo, M. W. (2003). *Soil improvement: prefabricated vertical drain techniques*. Singapore, Thomson.

Boussinesq, J. (1885). *Application des Potentials à L'Etude de L'Équilibre et du Mouvement des Solides Élastiques*. Gauthier-Villars, Paris, France (in French).

Budhu, M. (2000). *Soil mechanics and foundations*. John Wiley & Sons, INC, New York, USA.

Carrillo, N. (1942). Simple two and three dimensional cases in the theory of consolidation of soils. *Journal of Mathematics and Physics*, **21**(1): 1-5

Cascone, E. and Biondi, G. (2013). A case study on soil settlements induced by preloading and vertical drains. *Geotextiles and Geomembranes*, **38**: 51-67.

Chai, J. C. and Miura, N. (1999). Investigation of factors affecting vertical drain behavior. *Journal of Geotechnical and Geoenvironmental Engineering*, **125**(3): 216-226.

Chai, J. C., Shen, S. L., Miura, N. and Bergado, D. T. (2001). Simple method of modeling PVD-improved subsoil. *Journal of Geotechnical and Geoenvironmental Engineering*, **127**(11): 965-972.

Chai, J. C. and Miura, N. (2002). Long-term transmissivity of geotextile confined in clay. *Proceeding 7th International Conference on Geosynthetics*, Nice, France, Balkema Publishers, Vol. 1, pp. 155-158.

Chai, J., Hayashi, S. and Carter, J. (2005). Characteristics of vacuum consolidation. *Proceedings of the International Conference on Soil Mechanics and Geotechnical Engineering*, Osaka, Japan, vol. 3, pp. 1167-1170.

Chai, J. C., Carter, J. P. and Hayashi, S. (2005). Ground deformation induced by vacuum consolidation. *Journal of Geotechnical and Geoenvironmental Engineering*, **131**(12): 1552-1561.

Chai, J. C., Miura, N., Kirekawa, T. and Hino, T. (2009). Optimum PVD installation depth for two-way drainage deposit. *Geomechanics and Engineering*, **1**(3): 179-192.

Chai, J. C., Matsunaga, K., Sakai, A. and Hayashi, S. (2009). Comparison of vacuum consolidation with surcharge load induced consolidation of a two-layer system. *Géotechnique*, **59**, No. 7, 637-641.

Chai, J. C., Hong, Z. S. and Shen, S. L. (2010). Vacuum-drain consolidation induced pressure distribution and ground deformation. *Geotextiles and Geomembranes*, **28**(6): 525-535.

Chai, J. C. and Carter, J. P. (2011). *Deformation analysis in soft ground improvement*. Springer.

Chai, J. C., Ong, C. Y., Bergado, D. T. and Carter, J. P. (2013). Lateral displacement under combined vacuum pressure and embankment loading. *Géotechnique*, **63**(10): 842 –856.

Chai, J. C., Bergado, D. T. and Shen, S. L. (2013). Modelling prefabricated vertical drain improved ground in plane strain analysis. *Proceedings of the ICE-Ground Improvement*, **166**(2): 65-77.

Chai, J. C., Horpibulsuk, S., Shen, S. L. and Carter, J. P. (2014). Consolidation analysis of clayey deposits under vacuum pressure with horizontal drains. *Geotextiles and Geomembranes*, **42**(5): 437-444.

Chu, J., Yan, S. W. and Yang, H. (2000). Soil improvement by the vacuum preloading method for an oil storage station. *Géotechnique*, **50**(6): 625-632.

Conte, E. and Troncone, A. (2009). Radial consolidation with vertical drains and general time-dependent loading. *Canadian Geotechnical Journal*, **46**(1): 25-36.

Cowland, J. and Wong, S. (1993). Performance of a road embankment on soft clay supported on a geocell mattress foundation. *Geotextiles and Geomembranes*, **12**(8): 687-705.

Das, B. and Sobhan, K. (2010). *Principles of geotechnical engineering*. Cengage Learning, Stamford, USA.

Deng, X. (2009). *Improvement of soft highway foundation by combined vacuum pressure and surcharge load*. Master Thesis, Central South University, China (in Chinese).

Deng, Y. B., Xie, K. H. and Lu, M. M. (2013). Consolidation by vertical drains when the discharge capacity varies with depth and time. *Computers and Geotechnics*, **48**: 1-8.

Devata, M. and Darch, B. T. (1973). Settlement of an embankment constructed on marine clay. *Canadian Geotechnical Journal*, **10**(2): 161-179.

Fellenius, B. H. and Castonguay N. G. (1985). *The efficiency of band shaped drains: a full scale laboratory study*. Report to National Research Council and the Industrial Research Assistance Programme, 54 pp.

Feng, Y. C. (2013). *Comparative research on the two approaches of gravel pile and plastic drainage plate in reinforcing mountain weak subgrades*. Master Thesis, Chengdu University of Technology, Chengdu, China (in Chinese).

Geng, X., Indraratna, B. and Rujikiatkamjorn, C. (2011). Effectiveness of partially penetrating vertical drains under a combined surcharge and vacuum preloading. *Canadian Geotechnical Journal*, **48**(6): 970-983.

Geng, X., Indraratna, B. and Rujikiatkamjorn, C. (2012). Analytical solutions for a single vertical drain with vacuum and time-dependent surcharge preloading in membrane and membraneless systems. *International Journal of Geomechanics*, **12**(1): 27-42.

Ghandeharioon, A., Indraratna, B. and Rujikiatkamjorn, C. (2011). Laboratory and finite-element investigation of soil disturbance associated with the installation of mandrel-driven prefabricated vertical drains. *Journal of Geotechnical and Geoenvironmental Engineering*, **138**(3): 295-308.

Guo, Q. H., Zhou, S. H., Wang, B. L. and Wang, X. (2006). Soft ground treated with plastic drainage belt combined with surcharge preloading on express way. *Journal of Tongji University (Natural Science)*, **34**, No. 3, 340-344 (in Chinese).

Hansbo, S. (1977). *Geodrains in theory and practice*. Geotechnical Report from Terrafigo, Stockholm.

Hansbo, S. (1979). Consolidation of clay by bandshaped prefabricated drains. *Ground Engineering*, **12**(5): 16-25.

Hansbo, S. (1981). Consolidation of fine-grained soils by prefabricated drains. *Proceedings 10th International Conference on Soil Mechanics and Foundation Engineering*, Stockholm, Vol. 3, pp. 677-682.

Hansbo, S. (1987). Design aspects of vertical drains and lime column installations. *Proceeding 9th Southeast Asian Geotechnical Conference*, Southeast Asian Geotechnical Society, Bangkok, Thailand, Vol. 2, pp. 8-1–8-12

Hansbo, S. (1997). Aspects of vertical drain design: Darcian or non-Darcian flow. *Géotechnique*, **47**(5): 983-992.

Hart, E. G., Kondner, R. L. and Boyer, W. C., 1958. Analysis for partially penetrating sand drains. *Journal of Soil Mechanics and Foundation Division*, 812-815－1812-1911.

He, K. S. and Dai, J. Q. (2000). Surcharge preloading method with ultra-deep PVD. *Journal of Hydraulic Engineering*, No.6, 74-80 (in Chinese).

Heo, Y. and Bae, W. (2013). A statistical evaluation of consolidation properties of marine clay in South Korea. *Marine Georesources & Geotechnology*, **31**, No. 3, 209-224.

Hird, C. C. and Moseley, V. J. (2000). Model study of seepage in smear zones around vertical drains in layered soil. *Géotechnique*, **50**, 89-97.

Hu, Y., Zhou, W. H. and Cai, Y. (2014). Large-strain elastic visco-plastic consolidation analysis of very soft clay layers with vertical drains under preloading. *Canadian Geotechnical Journal*, **51**(2): 144-157.

Holtz, R. D., Jamiolkowski, M., Lancellotta, R. and Pedroni, S. (1991). *Prefabricated vertical drains: design and performance*, CIRIA ground engineering report: ground improvement. UK, Butterworth-Heinemann Ltd.

Holtz, R. D., Jamiolkowski, M., Lancellotta, R. and Pedroni, S. (1988). Behavior of bent prefabricated vertical drains. *Proceeding 12th International Conference Soil Mechanics and Foundation Engineering*, Rio De Janeiro, pp. 1657-1660.

Holtz, R. D. and Holm, G. (1973). Excavation and sampling around some sand drains Ska-Edeby, Sweden. *Proceeding Specialty Conference on Performance on Earth and Earth supported Structure,* Purdue University, Vol. 1, pp. 435-464.

Hong, Z. S., Bian, X., Cui, Y. J., Gao, Y. F. and Zeng, L. L. (2013). Effect of initial water content on undrained shear behaviour of reconstituted clays. *Géotechnique*, **63**(6): 441-450.

Hu, J. L. (2004). *Researeh on stabilty and settlement for soft soil road groulld combined with packed drain*. Master Thesis, Zhejiang University, China (in Chinese).

Indraratna, B., Balasubramaniam, A. S. and Sivaneswaran, N. (1997). Analysis of settlement and lateral deformation of soft clay foundation beneath two full-scale embankments. *International journal for numerical and analytical methods in geomechanics*, **21**, No. 9, 599-618.

Indraratna, B. and Redana, I. W. (1998). Laboratory determination of smear zone due to vertical drain installation. *Journal of Geotechnical and Geoenvironmental Engineering*, **124**(2): 180-184.

Indraratna, B. and Redana, I. W. (2000). Numerical modeling of vertical drains with smear and well resistance installed in soft clay. *Canadian Geotechnical Journal*, **37**(1): 132-145.

Indraratna, B., Rujikiatkamjorn, C. and Chu, J. (2007). Soft Clay Stabilization with Geosynthetic Vertical Drains beneath Road and Railway Embankments: A Critical Review of Analytical Solutions and Numerical Analysis. *Advances in Measurement and Modeling of Soil Behavior*, ASCE, pp. 1-20.

Indraratna, B., Rujikiatkamjorn, C., Balasubramaniam, A. S. and McIntosh, G. (2012). Soft ground improvement via vertical drains and vacuum assisted preloading. *Geotextiles and Geomembranes*, **30**: 16-23.

Jamiolkowski, M. and Lancellotta, R. (1981). Consolidation by vertical drains: Uncertainties involved in prediction of settlement rates. *Proceedings 10th International Conference on Soil Mechanics and Foundation Engineering*, Balkema, Rotterdam, The Netherlands, Vol. 4, pp. 593-595.

Jamiolkowski, M., Lancellotta, R. and Wolski, W. (1983). Precompression and speeding up consolidation. *Proceeding 8th European Conference on Soil Mechanics and Foundation Engineering*, Helsinki, pp. 1201-1226.

Japan Road Association (1986). *Guidelines and counter-measure for road and earthworks construction* . Tokyo, Japan: Japan Road Association (in Japanese).

Jimenez, R., Serrano, A. and Olalla, C. (2009). Consolidation charts for non-linearly time-increasing loads. *Proceedings of the ICE-Ground Improvement*, **162**(2): 103-108.

Karim, M. R. and Lo, S. C. (2015). Estimation of the hydraulic conductivity of soils improved with vertical drains. *Computers and Geotechnics*, **63**: 299-305.

Karunaratne, G. (2011). Prefabricated and electrical vertical drains for consolidation of soft clay. *Geotextiles and Geomembranes*, **29**(4): 391-401.

Kelln, C., Sharma, J., Hughes, D. and Gallagher, G. (2007). Deformation of a soft estuarine deposit under a geotextile reinforced embankment. *Canadian Geotechnical Journal*, **44**(5): 603-617.

Kim, H. J., Lee, K. H., Jamin, J. C. and Mission, J. L. C. (2014). Stochastic cost optimization of ground improvement with prefabricated vertical drains and surcharge preloading. *Geomechanics and Engineering*, **7**(5): 525-537.

Kjellman W. (1952). Consolidation of clay soil by means of atmospheric pressure. *Proceedings of the Conference on Soil Stabilisation*, Massachusetts Institute of Technology, Boston, USA, pp. 258–263.

Ladd, C. C. (1991). Stability evaluation during staged construction. *Journal of Geotechnical Engineering*, **117**(4): 540-615.

Lu, M. M., Wang, S. Y., Sloan, S. W., Sheng, D. C. and Xie, K. H. (2015). Nonlinear consolidation of vertical drains with coupled radial–vertical flow considering well resistance. *Geotextiles and Geomembranes*, **43**(2): 182-189.

Lekha, K., Krishnaswamy, N. and Basak, P. (1998). Consolidation of clay by sand drain under time-dependent loading. *Journal of Geotechnical and Geoenvironmental Engineering*, **124**(1): 91-94.

Leroueil, S., Tavenas, F., Samson, L. and Morin, P. (1983). Preconsolidation pressure of Champlain clays. Part II: Laboratory determination. *Canadian Geotechnical Journal*, **20**(4): 803-816.

Leroueil, S., Bouclin, G., Tavenas, F., Bergeron, L. and La Rochelle, P. (1990). Permeability anisotropy of natural clays as a function of strain. *Canadian Geotechnical Journal*, **27**(5): 568-579.

Lin, D. G. and Chang, K. T. (2009). Three-dimensional numerical modelling of soft ground improved by prefabricated vertical drains. *Geosynthetics International*, **16**, No. 5, 339-353.

Liu, S. Y., Han, J., Zhang, D. W. and Hong, Z. S. (2008). A combined DJM-PVD method for soft ground improvement. *Geosynthetics International*, **15**(1): 43-54.

Loganathan, N., Balasubramaniam, A. S. and Bergado, D. T. (1993). Deformation analysis of embankments. *Journal of Geotechnical Engineering*, **119**(8): 1185–1206.

Lu, M. M., Wang, S. Y., Sloan, S. W., Indraratna, B. and Xie, K. H. (2015). Nonlinear radial consolidation of vertical drains under a general time-variable loading. *International Journal for Numerical and Analytical Methods in Geomechanics*, **39**(1): 51-62.

Ma, S. D. (1995). Lateral displacement of soft clay ground under embankment. *Journal of Huaqiao University (Natural Science)*, **16**(2), 165-167 (in Chinese).

Marche, R. and Chapuis, R. (1974). Controle de la stabilite des remblais par mesure des deplacements horizontaux. *Canadian Geotechnical Journal*, **11**(1): 182-201 (in French).

Mesri, G. and Khan, A. Q. (2012). Ground Improvement Using Vacuum Loading Together with Vertical Drains. *Journal of Geotechnical and Geoenvironmental Engineering*, **138**(6): 680-689.

Mochizuki, K., Hiroyama, T., Morita, Y. and Sakamaki, A. (1980). Lateral deformation of soft ground-Case of Kurasiki. *Proceeding 15th Japan National Conference on Soil Mechanics and Foundation Engineering*, E-2. 216: 861-864 (in Japanese).

Oliveira, P. V. (2013). A formula to predict the effect of the variable discharge capacity of prefabricated vertical drains. *Geosynthetics International*, **20**(6): 408-420.

Olson, R. E. (1977). Consolidation under time-dependent loading. *Journal of the Geotechnical Engineering Division*, **103**(1): 55-60.

Olson, R. E. (1998). Settlement of Embankments on Soft Clays. *Journal of Geotechnical and Geoenvironmental Engineering*, **124**(4): 278-288.

Ong, C. Y. and Chai, J. C. (2011). Lateral displacement of soft ground under vacuum pressure and surcharge load. *Frontiers of Architecture and Civil Engineering in China*, **5**(2): 239-248.

Ong, C. Y. (2011). *Prediction of Lateral Displacement of Ground Induced by Surcharge Load and Vacuum Pressure*. PhD Dissertation, Saga University, Saga, Japan.

Ong, C. Y., Chai, J. C. and Hino, T. (2012). Degree of consolidation of clayey deposit with partially penetrating vertical drains. *Geotextiles and Geomembranes*, **34**: 19-27.

Onoue, A. (1988). Consolidation by vertical drains taking well resistance and smear into consideration. *Soils and Foundations*, **28**(4): 165-174.

Osterberg, J. O. (1957). Influence values for vertical stresses in a semi-infinite mass due to an embankment loading. *Proceedings 4th Intornational Conference on Soil Mechanics and Foundation Engineering*, London, Vol. 1, pp. 393-394.

Parsa-Pajouh, A., Fatahi, B., Vincent, P. and Khabbaz, H. (2014). Analyzing consolidation data to predict smear zone characteristics induced by vertical drain installation for soft soil improvement. *Geomechanics and Engineering*, **7**(1): 105-131.

Pothiraksanon, C., Bergado, D. T. and Abuel-Naga, H. M. (2010). Full-scale embankment consolidation test using prefabricated vertical thermal drains. *Soils and Foundations*, **50**(5): 599-608.

Poulos, H. G. (1972). Difficulties in prediction of horizontal deformations of foundations. *Journal of the Soil Mechanics and Foundations Division*, **98**(8): 843-848.

Redana, I. W. (1999). *Effectiveness of vertical drains in soft clay with special reference to smear effect*. PhD Thesis, University of Wollongong, Australia.

Rixner, J. J., Kraemer, S. R. and Smith, A. D. (1986). *Prefabricated vertical drains. Vol. II: Summary of Research Effort*, Federal Highway Administration Research Report No. FHWA/RD-86/169, Washington, DC, USA, 171 pp.

Runesson, K., Hansbo, S. and Wiberg, N. E. (1985). The efficiency of partially penetrating vertical drains. *Géotechnique*, **35**(4): 511-516.

Sathananthan, I. (2005). *Modelling of vertical drains with smear installed in soft clay*. PhD Thesis, University of Wollongong, Australia.

Sathananthan, I. and Indraratna, B. (2006). Laboratory evaluation of smear zone and correlation between permeability and moisture content. *Journal of Geotechnical and Geoenvironmental Engineering*, **132**(7): 942-945.

Sathananthan, I., Indraratna, B. and Rujikiatkamjorn, C. (2008). Evaluation of smear zone extent surrounding mandrel driven vertical drains using the cavity expansion theory. *International Journal of Geomechanics*, **8**(6): 355-365.

Shen, J. D. (2012). *Study on settlement-control of preloading method used to treat soft clay foundation*. Master Thesis, South China University of Technology, China (in Chinese).

Shibata, T., Nomura, K. and Sakai, S. (1982). The behavior of soft foundation under embankment. *Proceeding 17th Japan National Conference on Soil Mechanics and Foundation Engineering*, E-2. 505: 2017-2020 (in Japanese).

Smadi, M. M. (2001). *Lateral Deformation and Associated Settlement Resulting from Embankment Loading of Soft Clay and Silt Deposits*. PhD Thesis, University of Illinois, Urbana-Champaign, IL, USA

Suzuki, O. (1988). The Lateral flow of soil caused by banking on soft clay ground. *Soils and Foundations*, **28**(4): 1-18.

Tan, S. A. (1995). Validation of hyperbolic method for settlement in clays with vertical drains. *Soils and Foundations*, **35**(1): 101-113.

Tang, X. W. and Onitsuka, K. (1998). Consolidation of ground with partially penetrated vertical drains. *Geotechnical Engineering Journal*, **29**, 209-231.

Tang, X. W. and Onitsuka, K. (2000). Consolidation by vertical drains under time-dependent loading. *International journal for numerical and analytical methods in geomechanics*, **24**(9): 739-751.

Tang, M. and Shang, J. Q. (2000). Vacuum preloading consolidation of Yaoqiang Airport runway. *Géotechnique*, **50**(6): 613-623.

Tavenas, F., Mieussens, C. and Bourges, F. (1979). Lateral displacements in clay foundations under embankments. *Canadian Geotechnical Journal*, **16**(3): 532-550.

Tavenas, F. and Leroueil, S. (1980). The behaviour of embankments on clay foundations. *Canadian Geotechnical Journal*, **17**(2): 236-260.

Terzaghi, K. (1925). *Erdbaumechanik auf Bodenphysikalischer Grundlager*. Deuticke, Vienna.

Terzaghi, K. (1943). *Theoretical soil mechanics*. John Wiley & Sons, INC, New York, USA.

Tominaga, M., Echigo, Y. and Hasimoto, M. (1973). Measurement of lateral deformation to be caused by embankment loading in two layeres ground (1). *Proceeding 8th Japan National conference on Soil Mechanics and Foundation Conference on Soil Mechanics and Foundation Engineering*, E-2. 104: 411-414 (in Japanese).

Tominaga, M., Echigo, Y. and Hasimoto, M. (1973). Measurement of lateral deformation to be caused by embankment loading in two layeres ground (2). *Proceeding 8th Japan National conference on Soil Mechanics and Foundation Conference on Soil Mechanics and Foundation Engineering*, E-2. 118: 465-468 (in Japanese).

Tran, T. A. and Mitachi, T. (2008). Equivalent plane strain modeling of vertical drains in soft ground under embankment combined with vacuum preloading. *Computers and Geotechnics*, **35**(5): 655-672.

Vu, V. T. (2015). Optimal layout of prefabricated vertical drains. International. *International Journal of Geomechanics*, 06014020.

Walker, R., Indraratna, B. and Rujikiatkamjorn, C. (2012) Vertical drain consolidation with non-Darcian flow and void-ratio-dependent compressibility and permeability. *Géotechnique* **62**, 985-997.

Walker, R. (2006). *Analytical solutions for modeling soft soil consolidation by vertical drains*. PhD Dissertation, University of Wollongong, Wollongong, Australia.

Wang, Y. G. (2010). *Theory and experiment of vacuum combined surcharge preloading method for foundation improvement*. PhD Thesis, Central South University, China (in Chinese).

Xiong, P. H. (2012). *Research on the Consolidation and Settlement Law of Soft Soil Foundation Improved by Plastic Drainage Board Method*. Masters thesis, Chengdu University of Technology, Chengdu, China (in Chinese).

Xu, F. and Chai, J. C. (2014). Lateral displacement of PVD-improved deposit under embankment loading. *Geosynthetics International*, **21**(5): 286-300.

Yamaguchi, H., Nakanodo, H. and Kitazume, M. (1981). Consolidation deformation behavior of normal consolidation clay ground in the model test. *Proceeding 16th Japan National Conference on Soil Mechanics and Foundation Engineering*, E-2 205:817-820 (in Japanese).

Yoshikuni, H. and Nakanodo, H. (1974). Consolidation of soils by vertical drain wells with finite permeability. *Soils and Foundations*, **14**(2): 35-46.

Yoshioka, S., Miura, N. and Park, Y. M. (1994). Laboratory and field tests for Saga airport project. *Soil mechanics and foundation engineering*, **42**, No. 4, 33-38 (in Japanese).

Zeng, G. X. and Xie, K. H. (1989). New development of the vertical drain theories. *Proceedings 12th International Conference on Soil Mechanics and Foundation Engineering*, vol. 2, pp. 1435-1438.

Zhang, Y. G., Xie, K. H., Zhuang, Y. C. and Wang, Z. (2005). Calculation and analysis of consolidation theory of ground by partially penetrated sand drain. *Chinese Journal of Rock Mechanics and Engineering*, **24**(22): 4164-4171 (in Chinese).

Zheng, W. F. (2006). *Study on the settlement behavior of soft ground during the subgrade constuction of Zha-Jia-Su Express Way*. Master Thesis, Central South University, China (in Chinese).

Zhu, G. and Yin, J. H. (2001). Design charts for vertical drains considering construction time. *Canadian Geotechnical Journal*, **38**(5): 1142-1148.

Zhu, G. and Yin, J. H. (2004). Consolidation analysis of soil with vertical and horizontal drainage under ramp loading considering smear effects. *Geotextiles and Geomembranes*, **22**(1): 63-74.